APPENDIX M

Groundwater Model Update – Core Lithium Grants and BP33 Mine Groundwater Dewatering Model Update

(Artesium, 2026)

Groundwater Model Update

Core Lithium BP33 Mine Groundwater Dewatering Model Update

Technical Report

Project no: 2026-002

Prepared for: Core Lithium

13 April 2026

Artesium Consulting Services

Hydrogeological & Mine Water Solutions

Artesium Consulting Services (Pty) Ltd

Reg no 2021/447309/07

Email: koos@artesiumconsulting.com

Mobile: +27 64 512 4776

249 Draaihals Street

Leeuwfontein Estates

Kameeldrift East

Pretoria

0005

CSIR Campus,

Mering Naude Rd,

Building 4E 2nd Floor,

Pretoria

0184

South Africa

Groundwater Model Update

Core Lithium BP33 Mine Groundwater Dewatering Model Update

Technical Report

13 April 2026

Conducted on Behalf of:

Core Lithium

Level 4,

186 St Georges Terrace,

Perth,

WA 6000.

Compiled by:

Rudolf van Heerden (B.Sc, Hons Hydrogeology)

Reviewed by:

Dr Koos Vivier (PhD, M.Sc, Hydrogeology Pr.Sci.Nat)

Artesium Consulting Services (Pty) Ltd

Hydrogeologists & Mine Water Solutions

REPORT DISTRIBUTION LIST

Name	Institution
Helen Astill	Core Lithium
Anthony Kirke	
James Barratt	AGE
Keith Phillipson	

DOCUMENT HISTORY

Report no	Date	Version	Status
2026-002	13 April 2026	2	Final

LIST OF ABBREVIATIONS

Abbreviation	Description
a	Annum
BDL	Below detection limit
CRD	Cumulative Rainfall Departure
GDE	Groundwater Dependent Ecosystems
GW	Groundwater
ha	hectare
Kx	Horizontal Conductivity in direction x
Ky	Horizontal Conductivity in direction y
Kz	Vertical Conductivity in direction z
mamsl	metres above mean sea level
MAP	Mean Annual Precipitation
MAR	Mean Annual Runoff
mbgl	metres below ground level
Mon	Month/s
OP	Open Pit
P5	5th Percentile (Lower range)
P50	50th Percentile (Median)
P95	95th Percentile (Upper range)
S	Storativity
SW	Surface Water
Ss	Specific Storage
TDS	Total Dissolved Solids
ZOI	Zone of Influence

EXECUTIVE SUMMARY

At the Core Lithium operations, a numerical model was previously developed for the Grants and BP33 mines to calculate expected groundwater dewatering rates and zones of influence. The numerical models were developed by CloudGMS (2018, 2019, 2021, 2023) and previously Artesium Consulting Services (ACS, the consultant). The applicant (Core Lithium Limited) tasked ACS to update the numerical groundwater flow model to include the newly planned BP33 underground expansion from 320 mbgl to 850 mbgl. The model results should inform the Environmental Referral for the Proposal and quantify potential impacts on local and regional groundwater hydrology and related Groundwater Dependent Ecosystems (GDEs).

The Grants and BP33 mines, located approximately ±88 km south of Darwin, are part of Core Lithium's Finniss Lithium Project. Previously, mining at Grants ceased in January 2024 with the associated processing plant closed by mid-2024, and is due to recommence in quarter 2 2026.

The BP33 Underground mine has an expected Life of Mine (LoM) of 133 months. Access will be through an existing box cut and decline, with underground stopes extending to –787mamsl. The mine plan at BP33 incorporates paste backfilling, with 82% of the total 3 982 963 m³ of void volume scheduled to be refilled. The BP33 Box Cut will be backfilled up to the surface upon achievement of Life of Mine.

Long-term monitoring (June 2017 to March 2025) of water levels at Grants Open Pit (OP) pre- and post-mining showed the following:

- Pre-mining baseline groundwater levels were dynamic with an amplitude of 5.0 m and range of 10 m between wet and dry seasons.
- The pre-mining average baseline water level depth was shallow at 3.32 mbgl with a maximum of 12.80 mbgl.
- Monitoring data spanning ±8 years (2017 - 2025) testifies that the maximum measured drawdown at Grants OP was 360 – 400 m radius from the Pit. No measurable drawdown greater than the seasonal fluctuations of groundwater levels was observed during the operational phase in monitoring data collected. It can be concluded that Grants fissure water inflow rates ranged from 600 – 750 m^3/d and caused limited drawdown of water levels locally (<400 m) in the intermediate aquifer with no observed impact in the shallow groundwater zone.
- Due to the wet (season) cycle, the average water level change since mining started showed a rise of 4.42 m and a rate of change of 2.21 m/a. The rate of water level rise in the last year was 2.67 m/a with no evidence of a drawdown effect from the pit.
- Intermediate/deep monitoring bore GWB08 (60 m deep) had a measured decline of 1.8 m. The pre-mining water level fluctuations driven by wet and dry seasons averaged ±5.0 m up and down, with a maximum range of 12 m drop in water level in the pre-mining baseline conditions.
- At Grants, where the Open Pit is 94 m deep and acts as a hydrological sink, groundwater levels have stabilised in recent years towards a quasi-steady state.

The BP33 Box Cut Area pre- and post-mining long-term monitoring showed the following:

- Pre-mining baseline groundwater levels are comparable with the Grants Area and dynamic with fluctuations between wet and dry seasons with an amplitude of 5.7 m and a range of 11.4 m.
- The pre-mining average baseline water level depth was shallow at 2.39 m with a maximum of 11.40 m.
- Monitoring data spanning 3 - 5 years (2020 - 2025) around the box cut showed no measurable drawdown that exceeded seasonal variability of the baseline conditions. Fissure water inflow rates of ±340 m^3/d had a limited influence of (<365 m) in the deep aquifer with no measurable effect in the shallow groundwater zone.
- Due to the development phase falling in a dry season, the average water level change since development of the box cut started in August 2023 showed a decline of 4.39 m and a rate of decrease of 10.55 meters per annum (m/a). Compared to the past year (2025), which had an increase in water level of 2.95 m with no evidence of drawdown effect from the Box Cut.
- The monitoring data at both sites demonstrates hydraulic semi-disconnection between shallow, intermediate, and deep aquifers, although there is no defined confining layer. The hydraulic semi-disconnected behaviour is supported by head differences of 0.25 - 5.66 m at Grants Pit and in nested bores at BP33. The measured vertical head differences ranged from 0.25 m to 15.40 m, further supporting the limited vertical connectivity between the groundwater zones and/or aquifers.

The distinct hydrochemical signatures of shallow, intermediate, and deep groundwater provide further evidence of limited vertical hydraulic connectivity between the shallow and intermediate-to-deep aquifers. The aquifer system can be classified as minor, with borehole yields generally low at < 1L/s, with some isolated blowout yields of up to 5.0 L/s.

The updated model incorporated depth-dependent decreasing hydraulic conductivity to reflect decreasing permeability with depth. The limited hydraulic connectivity observed in the monitoring data was represented in the model by decreasing the vertical hydraulic conductivity by an order of magnitude. Calibration was undertaken against measured pit inflows and transient groundwater levels.

The simulated dewatering results, supported by long-term monitoring data, confirm that groundwater responses at mining areas are predominantly controlled by natural seasonal variability, with mining-related impacts remaining comparatively limited.

At BP33 underground mine, simulated fissure inflows indicate that dewatering rates peak at approximately ±1 696 m^3/d around 75 months into mining under base-case conditions, before declining to ±1 100 m^3/d as aquifer storage is depleted. The average life-of-mine dewatering rate was simulated at ±1 139 m^3/d. Under the high-case scenario, dewatering at BP33 peaked at ±2 235 m^3/d and stabilised at approximately ±1 600 m^3/d. The BP33 Box Cut contributes comparatively minor groundwater inflows, peaking at ±260 m^3/d prior to underground development and reducing to an average of approximately ±51 m^3/d thereafter.

The simulated zones of influence (ZOI), defined using a 1 m drawdown cutoff between mining and no-mining scenarios, indicate that impacts remain spatially constrained across the shallow, intermediate, and deep aquifers.

At BP33, the shallow aquifer zone of influence (ZOI) is simulated to extend approximately ±2.25 km east–west and ±2.1 km north–south (±345 ha) in the shallow aquifer, with maximum drawdown of ±10 m confined to the decline footprint. The intermediate and deep aquifer ZOIs expanded to ±395 ha and ±685 ha respectively, with the deep cone extending ±3.5 km east–west and ±2.5 km north–south. Several low-potential GDEs are intersected by the shallow ZOI to the south and north of BP33.

Simulated groundwater discharge to drainage systems decreased from a mean of 27 181 m^3/d under no-mining conditions to 24 564 m^3/d during active mining, representing an overall reduction of 10%. The mean annual impact on low- and moderate-potential GDEs remains negligible (<2%) across both wet and dry seasons.

Overall, the numerical modelling results are consistent with pre-mining monitoring data and are sufficiently calibrated with operational phase monitoring data. The model is considered conservative because it overpredicts the simulated drawdown relative to monitoring data. The model does simulate the limited vertical hydraulic connectivity of the aquifers (shallow, intermediate, and deep aquifers). This semi-disconnected behaviour constrains the propagation of mining-induced drawdown, resulting in localised zones of influence with limited regional impact.

In conclusion, the updated numerical modelling, supported by long-term monitoring data, demonstrates that groundwater zones at mining areas are characterised by limited hydraulic connectivity and are predominantly governed by natural seasonal variability. As a result, mining-induced impacts are localised, with zones of influence remaining spatially constrained and groundwater-dependent ecosystems simulated to be affected to a limited extent. The model provides a defensible basis for assessing groundwater impacts for the proposed mine expansion and supports the conclusion that, with appropriate monitoring and adaptive management, the development can proceed with a low risk to regional groundwater resources and associated ecosystems.

TABLE OF CONTENTS

LIST OF FIGURES

LIST OF TABLES

1 INTRODUCTION

The Grants and BP33 mines—part of the Finniss Lithium Project — are located approximately 88 km south of Darwin. Mining at the Grants Mine was suspended in January 2024, and its processing plant was shut down by mid-2024. Preparations are underway for the recommencement of mining in quarter 2 of 2026. Early development activities at the BP33 underground deposit were paused in 2023 and recommenced in January 2026.

Following previous numerical groundwater models and updates developed by CloudGMS (2018, 2019, 2021, and 2023) Core Lithium Limited (the applicant) engaged Artesium Consulting Services (ACS) to update the numerical groundwater flow model to support environmental impact assessment of changes related to an increased depth of BP33 underground mine from 320 metres below ground level (mbgl) to 850 mbgl (the Proposal). The model results inform the Environmental Referral for the Proposal and quantify potential impacts on local and regional groundwater systems.

1.1 Objectives

The project objectives were to:

- Update the existing groundwater model for BP33 Underground Extension to determine groundwater inflow rates associated with the planned mine expansion.
- Quantify the impacts on surrounding groundwater systems associated with mine dewatering-depressurisation volumes and potential zone of influence (ZOI).

1.2 Scope of Work

To meet the main objectives, the scope of work (Table 1-1) was implemented for the investigation.

Table 1-1: Summary of the Scope of Work

1	Action
1.1	Data review of additionally provided data, and incorporate into the numerical groundwater model.
1.2	Update the numerical groundwater model to gauge the impact of the BP33 Underground expansion.
1.3	Model simulations will be used to quantify the impact of management decisions on: • Groundwater flow directions and velocities • Life of mine inflow estimates • Sensitivity analysis on relevant hydrogeological parameters to acquire a dewatering envelope • Post operational water management
1.4	Post-closure (operational) zone of influence modelling
1.5	Post-closure box cut conceptual optimisation, analytical modelling
1.6	Hydrogeological impact assessment of the relevant mining units
1.7	GIS spatial analysis and maps.
1.8	3D zone of influence maps and illustrations.
1.9	Compilation and review of the numerical modelling/mine water management report

2 DESCRIPTION OF THE STUDY AREA

2.1 Site Overview

The Grants and BP33 mines form part of Core Lithium Limited's Finniss Lithium Project, located on the Cox Peninsula in the Northern Territory of Australia, approximately 25 km and 30 km south of Darwin, respectively. The project area is in the Bynoe Pegmatite Field, a geologically prospective zone known for its lithium-bearing spodumene mineralisation hosted in rare-element pegmatites (refer to Figure 2-1).

The Grants deposit, situated on Mineral Lease (ML) 31726, was the first lithium resource approved for mining in the Northern Territory. It comprises a shallow, high-grade, spodumene-bearing pegmatite body that was initially developed as an open-pit operation. Mining commenced in October 2022, with ore processed through an on-site Dense Media Separation (DMS) plant to produce spodumene concentrate. Since early 2024 the site is under care and maintenance and is scheduled to recommence mining in quarter 2 2026.

The BP33 deposit, located approximately 4.5 km southeast of Grants, represents a higher-grade spodumene resource. Early site works began in late 2023, and full-scale development was deferred that same year; construction at BP33 recommenced in January 2026.

The planned underground workings at BP33 will be accessed via a decline system. Active mining is scheduled for approximately 9 months at Grants, after which the open-pit mine will be repurposed as a mine water dam, and for 10 years and 11 months at BP33, with the mine depth increased from 320 mbgl to 850 mbgl. Maintaining safe working conditions in the stopes will require continuous dewatering and depressurisation of the underground workings during operations. Estimating dewatering rates is the primary focus of this numerical modelling update, along with quantifying the potential surface impacts of mine dewatering.

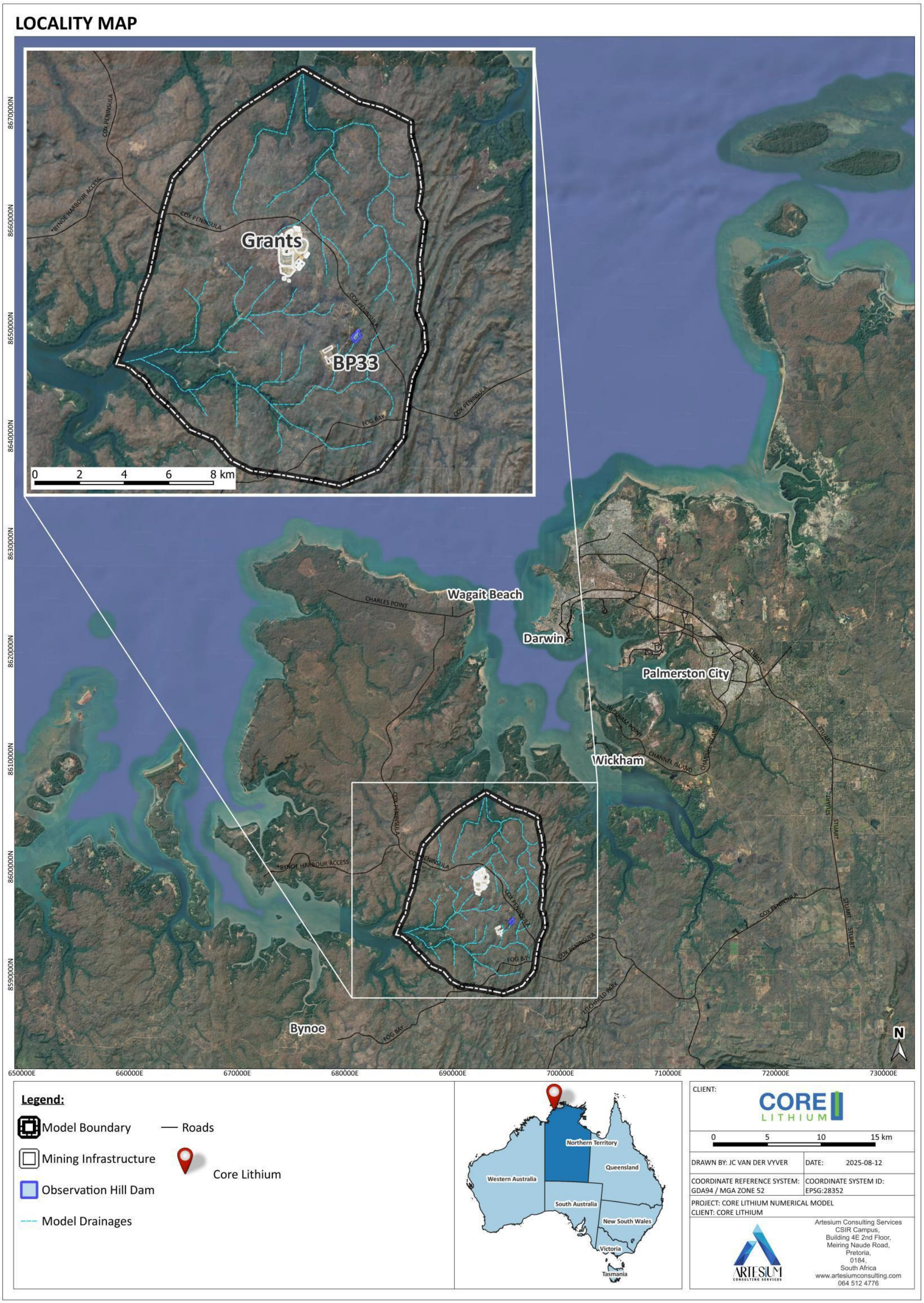

Figure 2-1: Locality Map

2.2 Local Climate

2.2.1 Precipitation

The measured on-site rainfall data provided by the client was reported to be variable. It was decided to use the same data source for this model update as was applied in the previous (CloudGMS model).

Rainfall and evaporation data were obtained from the SILO (2025) online database, maintained by the Queensland Government Department of Environment and Science. The modelled data, provided in grid format, was downloaded for the coordinate location (-12.65, 130.80). A summary of the monthly statistical distribution is presented in Table 2-1 and illustrated graphically in Figure 2-2.

Analysis of the statistical distribution of climate datasets is essential for assessing the probability of extreme rainfall events when sequencing rainfall records for future simulations. The Mean Annual Precipitation (MAP) of the dataset was 1 537 mm/a, which shows good correlation with the MAP used in the previous Grants model (1 570 mm/a).

Table 2-1: Monthly Statistical Summary of SILO Precipitation Data

SILO Precipitation Data from Latitude, Longitude: -12.65 130.80													
Month	**Jan**	**Feb**	**Mar**	**Apr**	**May**	**Jun**	**Jul**	**Aug**	**Sept**	**Oct**	**Nov**	**Dec**	**Annual**
P99	779	731	718	358	88	26	25	20	81	198	299	566	2 200
P98	738	687	628	288	64	22	13	15	72	175	286	543	2 162
P95	673	591	492	214	40	12	8	7	67	138	248	508	2 051
P90	588	523	435	186	29	5	1	2	45	120	196	458	1 967
P50	380	300	260	60	1	0	0	0	7	48	125	218	1 504
Average	389	320	277	83	9	2	1	1	14	59	131	250	**1 537**
P05	137	129	107	7	0	0	0	0	0	3	53	105	1 058

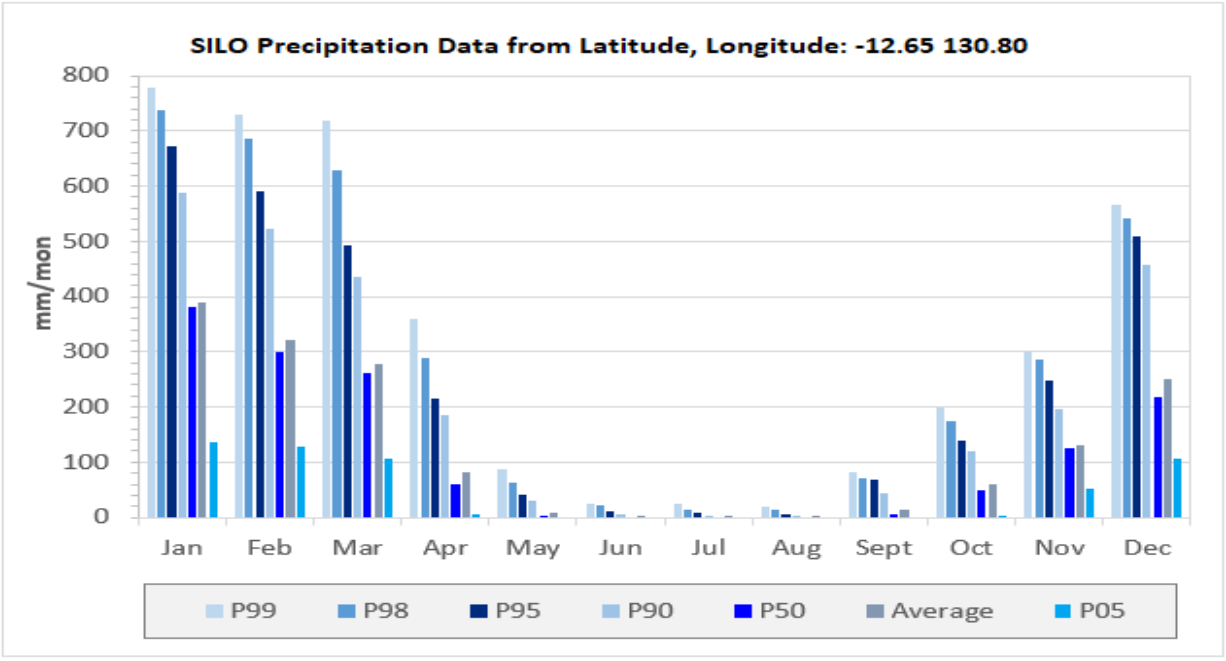

Figure 2-2: Monthly Statistical Summary of SILO Precipitation Data

The cumulative rainfall departures (CRD) method represents the cumulative deviation of monthly or annual rainfall from the long-term mean. Positive slopes in the CRD curve indicate periods of above-average rainfall (wet cycles), whereas negative slopes indicate below-average rainfall (dry cycles). This approach is particularly valuable in hydrogeological studies, as it provides insight into long-term recharge variability and assists in contextualising model inputs.

The Cumulative Rainfall Departure (CRD) trend for the downloaded SILO dataset covering the period January 1900 to June 2025 is presented in Figure 2-3. Historically, a prolonged dry cycle occurred between June 1925 and November 1965. The CRD highlights alternating long-term wet and dry cycles, with the most recent wet cycle beginning in November 1997 and continuing to the present. A marked inflection indicating elevated rainfall is evident from October 2010 onwards.

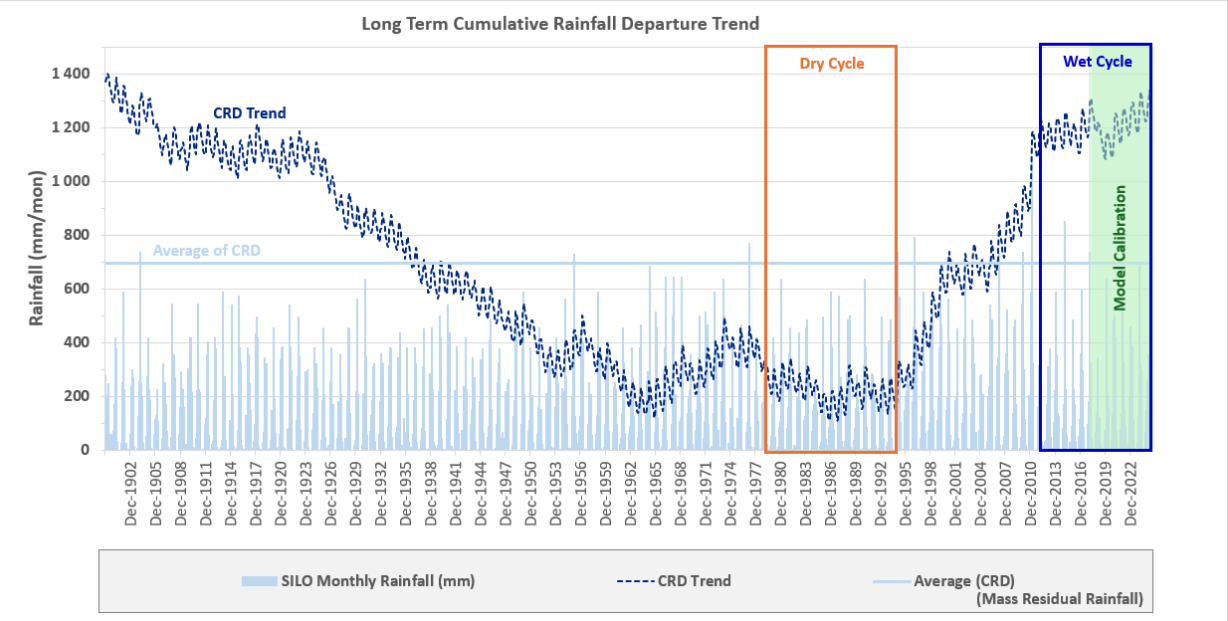

Figure 2-3: Long-term Cumulative Rainfall Departure (CRD) trend vs Modelled Monthly Rainfall (SILO, 2025)

2.2.2 Evaporation

The evaporation data for the site were also obtained from SILO (2025) for the period January 1990 to June 2025. The monthly statistical distribution is summarised in Table 2-2 and illustrated in Figure 2-4.

The evaporation dataset was applied in the analytical Grants pit inflow calculations. The Mean Annual Evaporation (MAE) rate for the site was calculated at 2 282 mm/a, which is consistent with the previously used value of 2 340 mm/a.

Table 2-2: Monthly Statistical Summary of SILO Potential Evaporation Data

SILO Evaporation Date from Latitude, Longitude: -12.65 130.80													
Month	**Jan**	**Feb**	**Mar**	**Apr**	**May**	**Jun**	**Jul**	**Aug**	**Sept**	**Oct**	**Nov**	**Dec**	**Annual**
P99	214	186	196	216	216	213	227	244	265	281	254	234	2 564
P98	209	179	195	211	215	210	222	243	258	275	246	227	2 524
P95	195	173	191	202	209	203	216	238	249	268	232	213	2 456
P90	182	161	183	193	203	195	209	227	238	256	225	209	2 418
P50	171	144	161	173	179	172	189	206	219	235	207	188	2 243
Average	172	147	163	176	184	178	193	211	223	237	209	190	**2 282**
P05	152	128	143	163	179	172	185	203	216	222	192	167	2 227

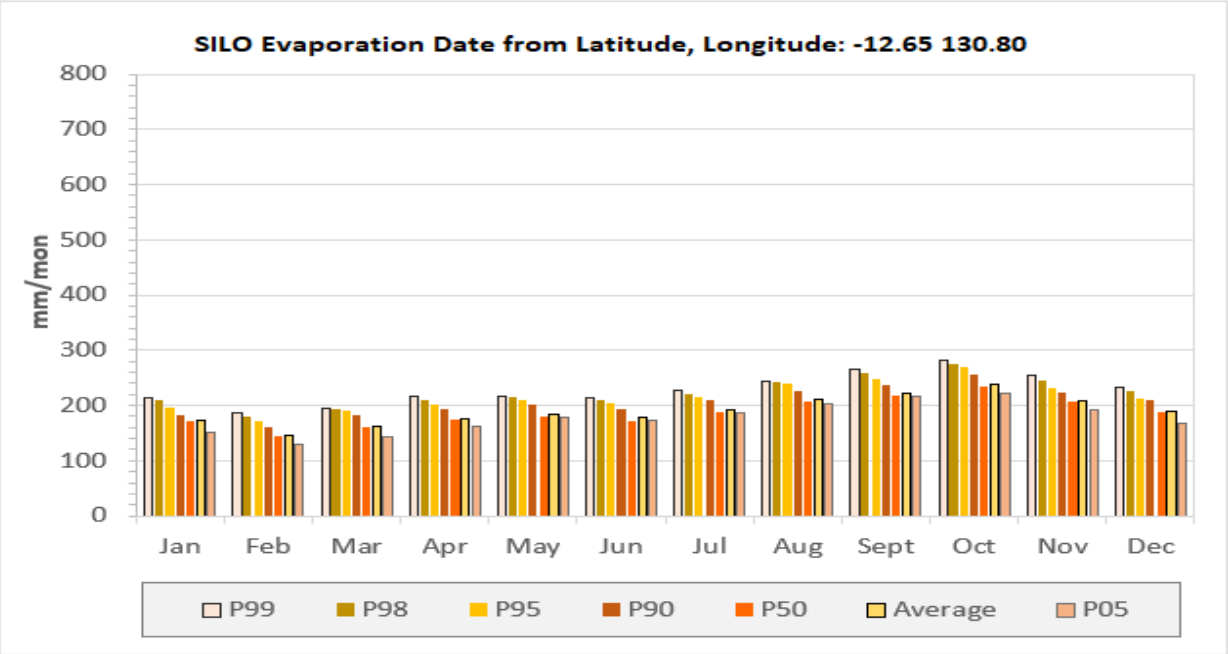

Figure 2-4: Monthly Statistical Summary of SILO Potential Evaporation Data

2.3 Topography and Drainage

Regional topography was derived from the Shuttle Radar Topography Mission dataset (SRTM, 2013) and compared with the topographic data used in the previous model. The datasets showed sufficient correlation, and according to Gallant et al. (2011), SRTM (2013) provides a vertical accuracy of ±9.8 m at 90% confidence. A watershed (surface catchment) was delineated from the Digital Elevation Model (DEM) and applied as the numerical groundwater model boundary (as shown in Figure 2-5). The regional topography is relatively flat, with a gently undulating slope from the higher elevations (±60 mamsl) in the south-east towards the catchment outlets, which occur as estuaries along the northern and south-western model boundaries. Most of the regional drainage systems are situated at low elevations (<5 mamsl).

Local topographic survey data provided by the client were used for the Grants Mine. The Grants site slopes from south to north, draining towards ephemeral streams that flank the surface infrastructure. The highest natural elevation at Grants is located to the south at 30 mamsl, while the Waste Rock Dumps (WRDs) have elevated the land surface to approximately 50 mamsl. The Grants Open Pit (OP) is currently □94 m deep, with

the pit floor at -73 mamsl and a decant (spillway) at 10 mamsl. In March 2025, the pit lake water level was measured at -53 mamsl.

For the BP33 deposit, surveyed box cut elevations were provided by the client. The box cut is currently 30 m deep, with the lowest point at -7 mamsl and a decant point at 19 mamsl located in the south-eastern corner. The box cut is inferred to be flooded; however, no measured water levels were available, and it was estimated to be situated at approximately 8 mamsl. In addition, an old underground pit lake south of the box cut is also flooded, and was reported by the client to be 6 m deep.

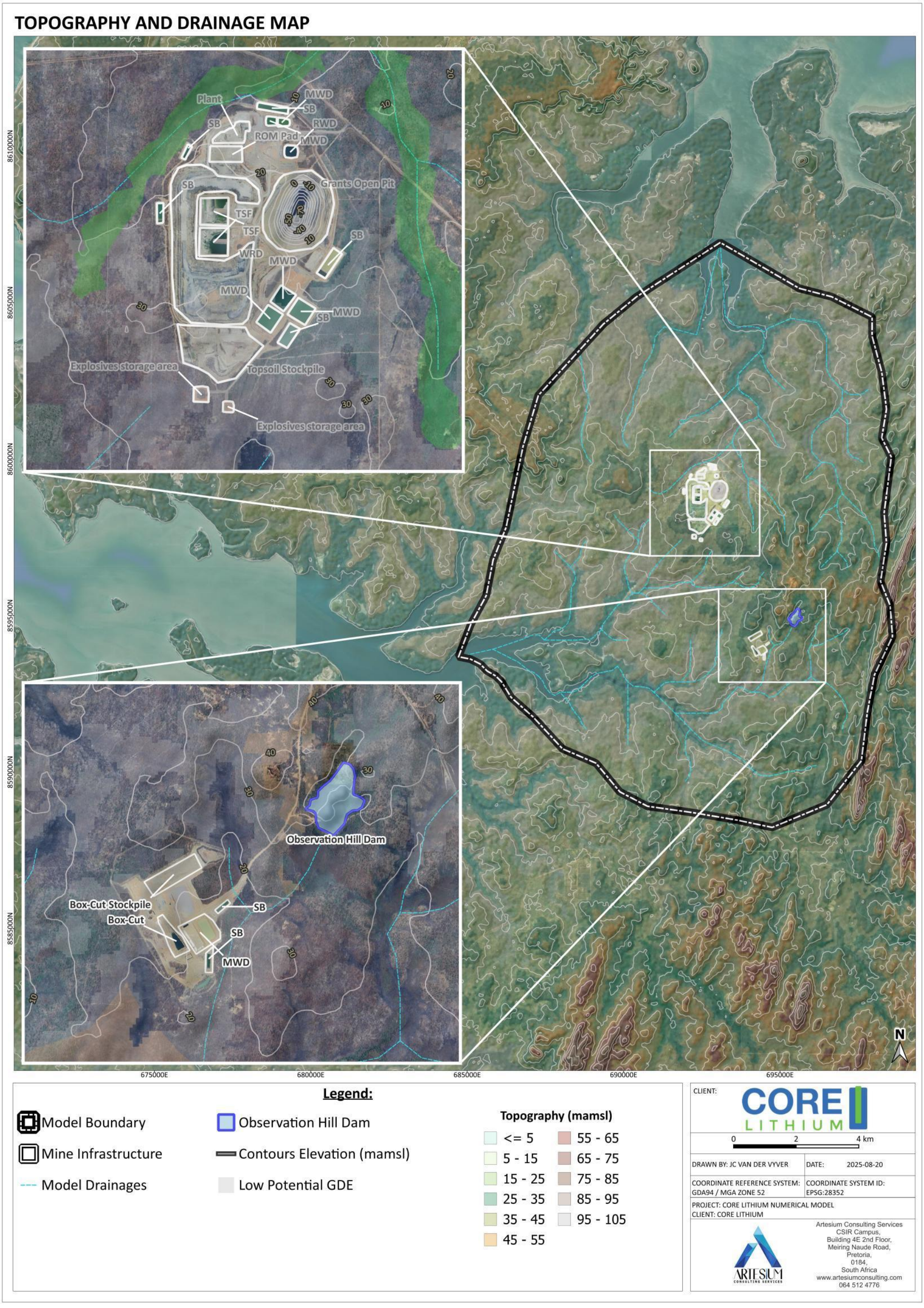

Figure 2-5: Regional and Local Topography Map

2.4 Geology

The regional and local geology, derived from the 1:250 000-scale geological map (SD 52-4 Darwin, 1988), is shown in Figure 2-6. The Grants Open Pit (OP) and associated surface infrastructure are underlain by Quaternary deposits (Qcl) of sand, silt, and clay. Along drainage channels and associated floodplains, alluvial deposits (Qa) of sand, silt, and clay are also present, with widths ranging from 100 to 450 m.

The Burrell Creek Formation (Pfb), a unit of the Finniss River Group, underlies much of the model domain. It is composed predominantly of shale, siltstone, and phyllite, with local occurrences of banded lithologies, fine- to very coarse-grained sandstone (quartz arenite and sublitharenite), pebble conglomerate, and minor graphitic phyllite. Outcrops of the Burrell Creek Formation occur to the east and south-east of the model boundary. Regionally, the unit represents one of the major successions of the Finniss River Group within the Palaeoproterozoic Pine Creek Orogen, consisting of thick turbiditic sediments deposited between □2.2 and 1.8 Ga (Ahmad & Hollis, 2013). The formation comprises interbedded slate, phyllite, fine- to medium-grained greywacke, siltstone, and minor conglomerate, displaying graded bedding and sedimentary structures typical of deep-water turbidite systems.

According to CloudGMS (2018), much of the near-surface geology across the study area is overlain by laterite, averaging up to 5 m in thickness. The laterite formed under prolonged tropical weathering during the Palaeoproterozoic, where feldspathic and volcanic-derived sediments of the Finniss River Group supplied abundant aluminosilicate minerals. Intense chemical leaching stripped mobile cations such as sodium (Na), calcium (Ca), potassium (K), and magnesium (Mg), leaving behind residual concentrations of iron and aluminium oxides. This process resulted in ferruginous and aluminous lateritic horizons. The Burrell Creek Formation is interpreted to extend to depths of up to □2 000 m beneath the surface, based on the cross-sections provided in the SD 52-4 Darwin (1988) geological map sheet.

2.5 Hydrogeological Setting

The surface Quaternary deposits (Qcl) of sand, silt, and clay and associated floodplains, alluvial deposits (Qa) of sand, silt, and clay along drainage channels forms the shallow (1-8 m deep) GDEs and upper groundwater zones. These shallow groundwater zones are either disconnected to the intermediate (15-30m) and deeper >50 m) zones or have limited and constrained vertical hydraulic connections.

The stratified rocks of the Burrell Creek Formation (BCF) are considered a minor aquifer in the region (Needham & Stuart-Smith, 1988), with typical borehole yields of ±0.5 L/s reported in both stratified and igneous rocks of the formation. Airlift yields and pumping rates are generally low, typically ranging from 0.5 to 5.0 L/s for water-supply bores. Typical yields are less than 1 L/s, with many bores producing 0.5 L/s or less. A significant proportion of bores drilled into the BCF failed to intersect productive fractures, resulting in very low or “dry” yields. Approximately 10–15% of bores in the BCF report essentially zero yield (Tickell et al., 2023).

The BCF is classified as a fractured-rock aquifer. The limited number of productive water strikes suggests that

significantly high-yielding fractures are uncommon, reflecting the tightly cemented and metamorphosed nature of the formation. Primary porosity is extremely low, and hydraulic testing (Groundwater Enterprises, 2020) has confirmed that permeability is limited in the absence of fracturing. There are 4 main hydraulic zones; (i) the shallow surface soils and alluvial surficial deposits, (ii) shallow saprolite zone, (iii) the weathered-fractured bedrock and the basal (iv) solid-fractured bedrock. The solid-fractured bedrock consists of fractures separated by matrix blocks.

2.5.1 Hydraulic Conductivity

Hydraulic conductivity (K) values in the BCF are typically low, except where enhanced by fracturing. Slug tests and pumping tests conducted in the Darwin region indicate that unfractured or poorly fractured BCF exhibits K-values in the order of 10e-3 to 10e-2 m/d. In contrast, zones intersecting significant fractures yield considerably higher conductivities. For example, tested K values in the BCF range from 0.27 to 2.6 m/d, illustrating the aquifer's dependence on secondary porosity. Permeability is therefore highly heterogeneous and anisotropic, controlled by the presence, orientation, and connectivity of fractures.

2.5.2 Water Strikes

Water strikes in the BCF are typically encountered at the base of the weathered zone or within deeper fracture zones. Drillers often report the first strike at the transition from saprolite (weathered rock) to fresh fractured rock, commonly 10 – 30 m below ground surface in the Darwin region, depending on the depth of weathering (Groundwater Enterprises, 2020). Deeper inflows correspond to specific fractures or quartz veins. At BP33 (Finniss Lithium Project, ±50 km south of Darwin), negligible water was encountered in the upper 50 m of weathered BCF; however, discrete quartz veins and fracture zones at depths of 50 – 70 m yielded significant inflows of ±2–3 L/s.

2.5.3 Storage and Porosity

Published values for porosity and storage in the BCF are limited. Specific yield (Sy) for fractured rock aquifers is generally very low, as storage is primarily fracture-controlled. The BCF behaves as a low-storage aquifer, with water released mainly from fractures during pumping. For this study, analogue values were adopted from literature values found for similar hydrogeological environments.

2.5.4 Groundwater Quality

Groundwater in the BCF is generally fresh due to high regional rainfall and significant recharge in the shallow saprolite zone. Total dissolved solids (TDS) are typically low, with electrical conductivity (EC) values ranging from 50 to 310 µS/cm, corresponding to TDS concentrations well below 200 mg/L. Groundwater salinity tends to decrease in floodplains and low-lying areas (Groundwater Enterprises, 2020). This pattern reflects strong annual flushing during the wet season and limited residence time for salt accumulation.

Water chemistry ranges from slightly acidic, to more acidic (pH values of below 6.0). This is due to the presence of sulphide minerals such as pyrite and arsenopyrite in the anaerobic (deeper) zones. Oxidation of

these minerals in the subsurface produces acid and mobilises metals. Regional studies around Darwin have reported naturally elevated concentrations of dissolved metals in BCF groundwater, including aluminium (Al), iron (Fe), manganese (Mn), zinc (Zn), lead (Pb), cadmium (Cd), and arsenic (As) (Greencap, 2018).

2.5.5 Recharge

Regional recharge to the BCF has been estimated using chloride mass balance and other methods. Annual diffuse recharge in the Darwin area is approximately 150 – 420 mm/a, equivalent to 9.8–27.3% of mean annual precipitation (Lee et al., 2024) in very shallow groundwater zones with much lower recharge rates of 1.5% in intermediate and deeper groundwater zones. Most of the recharge circulates in the shallow groundwater zones from where it discharges to the alluvial and surface drainage zones, including ephemeral creek lines.

2.5.6 Comparative Aquifers

Within the modelled area, medium-yielding aquifers (0.5 – 5 L/s) are associated with fractured and weathered non-carbonate rocks, with yields up to 10 L/s along major geological structures. Several mapped lineaments (Figure 2-6) may represent regionally significant faults, shear zones, or fracture corridors that controlled basin development, deformation of the Finniss River Group, and subsequent mineralisation (Needham & Stuart-Smith, 1988).

Dewatering rates, based on expected borehole yields from the regional aquifer in the vicinity of the project area, provide a range of dewatering rates that would be expected in the simulated numerical groundwater model. From a literature review perspective, dewatering rates in the Burrel Creek Formation are likely to range from approximately 0.5 to 5 L/s.

GEOLOGY MAP

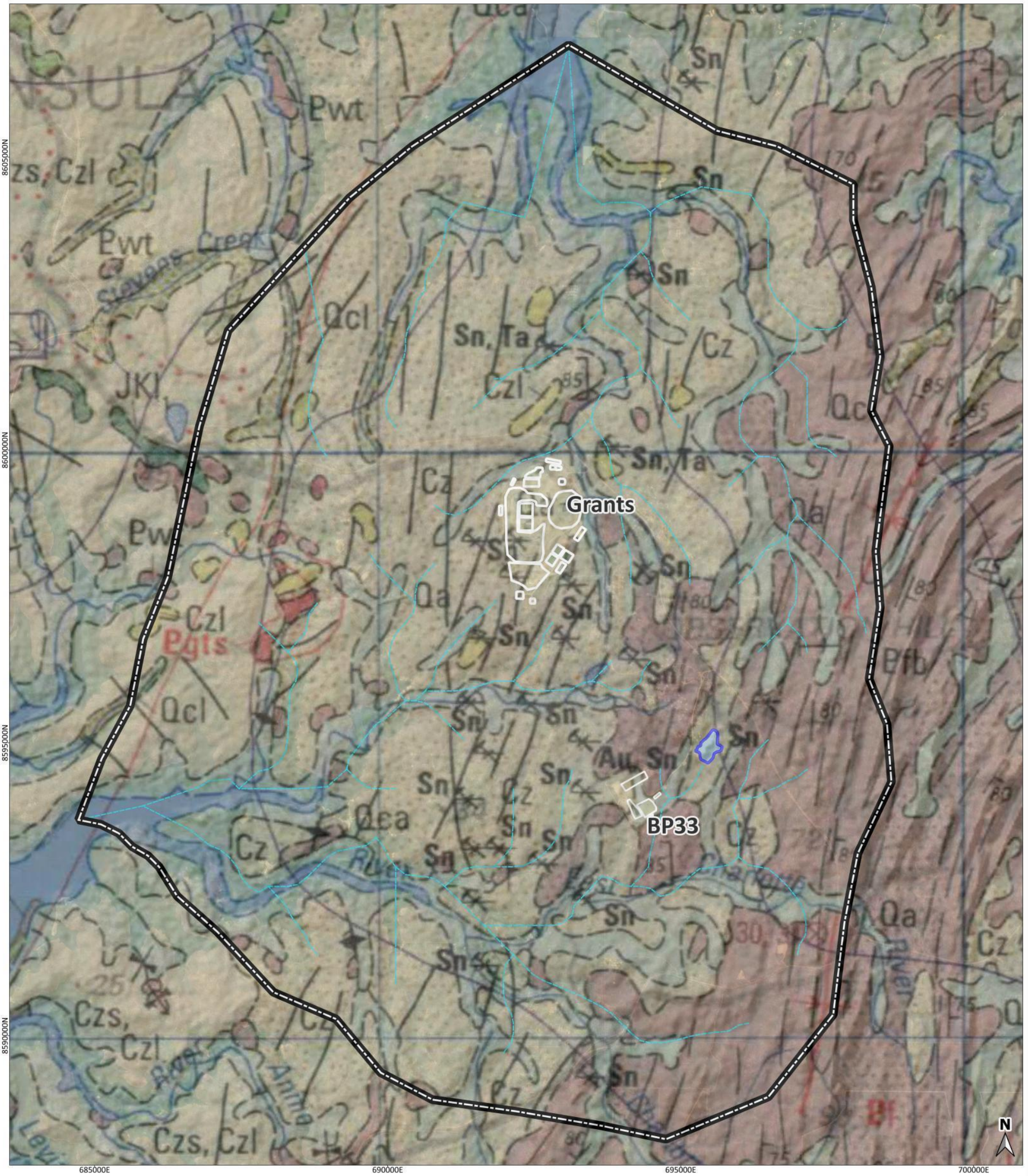

Figure 2-6: Regional and Local Geology Map

3 METHODOLOGY

The study approach included a review of historical reports to provide project background and incorporate data from previous studies used to characterise the underlying aquifers. Key datasets, including long-term monitoring data on water levels and dewatering rates, hydrochemistry and aquifer hydraulic parameters, were analysed. This informed the conceptual model and understanding of the groundwater behaviour.

Schedules for existing and planned future mine infrastructure were provided by the client and incorporated into the hydrogeological conceptual model. This conceptual framework then formed the basis for the numerical model simulations, which were undertaken to quantify the potential impacts of mine dewatering on the local groundwater environment.

3.1 Historical Reports Reviewed

The following 8 existing historical consultants' reports were available for the study area and were used to provide background for the numerical groundwater modelling:

1. Core Exploration Finniss Lithium Project Groundwater Investigation Report (GHD Report No.: 43/22625/02, dated July 2017). Referenced as GHD (2017).
2. Development of a Groundwater Model for the Grants Lithium Project (CloudGMS Report No.: V1.0 dated 20/09/2018). Referenced as CloudGMS (2018).
3. Grants Lithium Project Groundwater Model Addendum Report (CloudGMS Report No.: 1.3, dated 2019). Referenced as CloudGMS (2019).
4. BP33 Groundwater Investigation Report (Groundwater Enterprises Report dated November 2020).
5. BP33 Pumping Test Report (Groundwater Enterprises Report No dated September 2021). Referenced as Groundwater Enterprises (2021).
6. Finnis Lithium Project BP33 Groundwater Modelling Report (Report No.: 3.0, dated October 2021). Referenced as CloudGMS (2021).
7. BP33 Dewatering Assessment (Technical Memorandum, dated September 2023). Referenced as CloudGMS (2023).
8. Grants Lithium, Operational Water Management Plan (Report No.: 1727-17-C4, dated May 2024). Referenced as WRM (2024).

3.2 Previous Hydrogeological Studies Conducted

3.2.1 2017 Studies

A field investigation was conducted by GHD (2017) during which various aquifer tests were conducted on newly installed bores and groundwater hydrochemical sampling and analyses were conducted. The findings of the investigation were that the groundwater quality at Grants was mainly considered good (fresh water) with a number of metals present in the water. The hydraulic conductivity calculated from the tests ranged from 4.8e-03 to 1.7 m/d. The highest recorded blow yield (2 L/s) was obtained from deep (160 m) bore GWB01 located within the pit perimeter close to the deepest part of the Grants OP. The other airlift yields ranged from 0.005 – 1.0 L/s.

3.2.2 2018 Studies

A numerical groundwater model was developed by CloudGMS using FEFLOW to simulate potential groundwater impacts associated with the proposed Grants Lithium Project open cut mine (MLA31726). Life-of-mine simulations (25 months) predicted that dewatering would form a drawdown zone extending approximately 1 km from the Grants OP with no impacts expected beneath ephemeral drainage lines or beyond the mining lease. Groundwater inflows to the pit were forecast to peak at 2 000 m^3/d (23 L/s) during the wet season, stabilising at around 1 600 m^3/d (18.5 L/s). It should be noted that the Grants OP final depth extended to -150 mamsl in this model (CloudGMS, 2018).

Post-closure modelling indicated the pit would develop into a groundwater sink, filling over 50 years and stabilising at 12 – 13 mamsl (7 – 8 mbgl). Groundwater gradients would direct inflows to the pit lake, with a predicted water table decline of 5 m at the pit centre and 0.5 m at 500 m from the lake, with effects confined to the mine footprint and no changes anticipated at ephemeral streams or beyond the lease. Mass balance calculations suggested that 70 years post-closure, pit lake water quality would stabilise with an Electrical Conductivity (EC) of 50 – 300 µS/cm, dependent on groundwater inflow, though analogue sites with EC values of 19 – 26 µS/cm suggest final water quality will be at the lower end of the range (CloudGMS, 2018).

3.2.3 2019 Studies

The updated GL2 groundwater model for the Grants Lithium Project incorporated revised pit geometry and depth. The pit had a larger footprint and extended to a final depth of -190 mamsl. The mine schedule also had an extended Life of Mine (LoM) of 29 months. Re-run scenarios showed only marginal changes from the original model. During mining, the drawdown zone expanded slightly, with the 0.1 m contour crossing the western lease boundary and intersecting an ephemeral drainage line, while post-closure recovery resulted in minor additional drawdown extending southwest beyond the lease but not beneath drainage lines (CloudGMS, 2019).

Predicted pit inflows increased (peak 2 666 m^3/d) due to the larger pit, while post-mining pit lake salinity balances remained essentially unchanged (CloudGMS, 2019).

3.2.4 2020 Studies

The BP33 Groundwater Investigation Report (2020) established baseline hydrogeological conditions at the BP33 lithium deposit. Thirteen bores were drilled to characterise the Burrell Creek Formation (BCF) aquifer and adjacent alluvial sediments. Results showed the BCF is a low-yield, fractured rock aquifer with higher yields (up to 3 L/s) where discrete fractures or quartz veins are intersected. Hydraulic conductivity ranged from 0.003 – 0.08 m/day in unfractured zones to 0.27 – 2.6 m/day in fractured zones. Groundwater levels were shallow (3.4 – 7.9 mbgl), with EC ranging from 50 – 310 µS/cm.

3.2.5 2021 Fieldwork Investigations

The BP33 Pumping Test Report (Groundwater Enterprises, 2021) assessed groundwater availability through a 24-hour pumping test at monitoring bore BPG4d and 8-hour tests at bores BPG1, BPG5i, and BPG6. Results confirmed limited but variable yields, strongly influenced by fracture zones. Sustainable pumping rates were low, ranging from 1.8 to 2 L/s.

Analytical modelling suggested the BP33 pit-lake would be hydraulically connected to the surrounding aquifer and could provide supplementary water, with inflows dependent on fracture-controlled permeability. While groundwater can augment supplies, yields are modest and subject to decline with long-term pumping due to aquifer heterogeneity and fouling risks (CloudGMS, 2021).

The reports concluded that groundwater is a limited but manageable resource for mine operations, best utilised alongside surface water from Observation Hill Dam (Groundwater Enterprises, 2021; CloudGMS, 2021).

3.2.6 2021 Model Update

A numerical groundwater model was developed by CloudGMS using FEFLOW to assess the cumulative impacts of the proposed Grants Lithium Project (GLP, open cut) and BP33 (underground to 320 mbgl) mines, operating concurrently for 60 months. Life-of-mine forecasts indicated two separate drawdown zones: □1 km around the GLP pit (confined to the lease, with no impacts on ephemeral drainage lines) and □2 km around BP33, where the 0.1 m drawdown contour extended beyond lease boundaries, intersecting ephemeral drainage lines and areas of moderate groundwater-dependent ecosystem (GDE) potential (CloudGMS, 2021).

Groundwater inflows at BP33 were predicted to peak at 6 000 – 7 000 m^3/d (69 – 80 L/s). Post-closure forecasts suggested groundwater levels at BP33 would recover to pre-mining conditions within □3 years if the box-cut was backfilled with higher storage material, with any GDE impacts likely short-term (±5 years). At GLP, the pit void would form a lake that filled gradually over □50 years, stabilising 7 – 8 m below surface, consistent with earlier modelling (CloudGMS, 2019). The study concluded that cumulative impacts between GLP and BP33 were unlikely to occur, and overall post-mining effects were predicted to be limited and localised.

3.2.7 2023 Model Update

An update of the 2021 numerical model was conducted by CloudGMS (2023) to assess impacts from the proposed mine development at BP33. The update was aimed at reviewing inflow estimates and to assess changes in projected drawdown impacts with the planned extension of the BP33 underground mine depth from previous depth of 375 m to 820 m. The simulated Zone of Influence was approximately 1.97 km x 1.92 km and covered an area of 287 ha. Simulated groundwater inflows into the BP33 decline and stopes peaked at month 24 and stabilised after month 130 at about 3 000 to 4 000 m^3/d. Inflows to the decline and stopes were predicted to be relatively steady to the end of mining. The limitations listed by the author in the previous model update were that the groundwater model had only been roughly calibrated to the measured inflow volumes (assumed to be the Grants OP inflow volumes). The model was not calibrated to the observed groundwater levels, as it was inferred that calibrating towards the measured groundwater levels did not show any obvious effect due to dewatering at Grant's pit. It was assumed that the inflows to Grant's pit were considered representative of the fresh basement rock and the roughly calibrated parameters (K = 0.0025 m/d, and Specific Yield 0.01) were assigned across the model domain's basement rocks (CloudGMS, 2023).

3.3 BP33 Planned Future Mining Infrastructure

The planned future underground expansion schedule for BP33 is shown in Figure 3-3. The total life of mine (LoM) for the underground operation is projected at 133 months. The decline extends from the -5 mamsl, which is therefore considered the decant point for the underground workings. The deepest planned stopes will reach a depth of approximately -787 mamsl. Paste backfilling is included in the BP33 mine plan. According to the current schedule, backfilling will be initiated from month 18, with the final stope scheduled for backfilling in month 136 from the start of mining. The total cumulative mine void volume is 3 964 657 m^3, of which approximately 82% (3 279 706 m^3) will be backfilled. The distribution of void and backfill volumes with elevation is presented graphically in Figure 3-1.

In the numerical model simulations, it was assumed that no dewatering would be required once the backfilled voids were completed. The backfilled UG workings were assigned in the model according to the XYZ data provided by the client. The stopes not backfilled were dewatered up to LoM. It was assumed that the decline walls would not be sealed off, i.e. continuous dewatering would be required during the operational phase of the project. At LoM, the decline will be plugged with backfill paste material to limit the flow from the rewatered UG workings into the Box Cut.

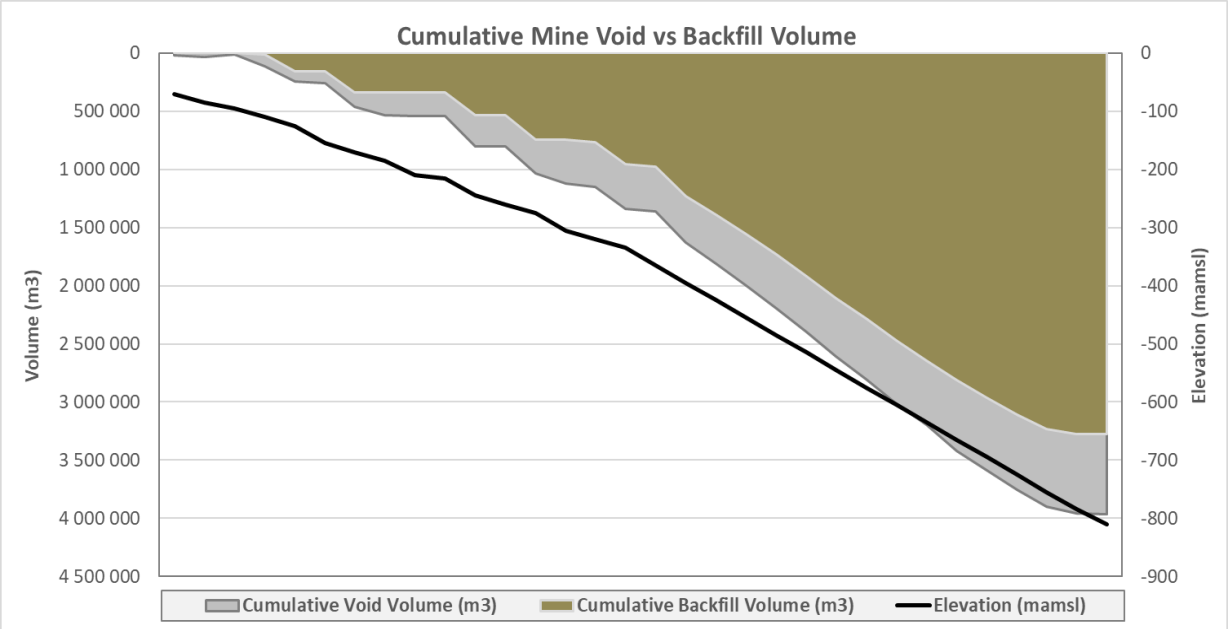

Figure 3-1: BP33 Stope Void Volume vs Backfilled Material Volume Relationship

The box cut was developed from August 2023 to December 2023 and is currently approximately ±35 m deep. The Box Cut decant point is located at the south-eastern corner of the surface perimeter, at an elevation of approximately 20 mamsl. At this elevation, the pit lake volume would be ±327 568 m^3. In the model simulations, it was assumed that the Box Cut would need to be fully dewatered prior to decline development.

The Box Cut will be backfilled to surface post-mining. The backfilled box cut will be backfilled with inert waste rock. Multiple sub-horizontal drains are located within the box cut (refer to Figure 3-2), that can be utilised both during the operational and post-operational phases. During the operational phase the drains can be used to drop pore pressures on the box cut walls. The drainage channels are assumed to be lined and sloped to a central sump pump and dewatering from there. The drains are also assumed to aid redirection of sub-surface flow from the backfilled cut into the surrounding host rock by increasing the surface area from which sub-surface discharge can occur.

Figure 3-2: View of BP33 Box Cut facing Nort-West

Derelict open pit workings are located immediately south of the Box Cut, directly overlying the planned future underground stopes. The bathymetry of these flooded workings is unknown. It is recommended that their depth and geometry (where possible) be surveyed and incorporated into future dewatering and re-watering assessments. In the current model simulations, the derelict pit lake was left in a flooded state to evaluate whether significant water ingress would occur from this feature and to assess whether complete dewatering would be required before mining could commence. However, without bathymetric data, reliable estimation of dewatering rates for this feature is not possible.

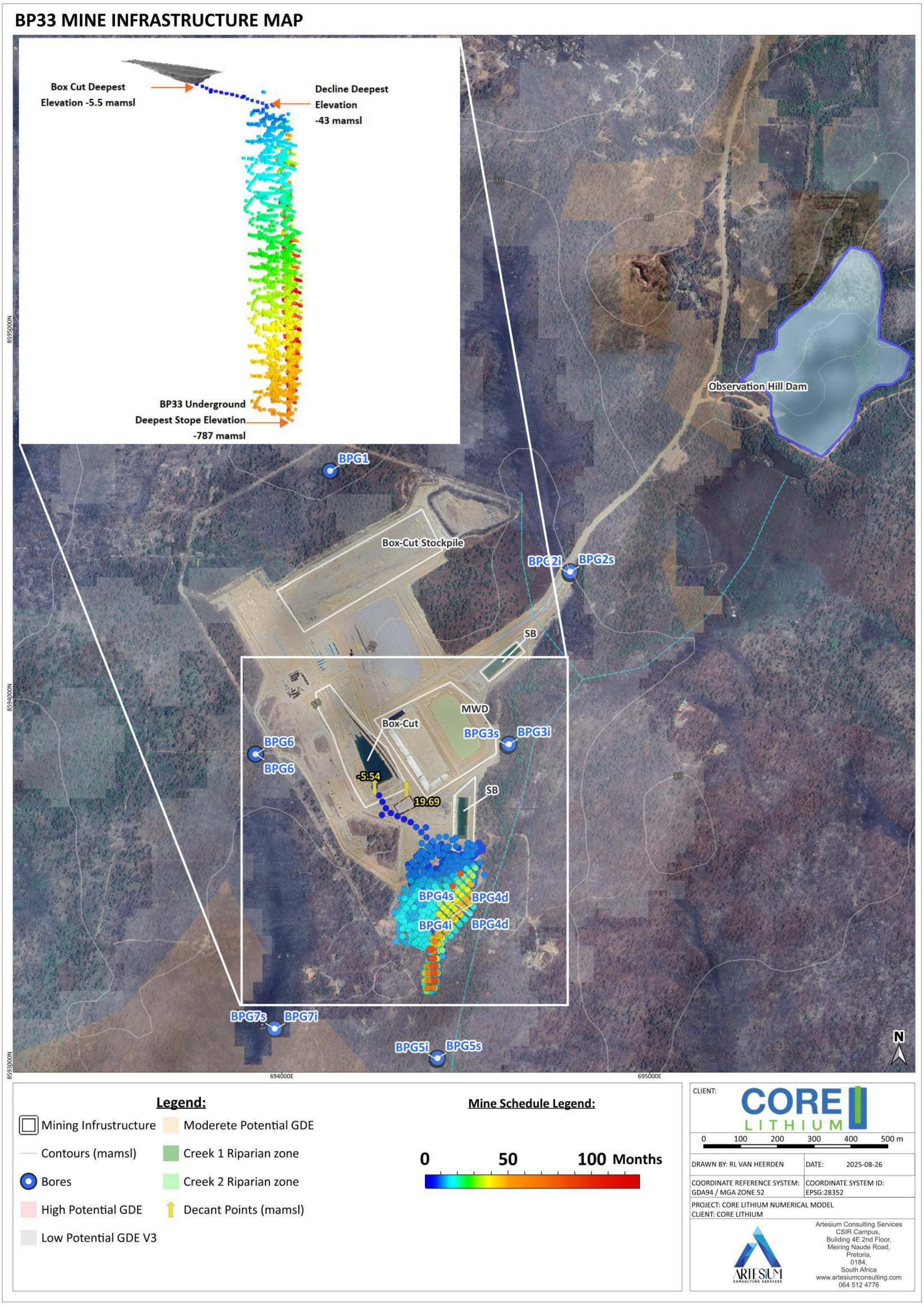

Figure 3-3: BP33 Existing Infrastructure vs Planned Future Underground Infrastructure Map

3.4 Groundwater Levels and Trends

Measured groundwater levels received from the client, and additional data were extracted from historical reports (refer to section 3.2).

3.4.1 Pre-mining baseline water levels

At Grants, the pre-mining baseline groundwater levels were dynamic with fluctuations between wet and dry seasons, with an amplitude of 5.0 m and a range of 10 m. The pre-mining average baseline water level depth was shallow at 3.32 m with a maximum of 12.80 m. The surface elevation vs hydraulic head elevation is shown in Figure 3-4. The first measured values were compared with the last measured values, along with the average from the pre-mining database. The first and average measured water levels showed a good correlation with surface topography (R^2 = 0.94 and 0.97), whereas the last measured level had a lower correlation (R^2 = 0.80). This can be attributed to lower rainfall received prior to mining.

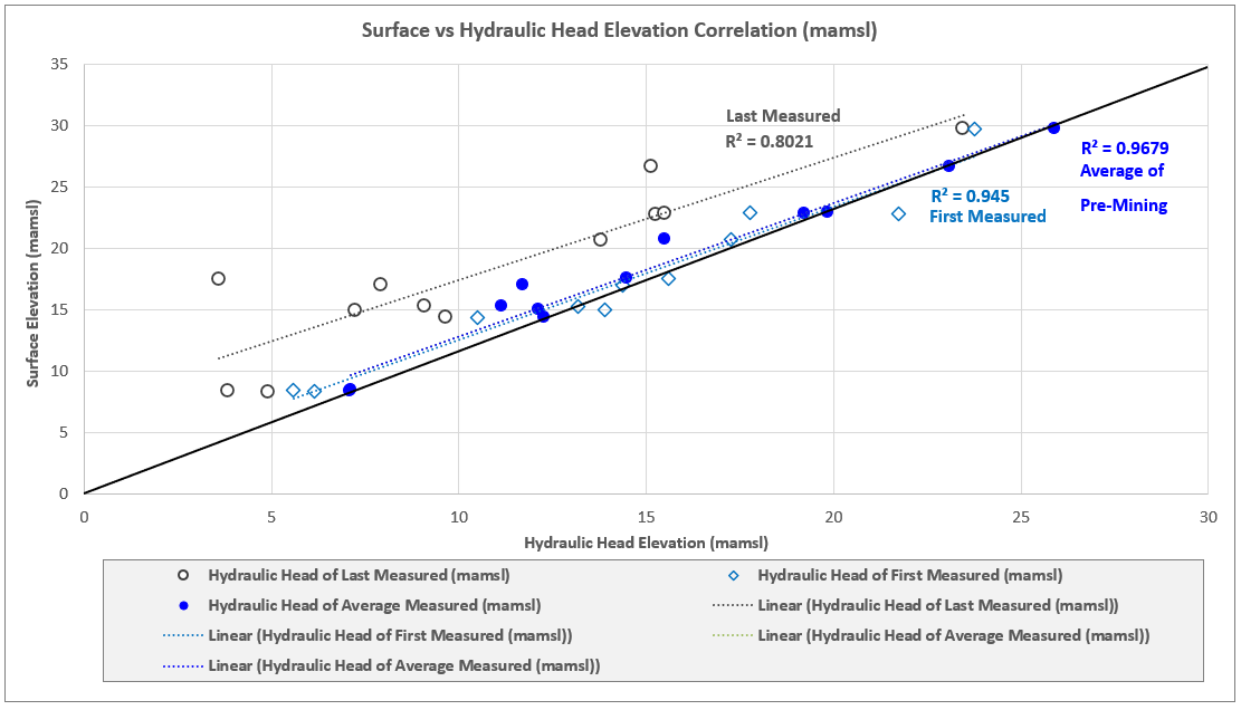

Figure 3-4: Baseline Surface Elevation vs Hydraulic Head Elevation Correlation Water Levels at Grants

In the BP33 area, the pre-mining baseline groundwater levels are comparable to those in Grants. The water levels are dynamic with fluctuations between wet and dry seasons, with an amplitude of 5.7 m and a range of 11.4 m. The pre-mining average baseline water level depth was also shallow at 2.39 m with a maximum of 11.40 m. A strong positive correlation (refer to Figure 3-5) exists between ground surface elevation and hydraulic head elevation across the monitoring network, with R^2 values ranging from 0.77 to 0.98. The weaker first measured correlation can be attributed to the mini-dry cycle experienced in 2020. This correlation plotting above the 1:1 relationship line at both Grants and BP33 indicates that groundwater levels are largely controlled by surface topography, consistent with an unconfined aquifer system where recharge occurs on

elevated terrain and groundwater flow follows local hydraulic gradients toward lower elevation.

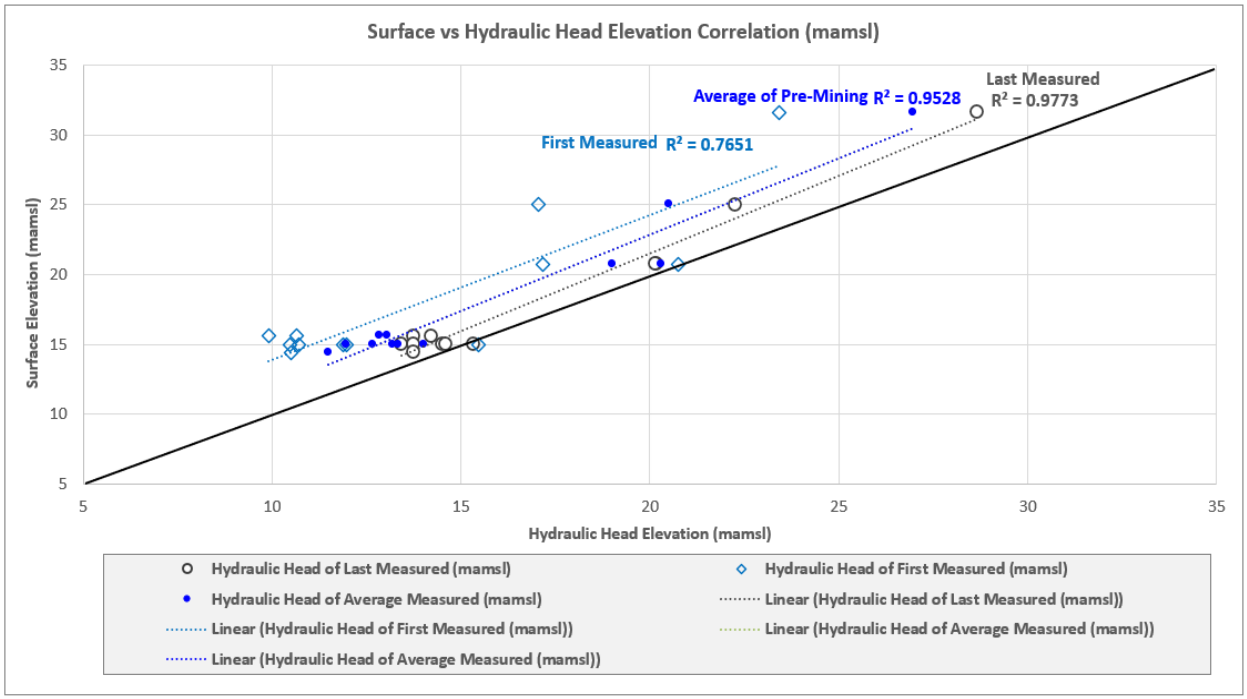

Figure 3-5: Surface Elevation vs Hydraulic Head Elevation Correlation for Pre-mining Water Levels at BP33

The depth to groundwater (DTGW) maps for Grants are shown in Figure 3-6 (shallow groundwater zone) and Figure 3-7 (intermediate and deep aquifer). The groundwater flow direction in the shallow groundwater zone was predominantly towards the south. For the intermediate and deep aquifers, the flow follows the same direction with vectors towards the south-east as well. The hydraulic head plateaus in the south-western portion of the site, beneath the current TSF.

The pre-mining baseline DTGW maps for BP33 are shown in Figure 3-8 and Figure 3-9. The groundwater flow pre-mining in the shallow groundwater zone was mainly southward, with the deepest measured water level at BPG5s (2.7 mbgl). The intermediate and deep aquifer flow vectors were oriented north-west, with the deepest point measured at BPG1 in the north (4.7 mbgl).

Figure 3-6: Grants Pre-Mining Depth to Groundwater (DTGW) Contour Map for Shallow Groundwater Zone

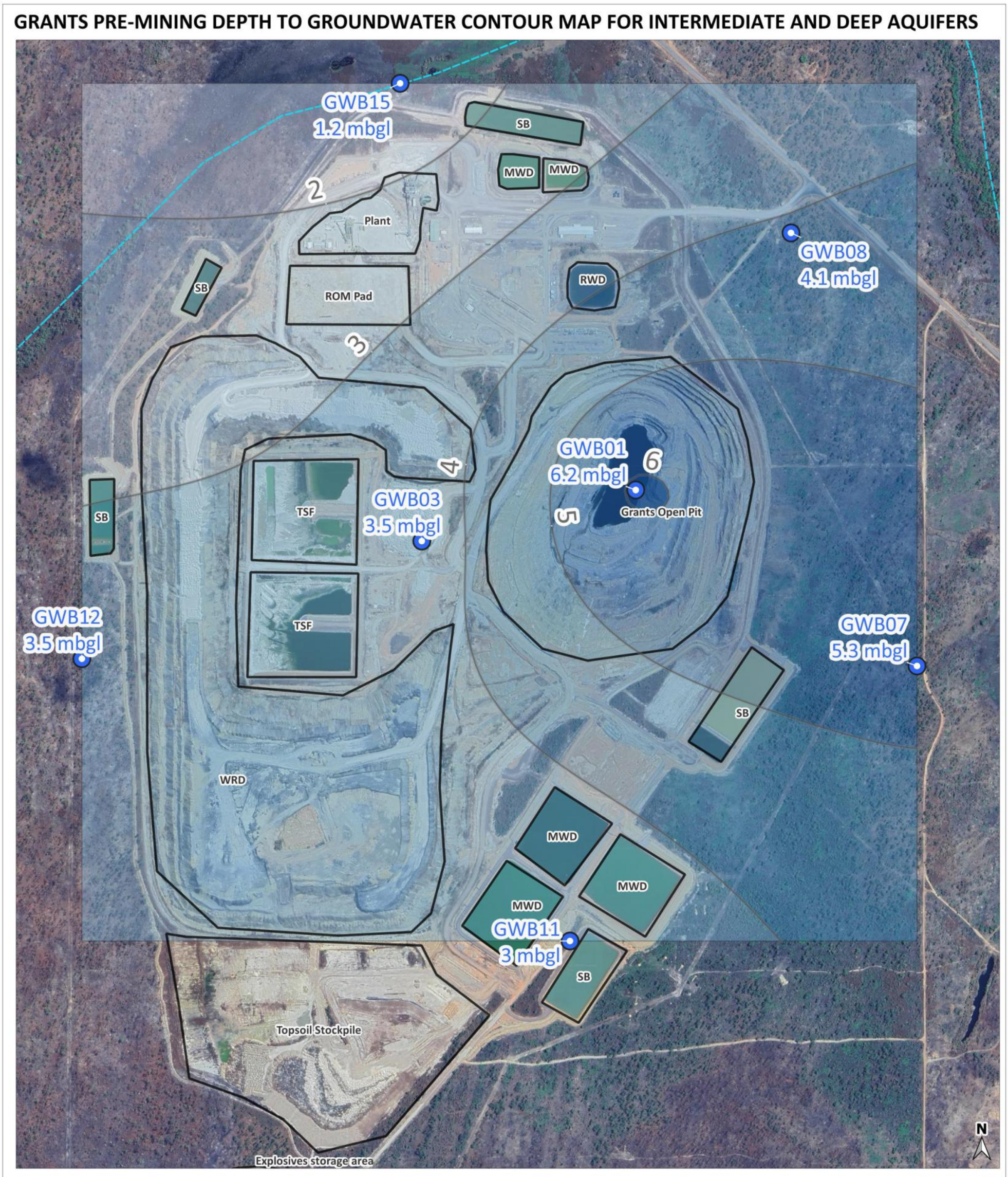

Figure 3-7: Grants Pre-Mining Depth to Groundwater (DTGW) Contour Map for the Intermediate and Deep Aquifers

Figure 3-8: BP33 Pre-Mining Depth to Groundwater (DTGW) Contour Map for Shallow Groundwater Zone

Figure 3-9: BP33 Pre-Mining Depth to Groundwater (DTGW) Contour Map for the Intermediate and Deep Aquifers

3.4.2 Grants Post-Mining Water Levels

The monitoring database for Grants is plotted vs the CRD trend in Figure 3-10 along with the measured water level for the Grants Pit during the operational and post-operational (current) phases. The Grants Pit was mined from approximately January 2022 to November 2024, with the pre-mining (baseline) water levels first measured in June 2017.

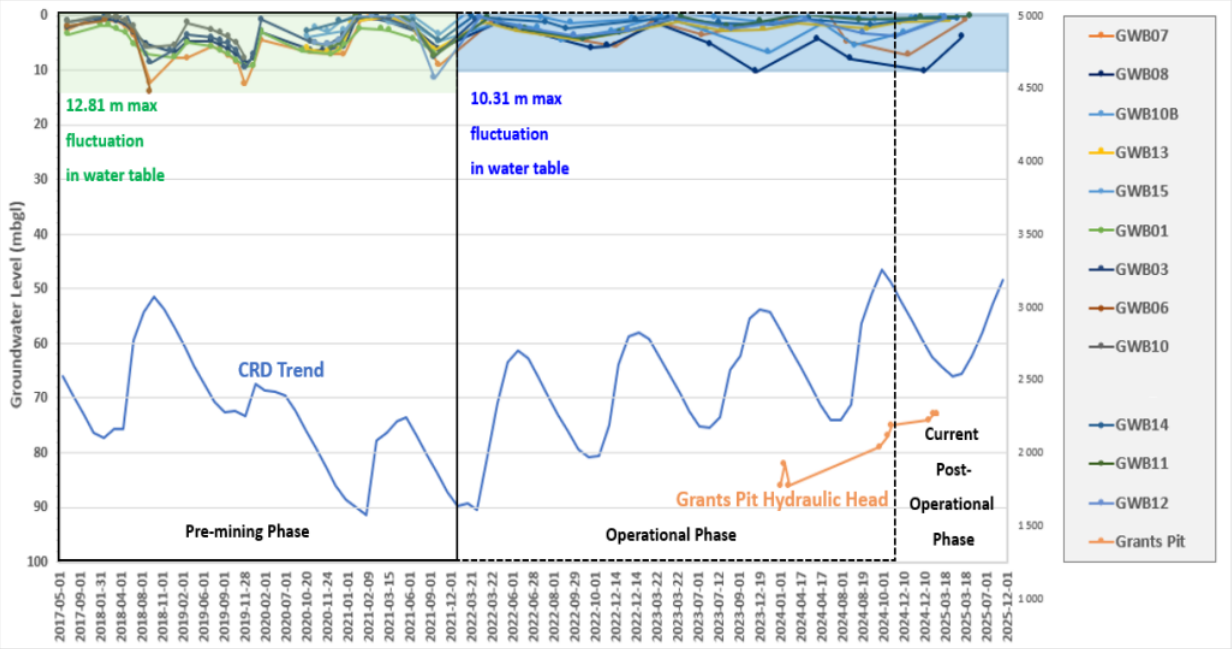

Figure 3-10: Grants Monitoring Bores Groundwater Level Trends

The total change and rate of change in water levels for the monitoring bores surrounding Grants OP are summarised in Table 3-1. The table provides an analysis of the rate of change measured in the bore over the monitoring period, expressed as a change in water level per annum. The monitoring data at Grants is unique because it allows comparison of the rate of change pre-mining (June 2017), during the operational phase (January 2022 – November 2022), and in the recovery or post-closure phase (January 2023 – March 2025), when the mine was in care and maintenance. The monitoring data effectively enable analysis of a bulk aquifer test across the shallow, intermediate (weathered zone), and the top of the deep aquifer (fresh rock).

Table 3-1: Grants Rate of Water Level Change in Bores

Site ID	Years	Pre-mining Change in Water Level (m)	Pre-mining Rate of Change in Water Level (m/a)	Operational Change in Water Level (m)	Operational Rate of Change in Water Level (m/a)	Post-operational (Current) Drawdown (m/a)	Rate of Change (m/a)	Total Change in Water Level (m)	Total Rate of Change in Water Level (m/a)
GWB01	4	-3.48	-0.87					-3.48	-0.82
GWB03	5	-6.50	-1.63	6.77	3.39			0.27	0.06
GWB10B	4	-0.86	-0.22	1.98	0.99	2.33	7.77	3.45	0.78
GWB10	2	-6.65	-1.66					-6.65	-2.75
GWB08	8	-4.10	-1.03	0.99	0.50	1.31	4.37	-1.80	-0.23
GWB07	8	-6.45	-1.61	5.50	2.75	2.85	9.50	1.90	0.25

Site ID	Years	Pre-mining Change in Water Level (m)	Pre-mining Rate of Change in Water Level (m/a)	Operational Change in Water Level (m)	Operational Rate of Change in Water Level (m/a)	Post-operational (Current) Drawdown (m/a)	Rate of Change (m/a)	Total Change in Water Level (m)	Total Rate of Change in Water Level (m/a)
GWB11	4	-2.28	-0.57	5.37	2.69	1.96	6.53	5.05	1.15
GWB15	4	-1.24	-0.31	3.22	1.61	1.02	3.40	3.00	0.68
GWB14	4	-1.74	-0.44	3.26	1.63	0.79	2.63	2.31	0.52
GWB13	4	-0.30	-0.08	3.58	1.79	1.90	6.33	5.18	1.17
GWB12	4	-6.54	-1.64	9.13	4.57	1.94	6.47	4.53	1.03
P95		-6.60	-1.65	1.39	0.69	0.87	2.90	-5.07	-1.78
Average		-3.65	-0.91	4.42	2.21	1.76	5.88	1.25	0.17
P05		-0.58	-0.15	8.19	4.09	2.67	8.89	5.12	1.16

The baseline water levels declined due to the sub-dry cycle from August 2018 to February 2021. The rate of change was -0.91 m/a during the pre-mining phase, compared to the operational phase, where the water levels increased by an average of 2.21 m/a. Water levels in the post-operational phase increased by 5.88 m/a on average.

The change in water level compared to the distance from Grants OP is plotted in Figure 3-11. No bore had water-level changes exceeding the baseline amplitude. The greatest distance from the OP at which groundwater levels decreased was in bore GWB08 (intermediate aquifer), with a 1.8 m drop in water level. Beyond this point, water levels were observed to increase, with no decreases measured in the shallow aquifer. The maximum measured drawdown cone in the intermediate aquifer was observed to be 360 m to 400 m from the pit across the complete monitoring period, and there was no measurable corresponding drawdown in the shallow aquifer from the Grants OP.

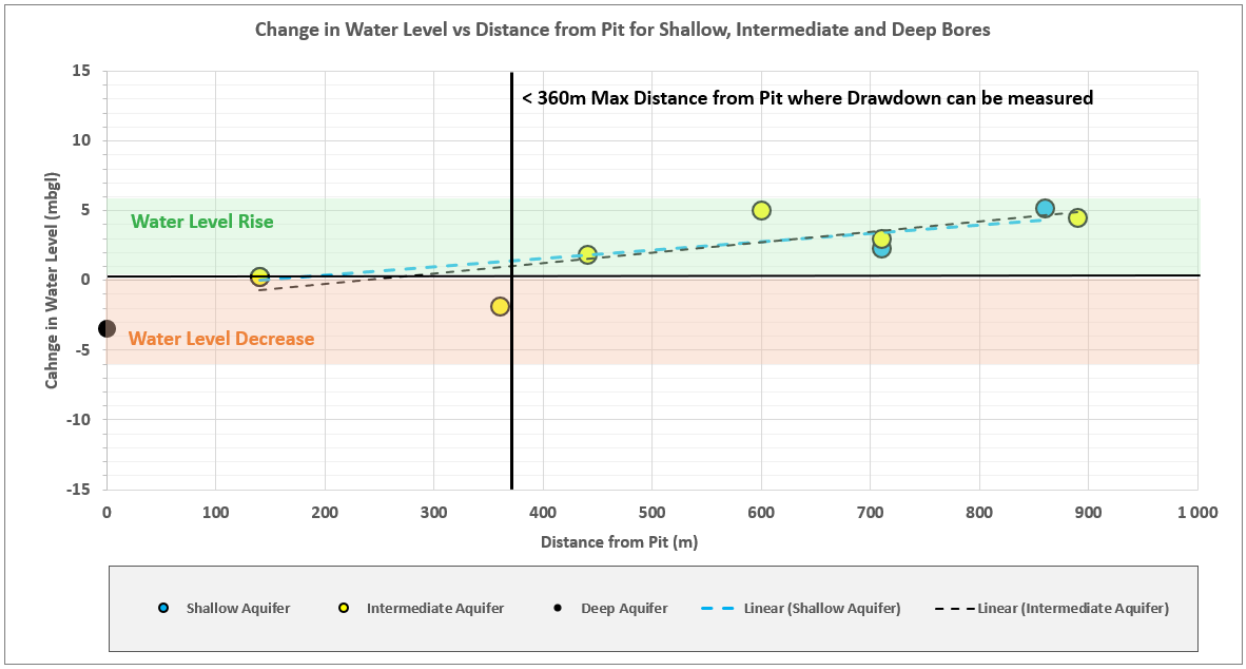

Figure 3-11: Change in Water Levels vs Distance from Grants OP

3.4.3 BP33 Groundwater Level Trend Analysis

The groundwater level monitoring data for BP33 is shown in Figure 3-12. The pre-mining water levels fluctuated between ±8.9 and 11.39 m, and during the operational phase, up to 11.12 m. The BP33 BC was developed between August 2023 and December 2023.

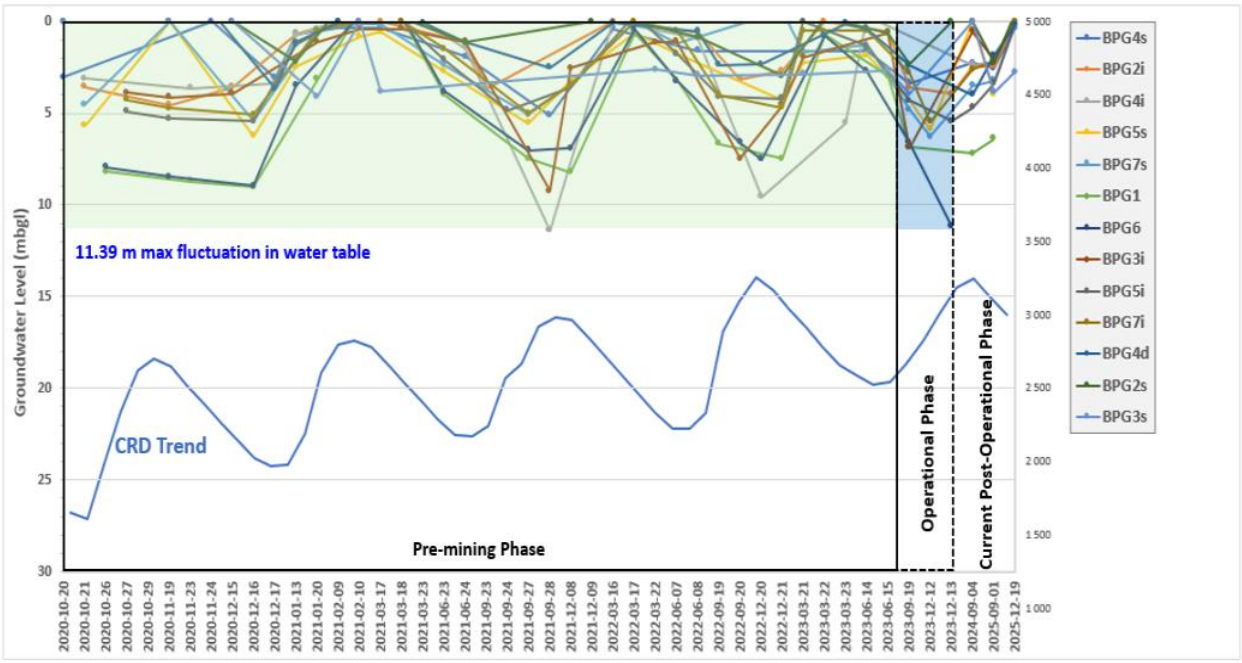

Figure 3-12: BP33 Monitoring Bores Groundwater Level Trends

The change in water levels, together with the rate of change, is summarised in Table 3-2. The average baseline rate of change was measured as an increase of 0.82 m/a over a three-year period. During development, the water levels decreased by a total of 4.39 m, at a rate of 10.55 m/a. It should be noted that the BP33 box cut was developed during the dry months over a period of five months. Therefore, the decline in water levels measured during the dry season is not considered representative of a rate of annual decline.

Table 3-2: Grants Rate of Water Level Change in Bores

Site ID	Years	Pre-mining Change in Water Level (m)	Pre-mining Rate of Change in Water Level (m/a)	Operational Change in Water Level (m)	Operational Rate of Change in Water Level (m/a)	Post-operational (Current) Drawdown (m/a)	Rate of Change (m/a)	Total Drawdown Hydraulic Head 3 – 5 years (m)	Drawdown Rate 2023 – 2025 (m/a)
BPG6	3	5.22	1.74	-8.43	-20.26				
BPG3i	5	3.23	1.08	-6.22	-14.95	7.08	5.49	4.09	0.79
BPG3s	5	-2.66	-0.89						
BPG4s	5	1.45	0.48	-1.77	-4.25	2.98	2.31	2.66	0.51
BPG4i	3	3.43	1.14					3.04	1.15
BPG4d	5	-0.89	-0.30	-1.99	-4.78	2.21	1.71	-0.67	-0.13
BPG1	5	5.24	1.75	-3.89	-9.35	0.45	0.35	1.80	0.37
BPG7s	5	3.26	1.09	-5.03	-12.09	6.05	4.69	4.28	0.83
BPG7i	5	3.78	1.26	-4.97	-11.95	5.47	4.24	4.28	0.83

Site ID	Years	Pre-mining Change in Water Level (m)	Pre-mining Rate of Change in Water Level (m/a)	Operational Change in Water Level (m)	Operational Rate of Change in Water Level (m/a)	Post-operational (Current) Drawdown (m/a)	Rate of Change (m/a)	Total Drawdown Hydraulic Head 3 – 5 years (m)	Drawdown Rate 2023 – 2025 (m/a)
BPG2i	5	3.01	1.00	-3.40	-8.17	3.97	3.07	3.58	0.69
BPG2s	5	-0.60	-0.20						
BPG5s	5	3.83	1.28	-4.07	-9.78	1.90	1.47	1.66	0.34
BPG5i	5	3.57	1.19	-4.11	-9.88	5.32	4.12	4.78	0.93
	P95	-1.60	-0.53	-7.44	-17.87	1.03	0.80	-2.95	-0.74
	Average	2.45	0.82	-4.39	-10.55	3.94	3.05	1.84	0.37
	P05	5.23	1.74	-1.87	-4.49	6.67	5.17	4.48	1.02

The Grants OP is substantially deeper (50–55 m) than the BP33 box cut (BC). Given that dewatering at Grants OP did not produce a measurable regional groundwater response beyond the range of seasonal water-level fluctuations, it is not expected that the BP33 BC will generate a drawdown (response) on the aquifer surrounding BP33, greater than that of the Grants OP.

This assumption is supported by post-operational water levels, which increased to 3.94 m at a rate of 3.05 m/a, exceeding the measured baseline increase rate. The maximum measured deep drawdown at BP33 BC would be 365 m, with no measured drawdown in the shallow or intermediate aquifers.

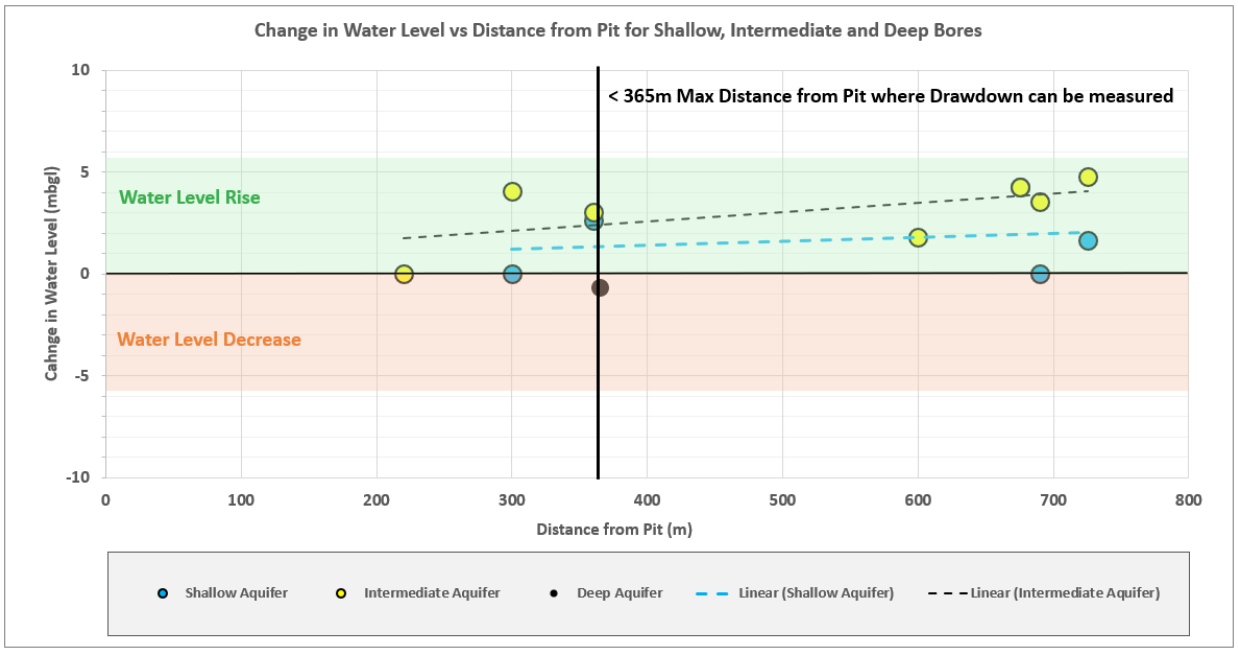

Figure 3-13: Change in Water Levels vs Distance from BP33

Limited vertical hydraulic connectivity is observed at the BP33 nested bores (BPG42, BPG4i, and BGP4d). The bores are situated ±10 m apart and provide a good indication of the limited vertical connectivity between the shallow, intermediate and deep aquifers.

A clear vertical differentiation in groundwater response to climatic variability, as represented by the CRD

cycle, is evident in long-term borehole water levels. The shallow bore (BPG4s) exhibits the strongest and most immediate response to CRD fluctuations, with groundwater levels rising during wetter-than-average periods and declining during drier periods. This suggests that the shallow aquifer is directly influenced by rainfall recharge, likely occurring through infiltration into the weathered zone. The relatively rapid response implies a short lag time between rainfall events and groundwater level changes, indicating good hydraulic connectivity between the surface and the shallow groundwater system.

The intermediate bore (BPG4i) exhibits a more subdued, slightly delayed response than the shallow bore. While some fluctuations correspond to CRD trends, the magnitude of change is smaller, and several water-level variations appear independent of short-term rainfall signals. This behaviour suggests that the intermediate zone acts as a transitional unit between the shallow weathered aquifer and the deeper fractured bedrock system. Recharge to this zone is therefore likely to occur through vertical leakage from the shallow aquifer and through fracture-controlled pathways, resulting in a dampened and delayed groundwater response relative to surface recharge events.

In contrast, groundwater levels in the deep bore (BPG4d) remained relatively stable throughout the monitoring period, with only minor fluctuations. The deep system shows limited correlation with short-term CRD variability, suggesting that it is largely buffered from seasonal climatic effects. This indicates that the deep bore intersects a fractured bedrock aquifer characterised by greater storage capacity and slower recharge, in which groundwater levels are influenced more by long-term regional groundwater flow than by direct rainfall infiltration.

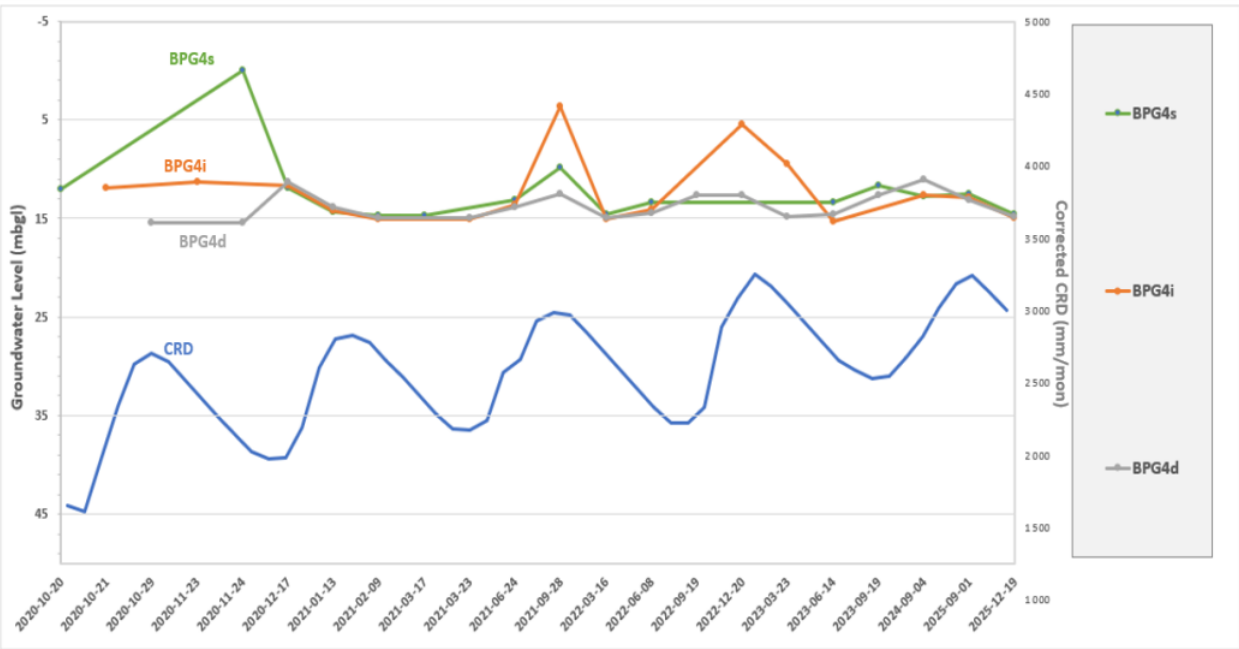

Figure 3-14: Nested Bores (BPG4s, BPG4i, and BPG4d) Measured Groundwater Levels

Collectively, the nested borehole data suggests a decreasing hydraulic sensitivity to climatic recharge with increasing depth. Strong hydraulic connectivity exists between rainfall recharge and the shallow aquifer, moderate connectivity is inferred between the shallow and intermediate zones, and relatively weak connectivity is evident between the intermediate and deeper aquifer units. This pattern is consistent with groundwater systems developed in weathered and fractured bedrock environments, where recharge enters the shallow weathered zone and progressively propagates downward through fracture networks, becoming increasingly attenuated with depth.

3.4.4 Summary

Long-term monitoring (June 2017 to March 2025) of water levels at Grants Open Pit showed the following:

- Pre-mining baseline groundwater levels were dynamic with an amplitude of 5.0 m and a range of 10 m between wet and dry seasons.
- The pre-mining average baseline water level depth was shallow at 3.32 m, with a maximum depth reached during the dry season of 12.80 m.
- Monitoring data spanning ±8 years (2017 - 2025) testifies that the maximum measurable drawdown at Grants OP was between 360 – 400 m from the pit. No measurable drawdown beyond seasonal fluctuations in groundwater levels was observed during the operational phase. It can be concluded that the Grants fissure water inflow rate, ranging from 600 – 750 m^3/d, caused a limited zone of influence of <400 m in the intermediate aquifer with no observed impact in the shallow groundwater zone due to operations.
- Due to the wet cycle, the average water level change since mining started shows a rise of 4.42 m and a rate of change of 2.21 m/a. The rate of water level rise in the last year was 2.67 m/a with no evidence of drawdown effect from the pit.
- Intermediate/deep bore GWB08 (60 m deep) had a measured decline of 1.8 m across the whole monitoring period. The pre-mining water level fluctuations driven by wet and dry seasons averaged ±5.0 m up and down, with a maximum range of 12 m drop in water level in the pre-mining baseline conditions.
- At Grants, where the Open Pit is 94 m deep and acts as a sink, water levels have stabilised in recent years towards a quasi-steady state.

The BP33 Box Cut Area pre- and post-construction long-term monitoring showed the following:

- Pre-construction baseline groundwater levels are comparable with those at Grants and are dynamic with fluctuations between wet and dry seasons of 5.7 m and a range of 11.4 m.
- The pre-construction average baseline water level depth was shallow at 2.39 m with a maximum of 11.40 m.
- Monitoring data spanning 3 - 5 years (2020 - 2025) around the box cut showed no measurable

drawdown that exceeded seasonal variability observed in baseline conditions. Fissure water inflow rates into the BP33 Box Cut of 340 m^3/d had a limited influence of <365 m in the deep aquifer with no measurable effect in the shallow groundwater zone. Water flowing into the box cut from groundwater creates a sink and removes water from the aquifer.

- Due to the development phase of the Box Cut falling in a dry season, the average water level change since construction started in August 2023 showed a decline to 4.39 m below ground level from 2.45 m and a rate of decrease of 10.55 m/a. The development phase of BP33 lasted 5 months throughout the dry season, which is thought to have exacerbated the annual average rate of change estimated from the five months of monitoring, and was a notable difference compared to the past year (2025), which saw an increase in water level of 2.95 m.

The monitoring data at both sites demonstrates hydraulic semi-disconnection between shallow, intermediate, and deep aquifers, although there is no defined confining layer. The hydraulic semi-disconnected behaviour is supported by head differences of 0.25 - 5.66 m at Grants Pit and in nested bores at BP33. The vertical head differences range from 0.25 m to 15.40 m, further supporting the limited vertical connectivity between the groundwater zones and/or aquifers.

3.5 Ternary Diagram for Shallow vs Intermediate/Deep Aquifer:

The differentiation between the shallow and deep aquifers is of particular interest in this investigation. The limited vertical hydraulic connectivity between shallow and deep groundwater zones, as detailed in Section 3.4 means that the impact of mining occurring in the intermediate and deeper groundwater zones would not necessarily translate directly to impacts in the shallow groundwater zone, which supports groundwater-dependent ecosystems (GDEs; riparian vegetation).

The ternary diagram (refer Figure 3-15) further illustrates the limited vertical hydraulic connectivity by plotting the calcium (Ca), magnesium (Mg), and sodium (Na) relationship between analytes. The shallow (GWB10B), intermediate (GWB08), and deep (GWB07) groundwater analyte concentration relationship measured in bore samples was cross-referenced with a sample from the Grants OP (refer Figure 3-18 for location of monitoring bores).

A clear distinction in the chemical profiles of water samples collected from the shallow and intermediate aquifers is observed. The intermediate water quality chemistry plots closer to the deep aquifer and the open pit. The pit lake chemistry signature closely resembles the concentrations measured in the deep aquifer, but not in the intermediate aquifer.

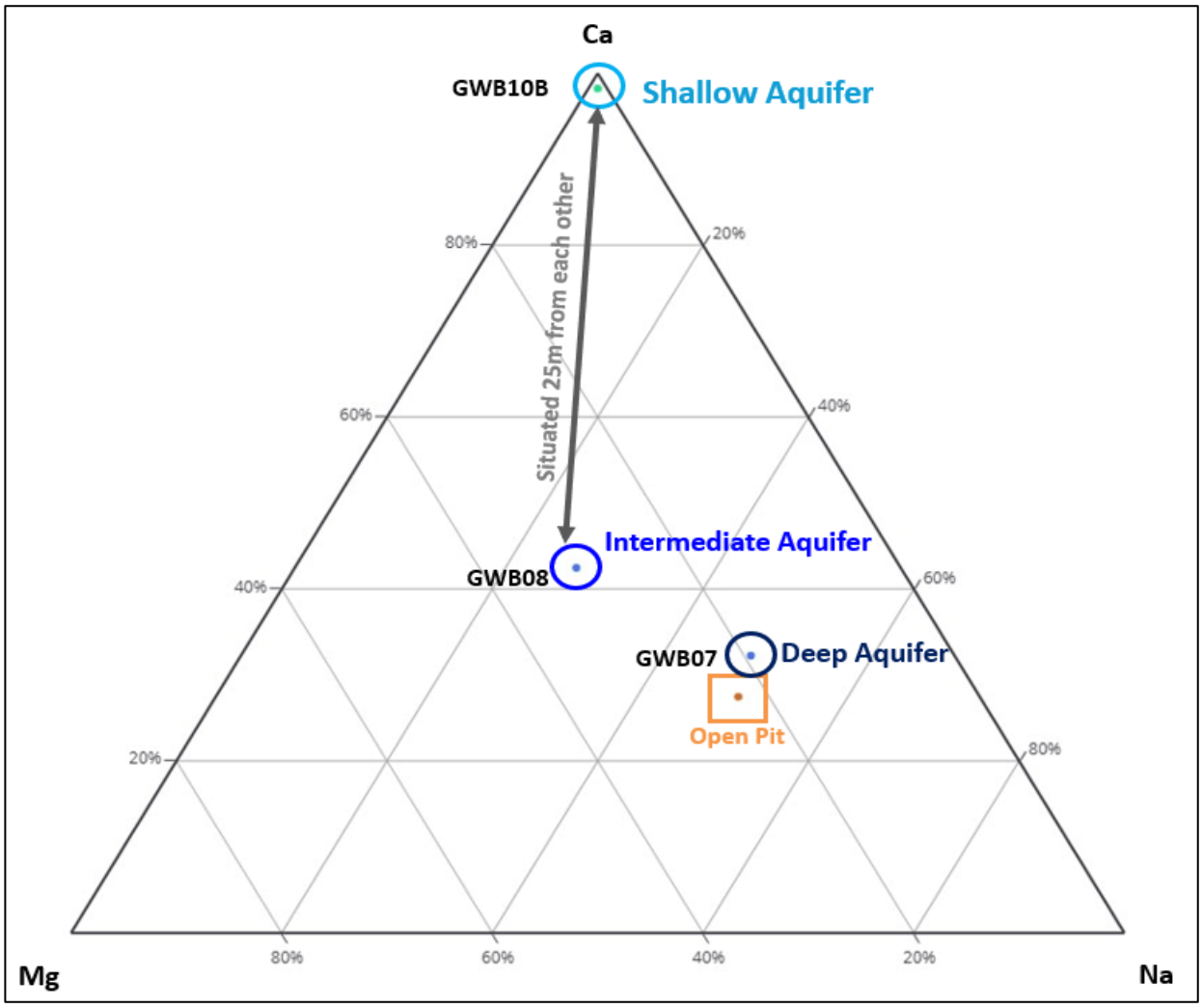

Figure 3-15: Ternary Diagram of the Relationship between Ca, Mg, and Na

3.6 Aquifer Characterisation and Hydraulic Testing

Aquifer test data available within the model boundary, derived from historical reports and the provided monitoring data, are summarised in Table 3-3 and illustrated in Figure 3-21. The hydraulic testing comprised slug tests, blow airlift recovery tests, and pumping tests. Data collected during these tests were used to calculate hydraulic conductivity (K, expressed in m/d), which is a key parameter in numerical groundwater modelling.

The summarised test data were superimposed on the K-values applied in the previous CloudGMS model and the current transiently calibrated model, plotted against depth (refer Figure 3-19). The maximum depth of the Grants Open Pit (dotted black line) is included as a reference to contextualise the depths at which aquifer tests were conducted. For each test, the maximum depth of the tested section was used to reference the test section elevation on the graph.

The current model is calibrated to lower K-values compared with the previous model, but both sets of values remain within the ranges indicated by the field tests. Importantly, the K-values for both models plot close to

the harmonic mean of the test results. This is significant, as upscaling to the harmonic mean provides a more representative K for regional aquifer behaviour when applied in numerical modelling (Steyl, 2011).

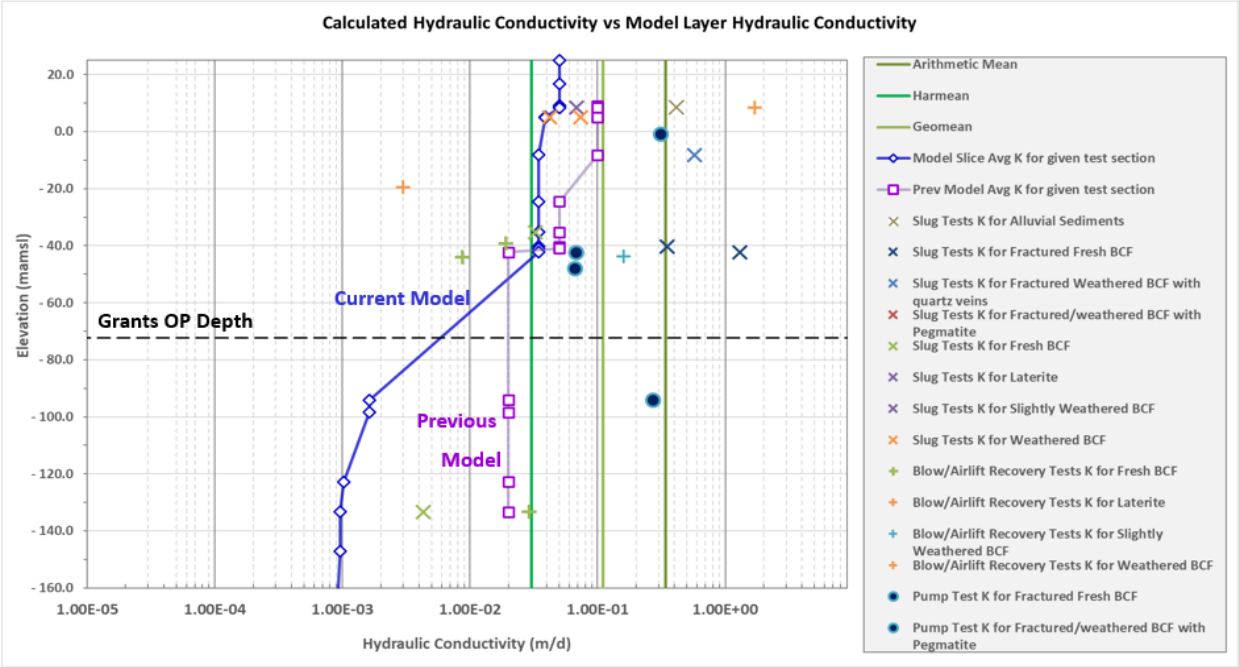

Figure 3-16: Calculated Hydraulic Conductivity vs Model Layer Hydraulic Conductivity Values

Upscaling heterogeneous aquifer parameters requires selecting an effective hydraulic conductivity (K) that preserves the aquifer's bulk flow behaviour. A common issue in this process is well-field bias, which arises when representative K-values are derived from borehole or pumping-test data. Since monitoring and production bores are often sited on preferential flow pathways, these tests may preferentially reflect higher-yielding zones with elevated K-values. The aquifer tests measure the horizontal component of hydraulic conductivity (Kxy). The vertical component (Kz) can be evaluated during model calibration and is lower than the horizontal component by at least an order of magnitude.

Groundwater flow occurs through a combination of high- and low-conductivity zones, reflecting both fracture flow and matrix flow. The harmonic mean of K-values provides a conservative estimate, as it places greater weight on lower conductivities. This makes it particularly appropriate for upscaling regional aquifers in numerical groundwater modelling. For layered aquifers, the effective conductivity perpendicular to the bedding is given by the harmonic mean of the individual layer conductivities (Prudic, 1991). Using a higher average, such as the arithmetic mean, would overestimate transmissivity (that is, a product of the aquifer thickness and hydraulic conductivity) and the aquifer's ability to transmit water. Calibrating a numerical model to the harmonic mean of measured K-values, therefore, ensures that the model reflects the realistic, lower bulk conductivity expected in a heterogeneous system.

Aquifer test data in the project area extends to a maximum elevation of -133 mamsl, or 154 mbgl (GWB01). As illustrated in Figure 3-17, the planned future mine workings extend deeper, reaching elevations of

-787 mamsl at BP33. Extrapolating the tested/calibrated K-values to these depths without adjustment would likely overestimate inflows. Scaling K-values downward with depth provides a more realistic representation of in-situ permeability, as increasing lithostatic stress with depth tends to close fissures and fractures, reducing both permeability and storage. The extrapolation needs to be verified with measured data up to the depth of the planned underground workings at BP333. Packer or Lugeon tests are recommended. The exception is sub-vertical fractures and faults, which may remain open to greater depths and locally enhance flow in discrete zones. The model layers incorporating depth-scaled K-values are shown in Figure 3-17.

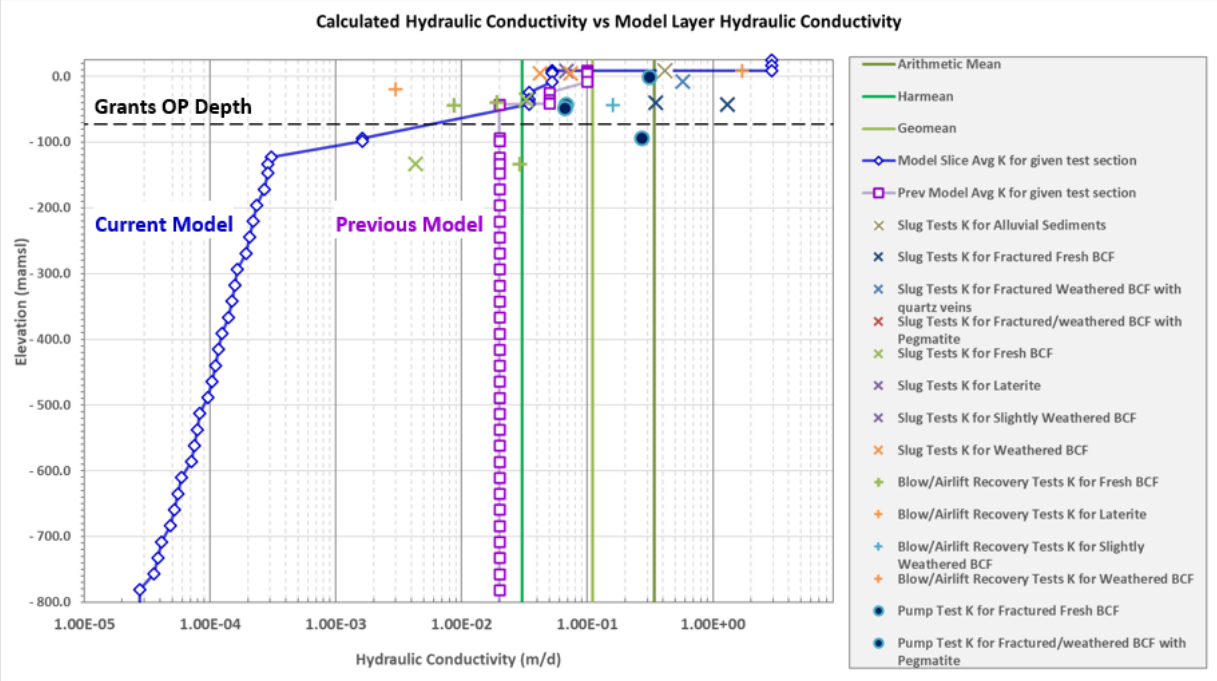

Figure 3-17: Calcualted Hydraulic Conductivity vs Model Layer Hydraulic Conductivity scaled with Depth

Table 3-3: Summary of the Hydraulic Tests vs Test Section Depths in Relation to the Calculated Hydraulic Conductivity for Grants and BP33

ID	ID with Test Type	X	Y	Z Topo (mamsl)	Test Type	Static Water Level (mbgl)	Bore-hole Depth (mbgl)	Bore-hole Depth (mamsl)	Hyd-raulic Head (mamsl)	Test Section From (mbgl)	Test Section To (mbgl)	Test Section From (mamsl)	Test Section To (mamsl)	Test Section Length (m)	Calcula-ted K (m/d)	Calcula-ted T (m^2/d)	Aquifer Thick-ness (m)	Blow Yield (l/s)	Blow Yield (m^3/d)	Blow Yield Dura-tion (h)	Date of Test	Lithology of Test Section_1	Data Source
GWB01	GWB01 - Blow/Airlift Recovery	693 066	8 599 025	20.69	Blow/Airlift Recovery	4.14	160	-139	16.55	88	154	-67	-133	66	2.90E-2	9.40E-1	32	2.00	173	1.0	May-2017	Fresh BCF	GHD, 2017
GWB03	GWB03 - Blow/Airlift Recovery	692 610	8 598 917	22.79	Blow/Airlift Recovery	1.86	63	-40	20.93	50	62	-27	HB-39	12	1.90E-2	1.50E-1	8	0.18	16	0.5	May-2017	Fresh BCF	GHD, 2017
GWB07	GWB07 - Blow/Airlift Recovery	693 666	8 598 650	17.06	Blow/Airlift Recovery	3.36	63	-46	13.70	49	61	-32	-44	12	8.70E-3	5.20E-2	6	0.04	3	0.5	May-2017	Fresh BCF	GHD, 2017
GWB08	GWB08 - Blow/Airlift Recovery	693 397	8 599 573	15.28	Blow/Airlift Recovery	2.60	60	-45	12.68	47	59	-32	-44	12	1.60E-1	1.10	7	1.00	86	0.5	May-2017	Slightly Weathered BCF	GHD, 2017
GWB10b	GWB10b - Blow/Airlift Recovery	693 371	8 599 562	14.40	Blow/Airlift Recovery	1.65	12	2	12.75	1	6	14	8	6	1.70	1.20	7.2	0.31	27	0.5	Jun-2017	Laterite	GHD, 2017
BPG4i	BPG4i - Blow/Airlift Recovery	694 486	8 593 420	15.03	Blow/Airlift Recovery	3.82	35	-20	11.21	29	35	-13	-19	6	3.00E-3				0			Weathered BCF	Groundwater Enterprises, 2020
BPG3s	BPG3s - N/A	694 614	8 593 869	13.56	N/A	Dry	5	9		4	5	10	9	1				Dry	N/A	N/A		Alluvial Sediments	Groundwater Enterprises, 2020
BPG1	BPG1 - Pump Test (Constant Discharge)	694 132	8 594 616	34.23	Pump Test (Constant Discharge)	2.80	36	-2	31.43	29	35	5	-1	6	3.11E-1	1.56E+1	50		0		Dec-2021	Fractured/weathered BCF with Pegmatite	Groundwater Enterprises, 2021
BPG4d	BPG4d - Pump Test (Constant Discharge)	694 493	8 593 423	14.88	Pump Test (Constant Discharge)	0.90	109	-94	13.98	47	109	-32	-94	62	2.71E-1	2.98E+1	110		0		Dec-2021	Fractured Fresh BCF	Groundwater Enterprises, 2021
BPG5i	BPG5i - Pump Test (Constant Discharge)	694 422	8 593 016	13.00	Pump Test (Constant Discharge)	1.52	57	-44	11.48	49	55	-36	-42	6	6.78E-2	3.39	50		0		Dec-2021	Fractured Fresh BCF	Groundwater Enterprises, 2021
BPG6	BPG6 - Pump Test (Constant Discharge)	693 929	8 593 846	24.01	Pump Test (Constant Discharge)	7.53	73	-49	16.48	66	72	-42	-48	6	6.64E-2	3.99	60		0		Dec-2021	Fractured Fresh BCF	Groundwater Enterprises, 2021
GWB01	GWB01 - Slug Test	693 066	8 599 025	20.69	Slug Test	4.14	160	-139	16.55	88	154	-67	-133	66	4.30E-3				0		May-2017	Fresh BCF	GHD, 2017
GWB03	GWB03 - Slug Test	692 610	8 598 917	22.79	Slug Test	1.86	63	-40	20.93	50	62	-27	-39	12	2.80E-3				0		May-2017	Fresh BCF	GHD, 2017
GWB07	GWB07 - Slug Test	693 666	8 598 650	17.06	Slug Test	3.36	63	-46	13.70	49	61	-32	-44	12	2.40E-2				0		May-2017	Fresh BCF	GHD, 2017
GWB08	GWB08 - Slug Test	693 397	8 599 573	15.28	Slug Test	2.60	60	-45	12.68	47	59	-32	-44	12	2.20E-2				0		May-2017	Slightly Weathered BCF	GHD, 2017
GWB10b	GWB10b - Slug Test	693 371	8 599 562	14.40	Slug Test	1.65	12	2	12.75	1	6	14	8	6	6.80E-2				0			Laterite	GHD, 2017
BPG1	BPG1 - Slug Test	694 132	8 594 616	34.23	Slug Test	7.87	36	-2	26.36	29	35	5	-1	6	1.83			1.50	130			Fractured/weathered BCF with Pegmatite	Groundwater Enterprises, 2020
BPG2i	BPG2i - Slug Test	694 784	8 594 336	20.11	Slug Test	3.51	28	-8	16.60	22	28	-2	-8	6	5.75E-1			0.40	35			Fractured Weathered BCF with quartz veins	Groundwater Enterprises, 2020
BPG2s	BPG2s - Slug Test	694 784	8 594 342	20.17	Slug Test	3.47	4	17	16.70	3	4	18	17	1	4.15E-1			Seepage	N/A			Alluvial Sediments	Groundwater Enterprises, 2020
BPG3i	BPG3i - Slug Test	694 618	8 593 873	13.57	Slug Test	4.22	49	-35	9.35	42	49	-28	-35	7	3.25E-2			0.10	9			Fresh BCF	Groundwater Enterprises, 2020
BPG4d	BPG4d - Slug Test	694 493	8 593 423	14.88	Slug Test	3.35	109	-94	11.53	47	109	-32	-94	62				2.60	225			Fractured Fresh BCF	Groundwater Enterprises, 2020
BPG4i	BPG4i - Slug Test	694 486	8 593 420	15.03	Slug Test	3.82	35	-20	11.21	29	35	-13	-19	6	6.50E-3			Seepage	N/A			Weathered BCF	Groundwater Enterprises, 2020
BPG4s	BPG4s - Slug Test	694 492	8 593 427	14.86	Slug Test	3.68	8	7	11.18	5	8	10	7	3	2.25E-2			Seepage	N/A			Weathered BCF	Groundwater Enterprises, 2020
BPG5i	BPG5i - Slug Test	694 422	8 593 016	13.00	Slug Test	4.72	57	-44	8.28	49	55	-36	-42	6	1.30			3.00	259			Fractured Fresh BCF	Groundwater Enterprises, 2020
BPG5s	BPG5s - Slug Test	694 423	8 593 020	13.02	Slug Test	5.17	8	5	7.85	5	8	8	5	3	4.20E-2			Seepage	N/A			Weathered BCF	Groundwater Enterprises, 2020
BPG6	BPG6 - Slug Test	693 929	8 593 846	24.01	Slug Test	7.53	73	-49	16.48	66	72	-42	-48	6	2.41			1.50	130			Fractured Fresh BCF	Groundwater Enterprises, 2020
BPG7i	BPG7i - Slug Test	693 984	8 593 099	11.94	Slug Test	4.03	53	-41	7.91	46	52	-34	-40	6	3.50E-1			0.50	43			Fractured Fresh BCF	Groundwater Enterprises, 2020
BPG7s	BPG7s - Slug Test	693 980	8 593 100	11.91	Slug Test	4.23	7	5	7.68	4	7	8	5	3	7.33E-2			Seepage	N/A			Weathered BCF	Groundwater Enterprises, 2020
	Maximum					7.87	160.00	16.67	31.43	88.00	154.00	17.67	16.67	66.00	2.41	29.84	110.00	3.00	259.20				
	Arithmetic mean					1.26	30.09	30.18	4.07	20.50	29.78	20.91	29.97	14.03	0.46	7.31	27.39	0.85	62.99				
	Std Dev					1.78	41.57	41.07	5.55	25.04	40.86	24.30	40.36	20.68	0.66	10.08	35.02	1.02	79.93				
	Geomean					3.27	35.96	N/A	13.53	21.29	33.70	N/A	N/A	7.97	0.07	1.58	22.14	0.58	N/A				
	Harmonic Mean					2.86	19.39	N/A	12.78	4.81	17.30	N/A	N/A	4.88	0.02	0.31	13.42	0.23	N/A				
	Minimum					0.90	3.50	-139.31	7.68	0.50	3.50	-67.31	-133.31	1.00	0.00	0.05	6.00	0.04	0.00				

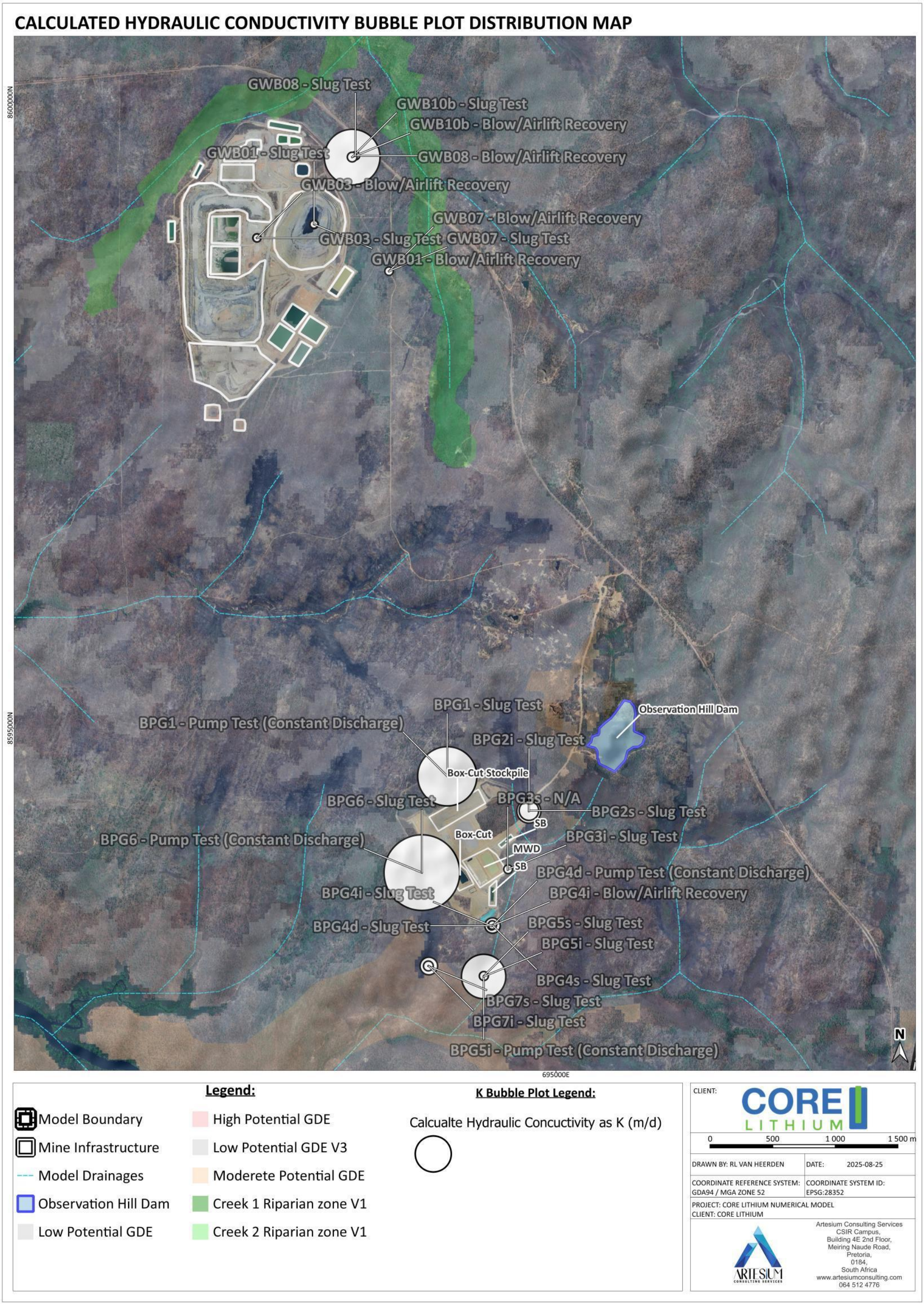

Figure 3-18: Calculated Hydraulic Conductivity Bubble Plot Distribution Map

3.7 Mine Water Abstraction Volumes and Measured Pit Lake Bathymetry

Dewatering volumes pumped from the Grants OP were provided by the client, who confirmed that the cumulative pumped volumes represent the most reliable record of dewatering rates. Statistical analysis of the data (Table 3-4) indicates an average abstraction rate of 3 856 m³/d, based on the two months of complete measured dewatering records available.

Table 3-4: Statistical Analysis of Grants OP Measured Dewatering Rates

Statistics	Date	Total Volume Pumped (m³/d)	Total Volume Pumped (ML/d)	Total Cumulative Volume (m³/d)
Max	2024/01/24	34 992	35	20 676
P95		14 045	14	13 638
P50		540	1	917
Average		**4 203**	**4**	**3 856**
P05		0	0	0
Min	2023/12/15	0	0	0

The measured pit lake water levels were given by the client in an Excel database and had the pit lake water level in metres above mean sea level (mamsl). The measured pit lake water level averaged -58 mamsl, based on an intermittent record spanning December 2023 to March 2025. The water level of the pit lake fluctuated from a maximum depth of –53 mamsl to a minimum depth of -66 mamsl. Given the variability in daily measurements, monthly averages were used as a reference.

Table 3-5: Statistical Analysis of Grants OP Measured Pit Lake Bathemetry

Statistics	Date	Pit Lake Water Level (mamsl)	Pit Lake Volume (ML)	Pit Lake Volume (m³)
Max	2025/03/18	-53	268	268 387
P95		-53	255	255 059
P50		-58	67	66 693
Average		**-58**	**104**	**103 686**
P05		-66	10	10 176
Min	2023/12/15	-66	3	2 672

The relationship between pit lake water level and pit lake volume is defined by the pit lake bathymetry. To establish this relationship, a stage curve of the as-built surveyed pit shell was generated using 1 m sliced intervals and cross-referenced with the stage curves provided by the client in Excel format. A strong correlation was achieved, confirming that a measured pit lake water level can be reliably converted to an equivalent pit lake volume. This assumption served as a critical input to the analytical water balance calculations at Grants and provided the primary supporting dataset for estimating groundwater inflows into the Grants OP.

The BP33 box cut was dewatered prior to 3 April 2024, after which dewatering activities ceased, and a surface water body was established. The surface water body established over a 7-month period following cessation of dewatering and was measured by a surveyor, enabling calculation of resident volume over time. The

sources and sinks of the water body in the box cut were isolated into individual components. Rainfall and runoff were calculated from climate data (sources), along with the evaporation data (sinks). The groundwater component was then estimated to balance the equation. The groundwater inflows were estimated to peak at 487 m^3/d and an average rate of 340 m^3/d.

The long-term forecast of groundwater inflow into BP33 Box Cut under current conditions for a 28-month period found that inflows would average approximately 10 m^3/d, with peaks forecasted at 102 m^3/d (refer to Table 3-6).

Table 3-6: Statistical Analysis of BP33 Box Cut Measured Pit Lake Bathemetry vs Groundwater Inflows

Statistics	Date	Box Cut Lake Water Level (mamsl)	Pit Lake Volume (ML)	Pit Lake Volume (m3)	Calculated Groundwater Inflows (m3/d)
Max	24/11/2024	4.84	63.08	63 078	487
Average		**-1.15**	**29.17**	**29 167**	**340**
Min	23/04/2024	-8.54	0	63 078	139

3.8 Numerical Model Development

The numerical modelling methodology is presented in Appendix A, Section 12. ACS was previously tasked to update the numerical groundwater model constructed by CloudGMS (2023). In this new numerical model (refer to report ACS, 2025) a larger model domain (watershed) was created to increase the model domain size and the previous CloudGMS (2023) parameters were used as initial model input values for steady state calibration.

The previous steady-state calibration focused on pre-mining (baseline) and operational (mining) conditions. Emphasis was placed on calibrating to the analytically calculated Grants OP fissure (groundwater) inflows as detailed in Section 3.8. The calculated fissure inflows were backed by observed values recorded by the operational team. From the steady-state calibration, limited verified transient water level data (monitoring data) were available at the time of the previous investigation and the transient calibration was once again anchored to the Grants fissure inflows and the measured zone of influence due to operations.

The progression of hydraulic conductivity values for both previously referenced models and the current (2026) model is summarised in Table 3-7 and shown in Figure 6-1.

Table 3-7: Summary of the Model Hydraulic Conductivity Progression

CloudGMS (2023)		ACS (2025)		% Difference from CloudGMS		ACS (2026)		% Difference from CloudGMS		% Difference from ACS 2025	
Kxy (m/d)	Kz (m/d)	Kxy (m/d)	Kz (m/d)	Kxy (m/d)	Kz (m/d)	Kxy (m/d)	Kz (m/d)	Kxy (m/d)	Kz (m/d)	Kxy (m/d)	Kz (m/d)
2.39E-2	2.39E-2	1.94E-2	1.30E-2	-19%	-46%	8.67E-1	8.65E-2	3522%	261%	3522%	261%
					Deep Aquifer	2.45E-4	1.63E-5	-99%	-100%	-99%	1.56E-04

The BP33 UG mine extends up to ± 800 m below surface with K values decreasing with depth due to an increase in lithostratigraphic pressure forcing possible water-bearing fractures closed. To represent this, the K-values were decreased with depth. This is an accepted method for representing deeper, fresher rock aquifers in numerical models (Belcher et al. 2002). The comparison of parameters between models can be seen in Figure 3-19. The comparison was made to gain more representative flows for the deep underground mining. Currently, there is a high degree of uncertainty with regards to the vertical hydraulic conductivity of the deeper (>150 mbgl) aquifer, and it is recommended that deep packer tests be conducted at depths where mining would occur.

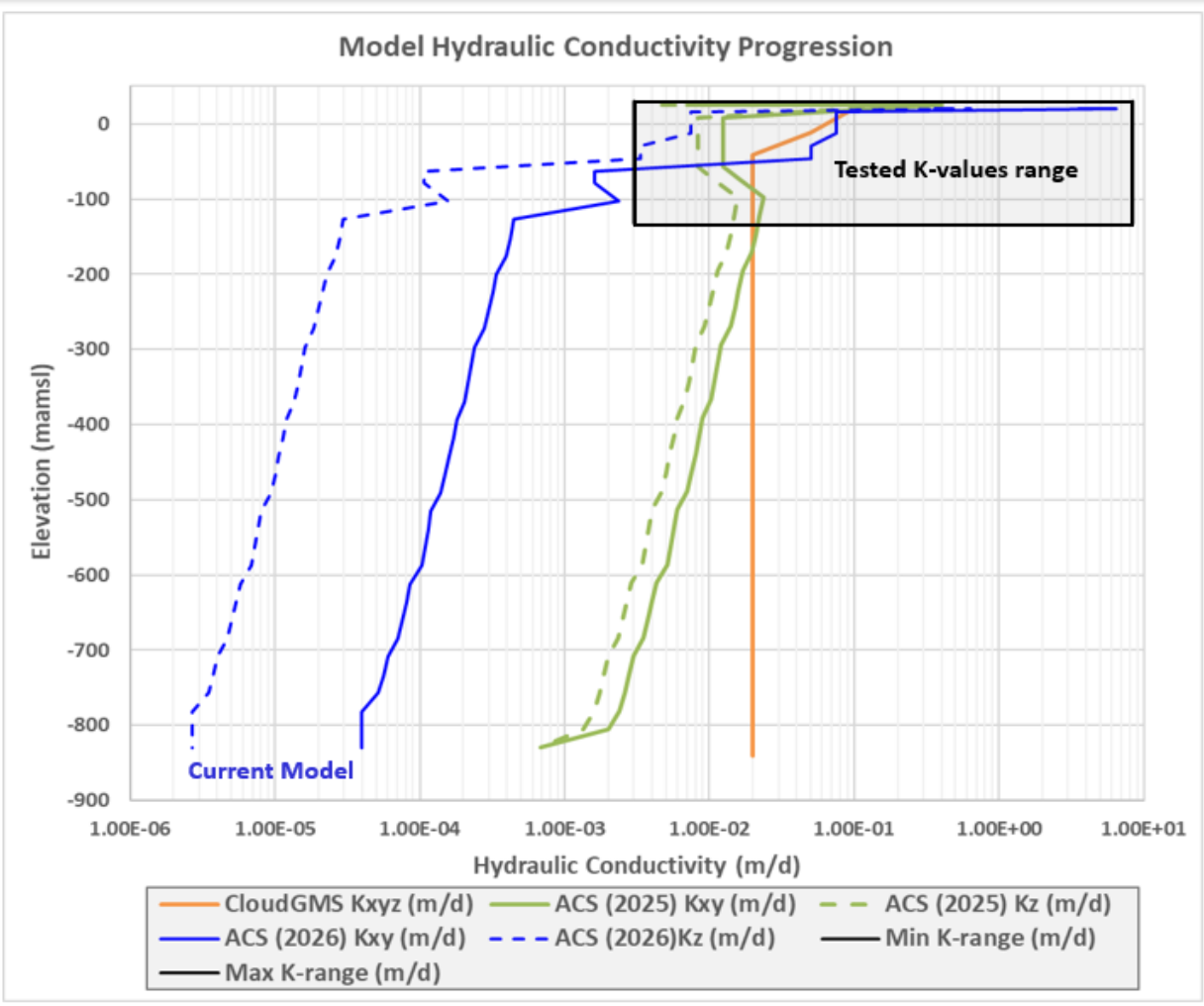

Figure 3-19: Model Hydraulic Conductivity Progression

In this investigation, additional long-term (±9 years) monitoring of bore water levels was received, and the model was recalibrated to more accurately represent seasonal fluctuations observed (Section 3.4). The specific storage (which is the 3D parameter, Ss) and Storativity (S, which is the 2D parameter), along with the specific yield (Sy), were calibrated towards the observed bore water levels and the progression of the parameters can be seen summarised in Table 3-8 and Table 3-9.

Table 3-8: Summary of Model-Specific Storage and Storativity Parameter Progression

CloudGMS (2023)		ACS (2025)		% Difference from CloudGMS		ACS (2026)		% Difference from CloudGMS		% Difference from ACS 2025	
Ss	S	Ss	S	Ss	S	Ss	S	Ss	S	Ss	S
1.00E-6	1.00E-6	2.61E-5	4.85E-4	2505%	48355%	2.31E-4	1.16E-3	23011%	116371%	787%	140%
					Deep Aquifer	7.54E-6	1.86E-4	654%	18471%	654%	18471%

Orders-of-magnitude increases in Ss and S were applied relative to the CloudGMS parameters used in the ACS (2025) model and were subsequently increased by 787% and 140% for the shallow aquifer, with regard to Ss and S, respectively. The Ss and S were further increased by 645 and 18 471% in the deeper model sections (Layers 14 – 43), respectively.

The specific yield (Sy) model progression is summarised in Table 3-9 and shown graphically in Figure 3-20. The Sy was reduced relative to previous models to account for seasonality in groundwater levels, as observed in measured borehole water levels. Specific yield was decreased by 62% compared to the previous ACS (2025) model. The decrease allowed for seasonal fluctuations to be observed in the modelled water levels.

Table 3-9: Summary of Specific Yield Parameter Progression

CloudGMS (2023)	ACS (2025)	% Difference from CloudGMS	ACS (2026)	% Difference from CloudGMS	% Difference from ACS 2025
Sy	Sy	Sy	Sy	Sy	Sy
1.25E-02	1.05E-02	-16%	5.84E-04	-95%	-94%

The bore logs at Grants and BP33 were derived from historical reports and data provided by the client. The logs were grouped into hydrogeological units and compared to Sy values found for the same hydrogeological units in the literature. This was done as no Sy values were found from cited scientific literature for the BCF specifically. Thus, analogue data were found in literature from similar hydrogeological environments, and this is summarised in Table 3-10.

Table 3-10: Literature values for Specific Yields considering similar hydrogeological environments

Hydrogeological unit	Geology	Sy Min Values from Literature	Sy Max Values from Literature	Source
Quaternary silt/silty sand cover	Silty sand, minor laterite	0.05	0.15	Morris & Johnson (1967) via Heath (1983)
Weathered schist/saprolite	Clay-rich, low permeability	0.01	0.1	Durand et al. (2017); Dewandel et al. (2017)
Transitional fractured zone (SFL top)	Weathered fractured schist/schist-quartz vein contact	0.01	0.02	Durand et al. (2017); Maréchal et al. (2015)
Deep fresh fractured rock	Fresh schist/sandstone, discrete fractures	0.001	0.005	Domenico & Schwartz (1990); Dewandel et al. (2017)

The Sy value applied (5.85E-04) was observed to be lower on average compared to the literature values (0.005 -0.15). If the Sy values were increased in the model to align with the lower and upper bounds reported in the literature, the predicted seasonality in groundwater levels was lost. To gain better seasonality in predictions, the recharge must then be increased, and the peak recharge was increased to match the upper limit of what was calculated using the Chloride Mass Balance Method (CMB) between 15.46 and 18.74%. Increasing the recharge peaks or the average recharge would require increasing the K-values even more. This was not considered viable, as the K-values were already at the upper limit observed in the tested site data.

Although the lower Sy values are at the limits of the literature data ranges, it is important to observe what the measured site data shows. Scaling up from, for example, lab scale to regional aquifer scale site could reduce the Sy to the geomean and could be an order of magnitude lower. When assumptions are developed from small-scale tests (like lab measurements) to a much larger, regional aquifer system (i.e. the model domain), the value of specific yield is expected to be an order smaller (10× smaller).

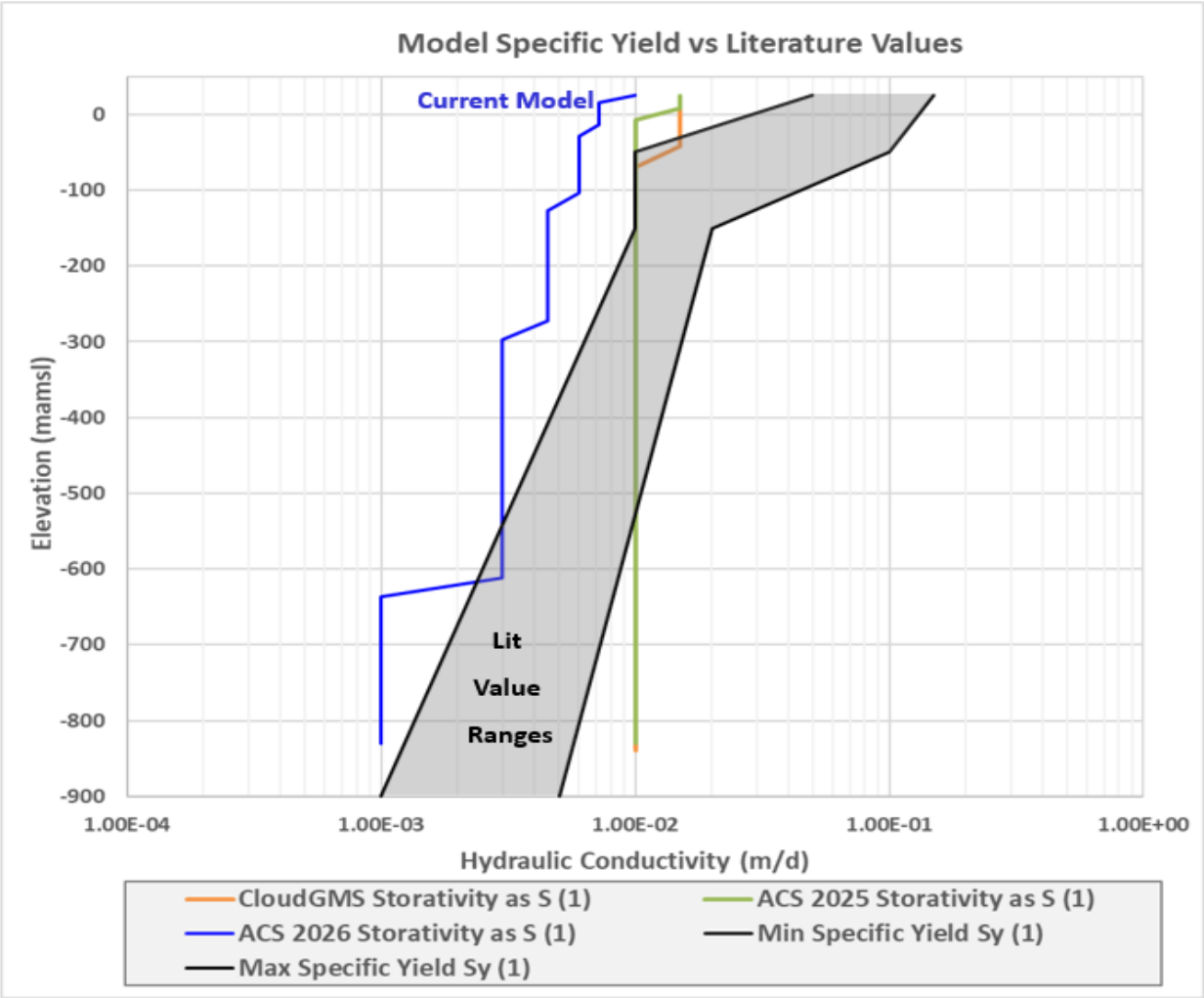

Figure 3-20: Model Specific Yield Progression

3.8.1 Model Scenarios (Sensitivity Analysis)

Using the calibrated model, sensitivity scenarios were set up to gauge potential impacts on GDEs by quantifying dewatering rates and resultant ZOIs. The following sensitivity scenarios were included:

1. Scenario 1.1a (Base Case) –the model was calibrated to scale Sy values with depth and be more representative of literature values as best possible while still achieving seasonal variability in water levels.

2. Scenario 1.1b (No Mining) – All mining was removed from the calibrated base case transient model (Scenario 1.1a) and run up to LoM.

3. Scenario 1.2 (Medium K) – Hydraulic conductivity for the deeper aquifer (Layer 14 to Layer 43, where the bulk of underground mining will occur) was increased by 5 times from the calibrated model used in Scenario 1.1a.

4. Scenario 1.3 (High K) - Hydraulic conductivity for the deeper aquifer (Layer 14 to Layer 43, where the

bulk of the underground mining will occur) was increased by 10 times from the calibrated model used in Scenario 1.1a.

5. Scenario 1.4 (High Sy) –Specific yield was scaled up by an order of magnitude (x10) from Scenario 1.1a for all model layers.

6. Scenario 1.5 (50% of recharge) – 50% of the transient non-linear recharge applied in the calibrated model was used.

7. Scenario 1.6 (Double recharge) – The transient non-linear recharge applied in the calibrated model was doubled.

8. Scenario 1.7 (Dry Cycle) – Scenario 1.1a parameters were used, and a dry sub-climate cycle was used to simulate LoM impacts.

These scenarios are discussed in more detail in Section 6.1.

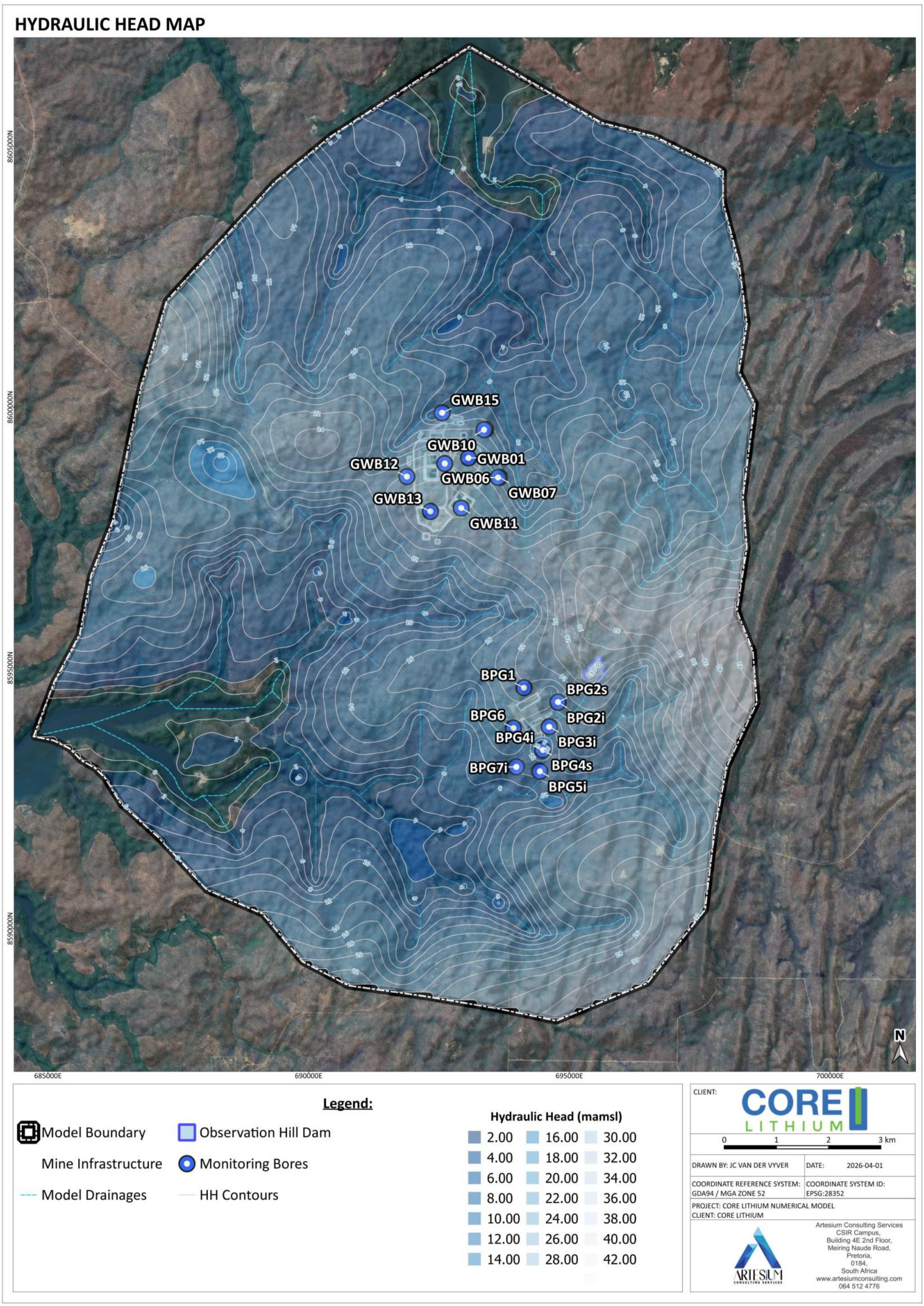

Figure 3-21: Calibrated Steady State Pre-mining Hydraulic Head Map

4 HYDROGEOLOGICAL CONCEPTUAL MODEL

A Conceptual Site Model (CSM) was developed using measured data at Grants to represent both current mining conditions (July 2025) and pre-mining conditions. The CSM consisted of a long-section (Figure 4-1) drawn from south-west to north-east:

1. Delineate the current measured drawdown zone of influence (ZOI) at the Grants OP.
2. Quantify the hydraulic semi-disconnect or limited vertical hydraulic connectivity between shallow weathered aquifer heads and intermediate/deeper solid/fractured aquifer heads.

4.1 Current Measured Zone of Influence

The measured hydraulic head trends (Section 3.4) were used to infer the current drawdown zone resulting from the Grants OP acting as a sink. The delineated drawdown zone for the intermediate aquifer is shown in the long section and in plan view in Figure 4-1.

From the monitoring data (Section 3.4) no boreholes at Grants measured changes in water levels that exceeded the baseline seasonal amplitude. The furthest distance (360 m) from the OP where groundwater levels were measured to decrease was in bore GWB08 (intermediate aquifer; -1.8 m); beyond this point, water levels were observed to increase, with no decreases measured in the shallow aquifer. The maximum measured drawdown cone in the intermediate aquifer was observed to be a maximum of 360 m to 400 m from the pit by <2 m change, and there was no commensurate measurable drawdown in the shallow aquifer monitoring bores from the Grants and BP33 during the operational phase for Grants OP (See Section 3.4).

4.2 Shallow weathered Aquifer and Deeper Solid/fractured Aquifer

The differences in measured hydraulic heads at depth-specific monitoring bores indicate limited, distinct vertical hydraulic connectivity between the shallow and deep aquifer zones. The numerical model does not sufficiently differentiate between shallow and deep drawdown zones at the same resolution. Although there is no defined confining layer, the system reacts as if there is; the hydraulic semi-disconnect is represented in the model by reducing the Kz by an order of magnitude for the intermediate and deep aquifers relative to the shallow aquifer.

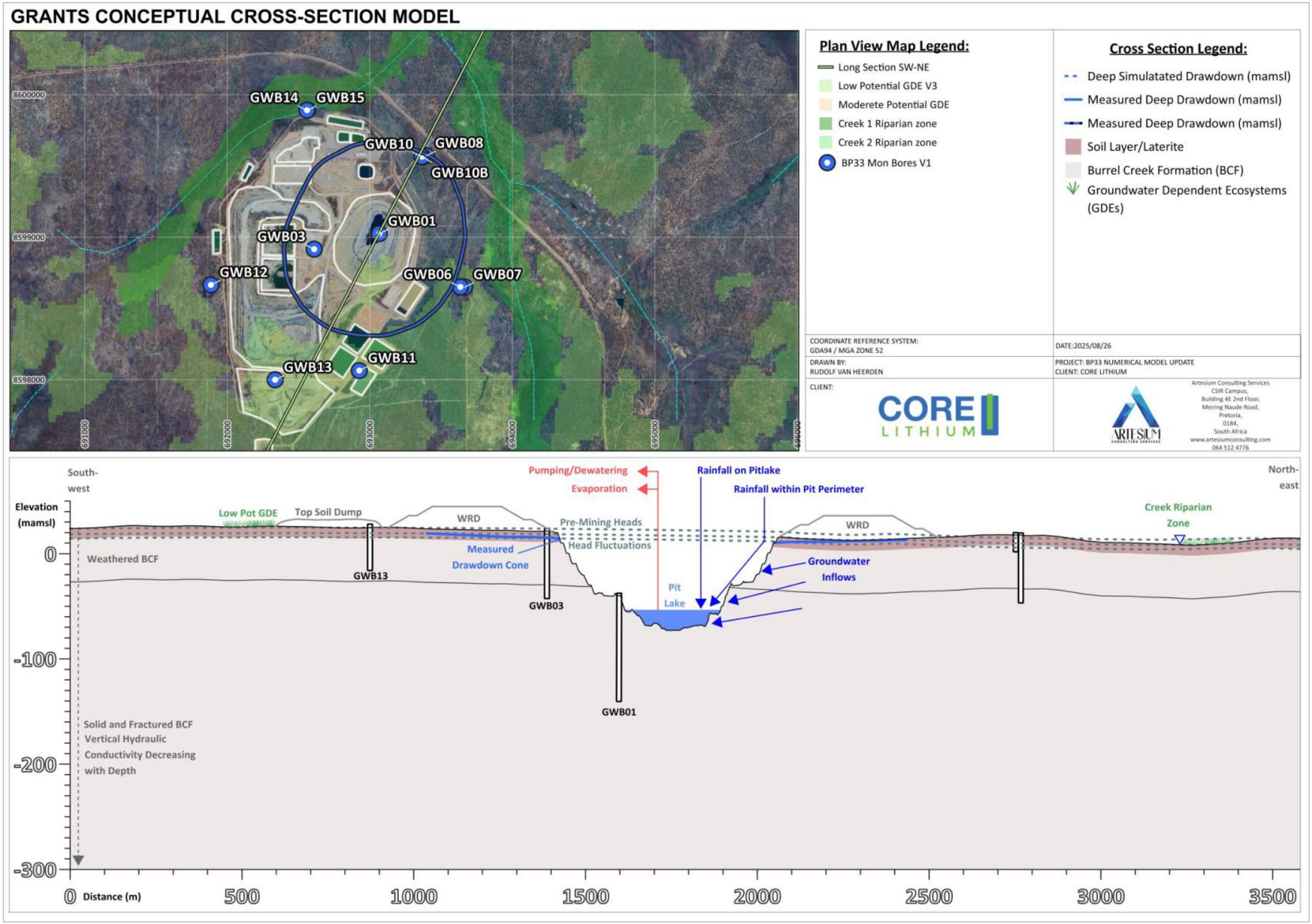

Figure 4-1: Grants Hydrogeological Conceptual Model in Long Section View

5 Model Confidence Level Classification

The model confidence-level classification provides a benchmark, based on Barnett et al. (2012), for assessing the reliability of groundwater model predictions. It establishes a common basis for stakeholders—including model owners, reviewers, regulators, and decision-makers—to form realistic expectations of model performance. This classification is important because model reliability is inherently constrained by the availability of data, as well as by project budget and timeframe.

Three confidence classes are defined: Class 1 (low confidence), Class 2 (medium confidence), and Class 3 (high confidence). The classification assigned to a model depends on factors such as the availability and quality of data, the robustness of calibration, and how predictions are formulated. Key considerations include:

- Data: spatial and temporal coverage, accuracy, and adequacy to support aquifer characterisation and calibration; and
- Calibration: the type and quality of data used, the model's ability to reproduce observed conditions, and the extent to which calibration represents current groundwater behaviour.

In practice, a Class 1 model may be adequate where predictive reliability is less critical for low-risk developments. By contrast, Class 2 and Class 3 models are more appropriate for high-value aquifers or high-risk developments, where decision-making demands greater predictive certainty.

5.1 BP33 Model Confidence Classification

The model classification for BP33 was considered Class 2 when applied to BP33, and the following updates or improvements are suggested:

- Hydraulic conductivity testing (packer testing) extending down to the final depth of underground workings (-850 mamsl) to improve characterisation of the deeper aquifer.
- Vibrating Wireline Piezometer (VWP) hydraulic head monitoring for the deep (>150 – 800 mbgl) aquifer, where mining will take place.
- Measurement of deep groundwater piezometric pressures and chemistry.

Table 5-1: Model Confidence level Classification adapted from Barnett et al. (2012)

Confidence level classification	Data	Calibration	Prediction	Key indicator	Examples of specific uses
Class 3	1. Spatial and temporal distribution of groundwater head observations adequately define groundwater behaviour especially in areas of greatest interest and where outcome are to be reported. 2. Spatial distribution of bore logs and associated stratigraphic interpretations clearly define aquifer geometry. 3. Reliable metered groundwater extraction and injection data is available. 4. Rainfall and evaporation data is available. (Site specific data can strengthen the data sets used for the model.) 5. Aquifer-testing data to define key parameters. Deep (>150 mbgl) testing to verify hydraulic parameters up to depth of UG mine. 6. Streamflow and stage measurements are available with reliable baseflow estimates at a number of points. 7. Good quality and adequate spatial coverage of digital elevation model to define ground surface elevation.	1. Scaled RMS error or other calibration statistics are acceptable. 2. Long-term trends are adequately replicate where these are important. 3. Seasonal fluctuations are adequately replicated where these are important. 4. Transient calibration is current, i.e. uses recent data. 5. Model is calibrated to heads and fluxes. 6. Observations of the key modelling outcomes dataset is used in calibration.	1. Length of predictive model is not excessive compared to length of calibration period. 2. Temporal discretisation used in the predictive model is consistent with the transient calibration. 3. Level and type of stresses included in the predictive model are within the range of those used in the transient calibration.	1. Key calibration statistics are acceptable and meet agreed targets. 2. Model predictive time frame is less than 3 times the duration of transient calibration. 3. Stresses are not more than 2 times greater than those included in calibration. 4. Temporal discretisation in predictive model is the same as that used in calibration. 5. Mass balance closure error is less than 0.5% of total. (Steady State). Transient State. 6. Model parameters consistent with conceptualisation. 7. Appropriate computational methods used with appropriate spatial discretisation to model the problem. 8. The model has been reviewed and deemed fir for purpose by an experienced, independent hydrogeologist with modelling experience.	1. Suitable for predicting groundwater responses to arbitrary changes in applied stress or hydrological conditions anywhere within the model domain. 2. Provide information for sustainable yield assessments for high-value regional aquifer systems. 3. Evaluation and management of potentially high-risk impacts. 4. ·Can be used to design complex mine dewatering schemes, salt-interception schemes or water-allocation plans. 5. Simulating the interaction between groundwater and surface water bodies to a level of reliability required for dynamic linkage to surface water models. 6. Assessment of complex, large-scale solute transport processes.
Class 2	1. Groundwater head observations and bore logs are available but may not provide adequate coverage throughout the model domain. 2. Metered groundwater-extraction data may be available but spatial and temporal coverage may not be extensive. 3. Streamflow data and baseflow estimates available at a few points. 4. Reliable irrigation-application data available in part of the area or for part of the model duration.	1. Validation is either not undertaken or is not demonstrated for the full model domain. 2. Calibration statistics are generally reasonable but may suggest significant errors in parts of the model domain(s). 3. Long-term trends not replicated in all parts of the model domain. 4. Transient calibration to historic data but not extending to the present day. 5. Seasonal fluctuations not adequately replicated in all parts of the model domain. 6. Observations of the key modelling outcome data set are not used in calibration.	1. Transient calibration over a short time frame compared to that of prediction. 2. Temporal discretisation used in the predictive model is different from that used in transient calibration. 3. Level and type of stresses included in the predictive model are outside the range of those used in the transient calibration. 4. Validation suggests relatively poor match to observations when calibration data is extended in time and/or space.	1. Key calibration statistics suggest poor calibration in parts of the model domain. 2. Model predictive time frame is between 3 and 10 times the duration of transient calibration. 3. Stresses are between 2 and 5 times greater than those included in calibration. 4. Temporal discretisation in predictive model is not the same as that used in calibration. 5. Mass balance closure error is less than 1% of total. (Steady State). Transient State. 6. Not all model parameters consistent with conceptualisation. 7. Spatial refinement too coarse in key parts of the model domain. 8. The model has been reviewed and deemed fit for purpose by an independent hydrogeologist.	1. Prediction of impacts of proposed developments in medium value aquifers. 2. Evaluation and management of medium risk impacts. 3. Providing estimates of dewatering requirements for mines and excavations and the associated impacts. 4. Designing groundwater management schemes such as managed aquifer recharge, salinity management schemes and infiltration basins. 5. Estimating distance of travel of contamination through particle-tracking methods. Defining water source protection zones.
Class 1	1. Few or poorly distributed existing wells from which to obtain reliable groundwater and geological information. 2. Observations and measurements unavailable or sparsely distributed in areas of greatest interest. 3. No available records of metered groundwater extraction or injection. 4. Climate data only available from relatively remote locations. 5. Little or no useful data on land-use, soils or river flows and stage elevations.	1. No calibration is possible. 2. Calibration illustrates unacceptable levels of error especially in key areas. 3. Calibration is based on an inadequate distribution of data. 4. Calibration only to datasets other than that required for prediction.	1. Predictive model time frame far exceeds that of calibration. 2. Temporal discretisation is different to that of calibration. 3. Transient predictions are made when calibration is in steady state only. 4. Model validation suggests unacceptable errors when calibration dataset is extended in time and/or space.	1. Model is uncalibrated or key calibration statistics do not meet agreed targets. 2. Model predictive time frame is more than 10 times longer than transient calibration period. 3. Stresses in predictions are more than 5 times higher than those in calibration. 4. Stress period or calculation interval is different from that used in calibration. 5. Transient predictions made but calibration in steady state only. 6. Cumulative mass-balance closure error exceeds 1% or exceeds 5% at any given calculation time. 7. Model parameters outside the range expected by the conceptualisation with no further justification. 8. Unsuitable spatial or temporal discretisation. 9. The model has not been reviewed.	1. Design observation bore array for pumping tests. 2. Predicting long-term impacts of proposed developments in low-value aquifers. 3. Estimating impacts of low-risk developments. 4. Understanding groundwater flow processes under various hypothetical conditions. 5. Provide first-pass estimates of extraction volumes and rates required for mine dewatering. 6. Developing coarse relationships between groundwater extraction locations and rates and associated impacts. 7. As a starting point on which to develop higher class models as more data is collected and used.

Table Legend:

Criteria met

Criteria met with room for improvement (update)

Criteria not met

6 GROUNDWATER NUMERICAL MODELLING RESULTS

6.1 Results for Life of Mine Dewatering Scenarios

The simulated bulk dewatering results up to LoM for the BP33 mine are presented graphically in Figure 6-1 and Figure 6-2, and in Table 6-5. The following general assumptions were made with regard to the simulated dewatering rates:

- Dewatering rates for BP33 UG are strictly for fissure/groundwater dewatering with no surface water runoff or rainfall accounted for in the numerical groundwater model.
- The Box cut is dewatered completely before the decline is constructed at BP33, as the decline is developed from the third bench at approximately 30 m depth.
- The BP33 Box Cut remains dewatered up to LoM for BP33.
- The old BP33 underground mine "pit lake" situated on top of the footprint of the planned BP33 underground infrastructure was not dewatered to gauge how much water would seep from this facility.

Table 6-1: Statistical Summary of Simulated LoM Dewatering Rates for BP33 Mine

Statistical Summary	Scenario 1.1 (Base Case)		Scenario 1.2 (High Case)	
	Dewatering Rates for BP33 Box Cut Scen_1.1 (m^3/d)	Dewatering Rates for BP33 UG Scen_1.1 (m^3/d)	Dewatering Rates for BP33 Box Cut Scen_1.6 (m3/d)	Dewatering Rates for BP33 UG Scen_1.4a (m^3/d)
Max	260	1 696	715	2 235
P95	105	1 558	256	2 007
Average	**51**	**1 139**	**106**	**1 359**
P50	36	1 314	62	1 474
Min	3	0	5	0

6.2 BP33 LoM Dewatering Rates

The estimated base-case groundwater flows for BP33 underground peaked at ±1 696 m^3/d 75 months after mining started. The dewatering rates steadily declined as aquifer storage was depleted and plateaued around month 95 at a rate of ±1 100 m^3/d. The average LoM dewatering rate for BP33 LoM base case was 1 139 m^3/d. The BP33 UG high case dewatering rate peaked at 2 235 m^3/d and stabilised around 1 600 m^3/d, with the average dewatering rate calculated for the BP33 LoM high case at 1 359 m^3/d. The dewatering rates are displayed graphically in Figure 6-1.

The estimated BP33 box cut dewatering rate (Figure 6-2) for the base case peaked at 260 m^3/d. The box cut dewatering was predicted to decrease as the decline is developed from the box cut and dewaters the immediate area. The average fissure dewatering rate applied to the Box Cut was 51 m^3/d up to LoM. The high-case scenario in which recharge was doubled yielded estimated peaks of up to 715 m^3/d, with an average dewatering rate that was double the base case (106 m^3/d).

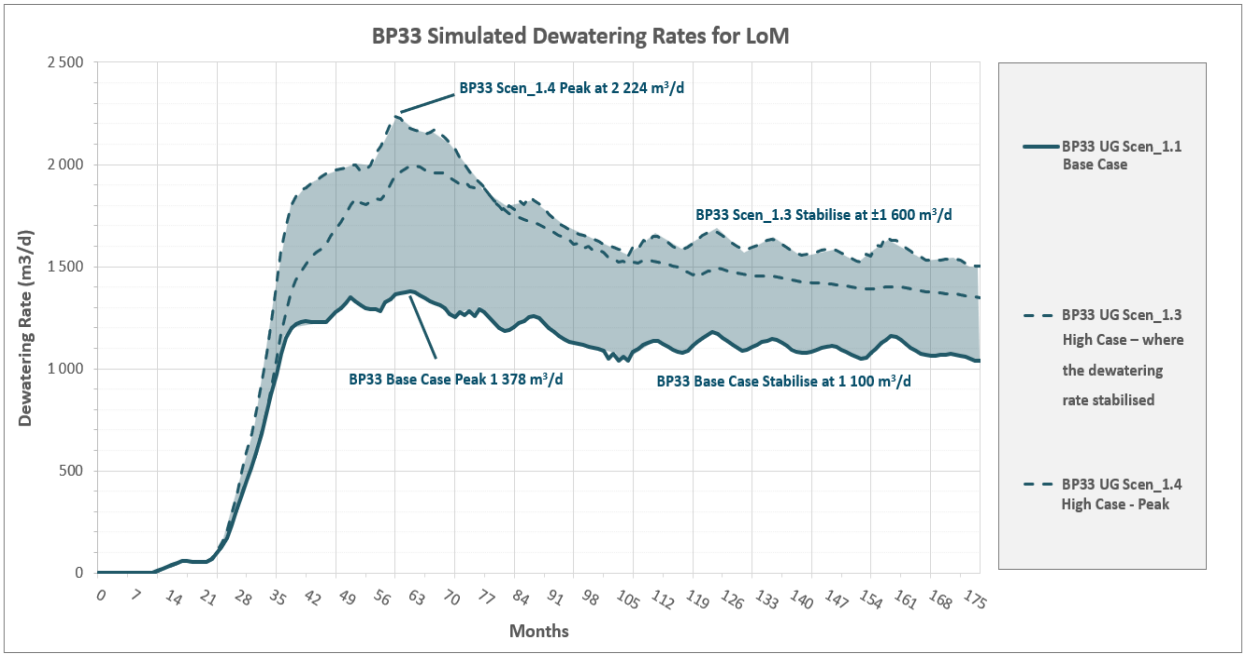

Figure 6-1: BP33 Underground Simulated Dewatering Rates for LoM

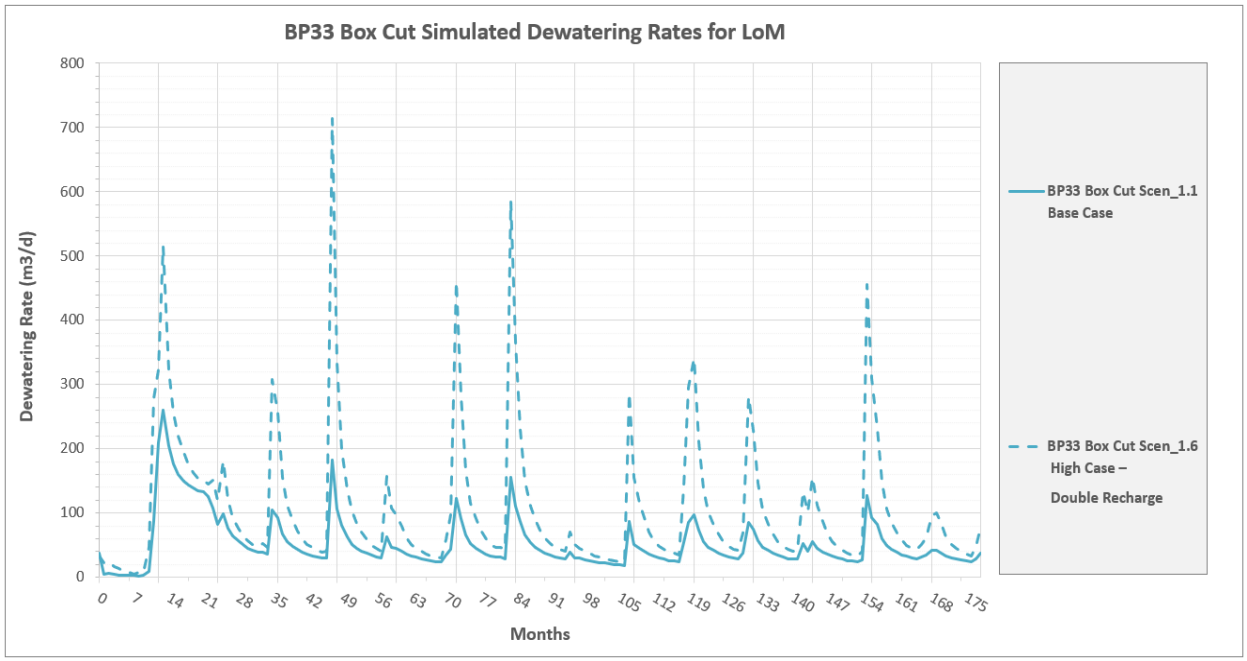

Figure 6-2: BP33 Box Cut Simulated Dewatering Rates for LoM

6.3 Simulated Maximum Zone of Influence (ZOI) for BP33 LoM

The simulated ZOI for the wet vs dry season observed in the shallow, intermediate and deep aquifer at LoM is shown in Figure 6-3. The ZOI was plotted with a 1 m boundary. At LoM for BP33 UG, the ZOI in the shallow aquifer extended ±2.25 km east–west and ±2.1 km north – south (±345 ha). The shallow ZOI intersects various low-potential GDEs to the south and north of the mine. The maximum simulated drawdown was ±10 m within the decline footprint relative to the shallow aquifer ZOI.

The intermediate aquifer ZOI had a slightly larger extent than the shallow ZOI and covered an area of approximately ±395 ha, with the deep ZOI, where the bulk of the UG mining will occur, covering a surface area of ±685 ha. The deep cone extended ±3.5 km east-west and ±2.5 km north-south. Currently, there are no known groundwater users located within the deep and intermediate simulated impact zones at BP33.

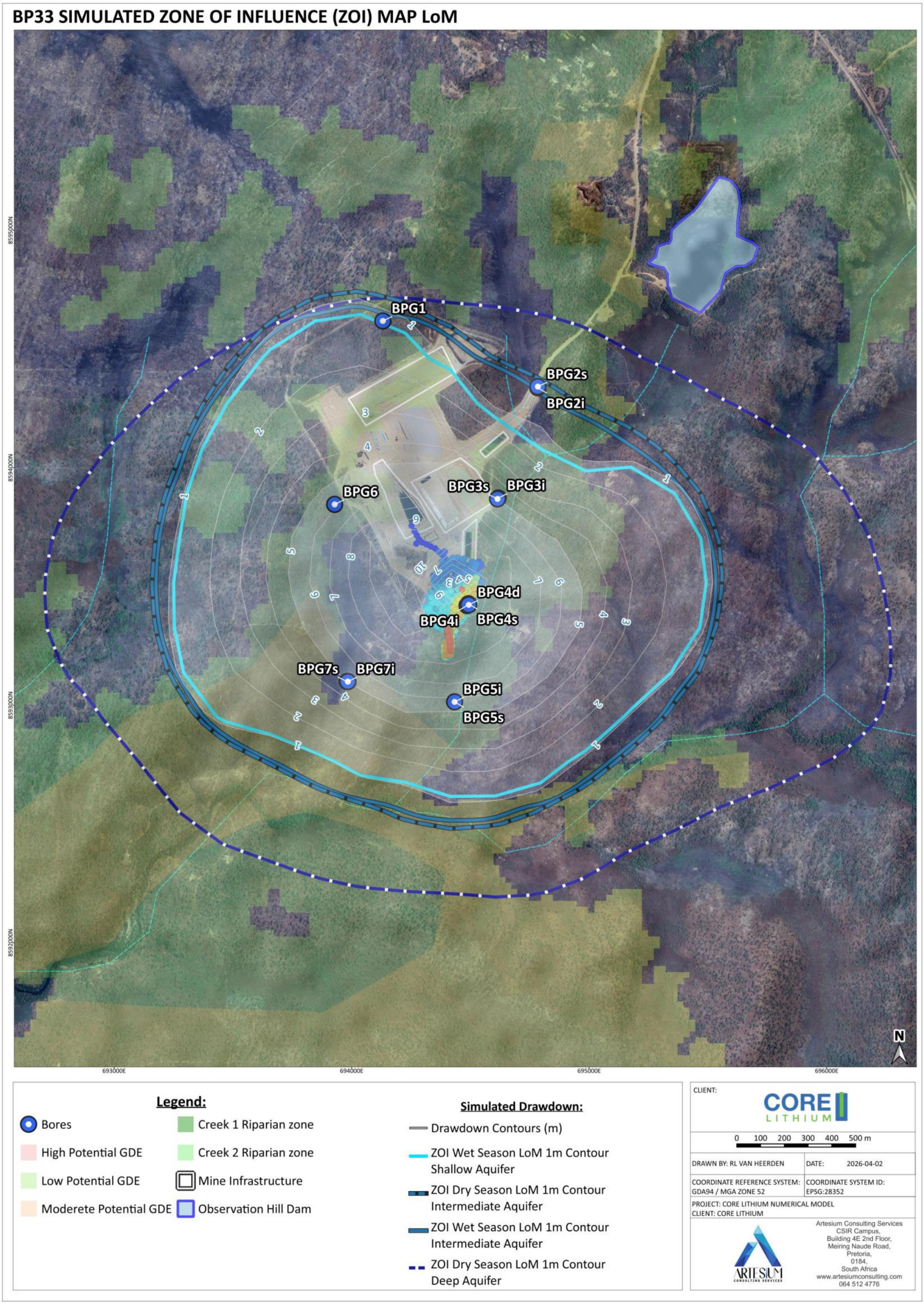

Figure 6-3: Simualted ZOI Map for BP33 Mine LoM

6.4 Groundwater Flow Budgets and Potential Impacts on GDEs

The potential impacts of mining on the GDEs within the model domain were calculated by running two scenarios: one with no mining and one with active mining. The simulations were conducted over the same time frame for pre-mining, previous construction phase, and future development/ operational phase up to LoM for BP33.

The GDEs were isolated as a separate feature within the domain water budget. All the sources and sinks within the model domain are accounted for, and the difference between the mining and no-mining scenarios was quantified to simulate the impact on GDEs. The results are presented in Table 6-2 'no mining' and 'with mining' Table 6-3.

Table 6-2: Domain Water Budgets for Scenario 1.1b with No Mining[1]

Groundwater Component		Mean Annual		Wet Season		Dry Season	
		Inflow (m^3/d)	Outflow (m^3/d)	Inflow (m^3/d)	Outflow (m^3/d)	Inflow (m^3/d)	Outflow (m^3/d)
1	Recharge	57 171		87 338		0	
2	Perennial Surface Water	2 505	-19 500	3 179	-24 075	2 897	-14 750
3	Inflow Outflow (from/to) Boundaries	822	-1 128	1 263	-247	1 004	-247
4	Groundwater Discharge to Drainages		-27 181		-36 882		-23 877
5	Groundwater Discharge to GDEs		-12 143		-18 969		-9 897
6	Mine dewatering Total		0		0		0
7	From (+) To (-) Aquifer Storage	34 012	-33 843	23 572	-54 054	45 764	-397
	Total	**94 510**	**-93 795**	**115 352**	**-134 228**	**49 665**	**-49 168**
	Balance	**715**		**-18 876**		**497**	
	Seasonal Balance Error (%)	**0.76%**		**-16.36%**		**1.00%**	

6.4.1 Results

The mean groundwater discharged to drainages within the model domain in the no mining scenario was simulated as 27 181 m^3/d, and in the mining scenario was simulated as 24 564 m^3/d; that is a 10% reduction due to mining. The groundwater discharge accounts for all model drainages, not all of which are received by GDEs. Table 6-4 summarises the areas where groundwater discharge would feed GDEs.

1 Although from (+) and to (-) storage are not strictly outflows and inflows it is used as such to demonstrate the balances.

Table 6-3: Domain Water Budgets for Scenario 1.1a with Mining

Groundwater Component		Mean Annual		Wet Season		Dry Season	
		Inflow (m^3/d)	Outflow (m^3/d)	Inflow (m^3/d)	Outflow (m^3/d)	Inflow (m^3/d)	Outflow (m^3/d)
1	Recharge	57 167		87 330		0	
2	Perennial Surface Water	2 521	-19 385	3 183	-23 888	2 915	-14 638
3	Inflow Outflow (from/to) Boundaries BCs	816	-1 130	1 260	-1 654	997	-248
4	Groundwater Discharge to Drainages		-24 564		-35 725		-21 022
5	Groundwater Discharge to GDEs		-15 516		-20 912		-13 096
6	Mine dewatering Total		-1 508		-2 146		-1 457
7	From (+) To (-) Aquifer Storage	34 159	-34 292	54 506	-23 449	46 269	-401
	Total	**94 664**	**-96 395**	**146 279**	**-107 775**	**50 181**	**-50 863**
	Balance	**-1 731**		**38 505**		**-681**	
	Seasonal Balance Error (%)	**-2%**		**26%**		**-1%**	

Table 6-4: Impact on GDEs from Model Water Budgets

Groundwater Discharge to Drainages (GDE's) Breakdown										
Groundwater Discharge to Drainages (GDE's) Breakdown		Mean Annual			Wet Season			Dry Season		
Nr	Feature	Pre-Mining	Min-ing	Diff (%)	Pre-Mining	Min-ing	Diff (%)	Pre-Mining	Min-ing	Diff (%)
5.1	Groundwater Discharge to Drainages High potential GDE's	0	0	0%	0	0	0%	0	0	0%
5.2	Groundwater Discharge to Drainages Moderate potential GDE's	-4 820	-4 733	-2%	-6 426	-6 267	-2%	-4 326	-4 249	-2%
5.3	Groundwater Discharge to Drainages Low potential GDE's	-8 937	-8 730	-2%	-12 300	-12 032	-2%	-7 652	-7 483	-2%

The predicted impact due to mining effect on drainage to low- and moderate-level risk GDEs was negligible, with a <2% reduction simulated.

7 MINE REWATERING MODELLING

7.1 BP33 Analytical Rewatering Model Results

For the fully backfilled BP33 Box Cut and fully backfilled BP33 UG, the model presented in Figure 7-2 was used to simulate the re-watering rate and potential for subsurface and surface decant. The box cut was assumed to be backfilled with a permeable (i.e. disturbed) material that has a porosity of 26%. The decline was assumed to be backfilled with paste backfill material, from where the stopes originate up to the entry point in the box cut. This assumption was made to constrain the flow volume from Underground with 90%. The net infiltration through the box cut top layer must be reduced to less than 15% to 20% mean precipitation. Under these conditions, the probability of surface decant is estimated at approximately 0.2% (equivalent to a 1:500 annual exceedance probability, or P99.8).

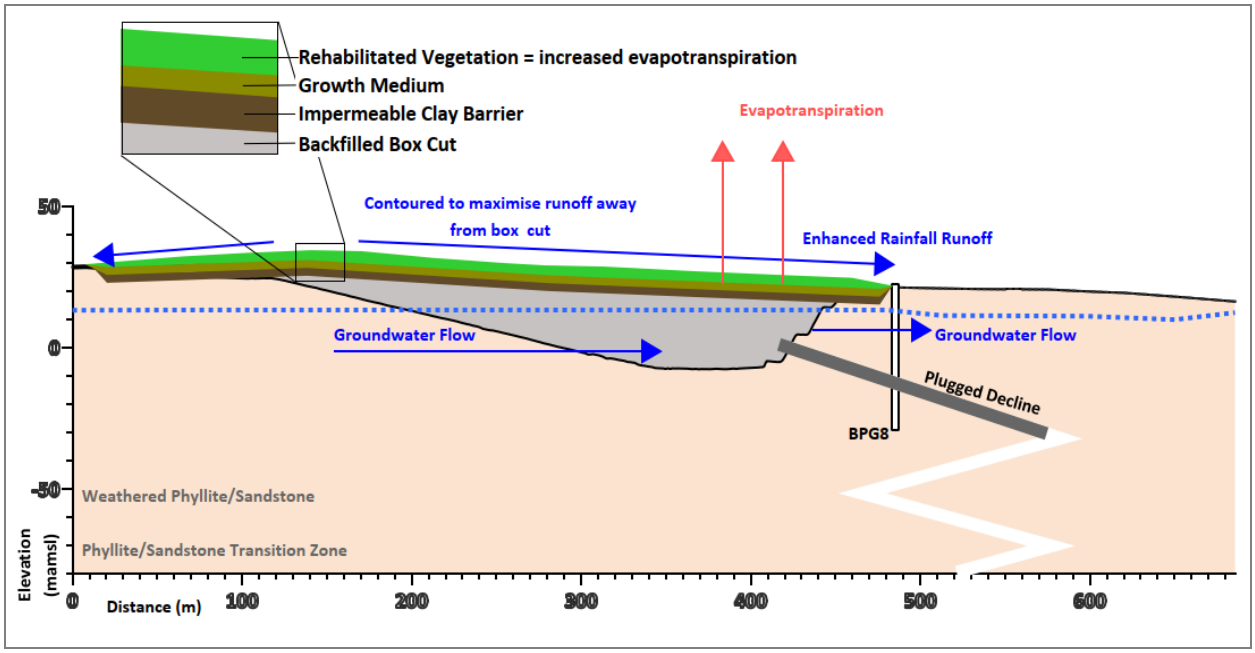

Figure 7-1: Conceptual Post-Closure Model for Box Cut

It is recommended that the box cut rehab design makes provision for a top layer of growth medium to maximise evapotranspiration up to 1-2 m underlain by a 0.3 m to 0.5 m low permeability barrier layer (Clayey). This will help reduce the net infiltration within the backfilled box cut to below 15% of the mean annual precipitation. This will mitigate the risk of surface decanting.

The upstream perimeter should also be contoured to divert surface water away from the box cut, limiting additional infiltration from runoff.

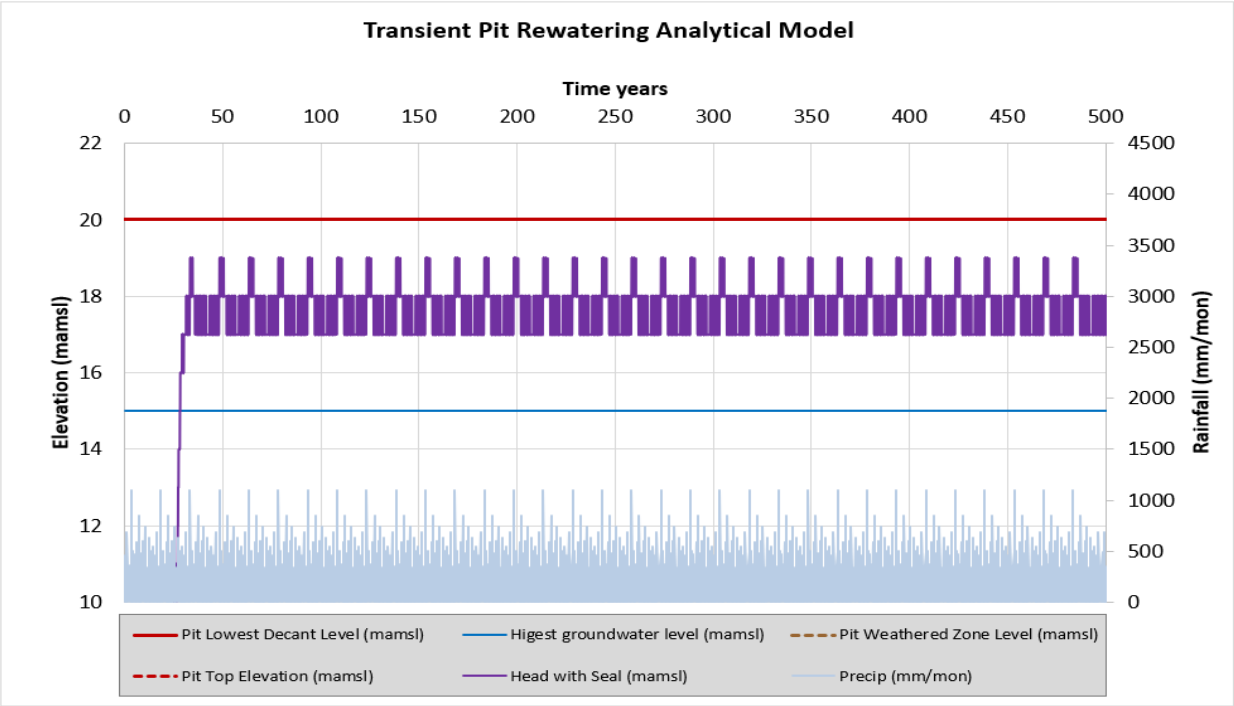

Figure 7-2: BP33 Backfilled Box Cut Transient Analytical Rewatering Model with BP33 UG Decant Added

8 GROUNDWATER MONITORING

The current monitoring network at BP33 is considered sufficient to measure if potential impacts occur from the proposed deep UG mining. It is recommended that the conceptual monitoring bores shown in Figure 8-1 be proactively drilled if the measured drawdown trend in the current monitoring bores is projected to exceed the simulated drawdown, as indicated by the simulated ZOI.

The boreholes can be either a) drilled from surface and subjected to packer testing, and a VW Pin installed to monitor the hydraulic head of the deep aquifer, or b) testing can be conducted during the operational phase and deep VW Pins, and packer testing can be conducted from underground stopes.

The position of bores shown in Figure 8-1 are only proposed. The bore locations should be drilled in identified impact zones informed by monitoring data. The exact drilling targets should be potential preferential flow pathways, to be verified by surface geophysical surveys.

Should the additional bores at BP33 be drilled, it is recommended that they be sampled for chemical and isotopic analyses. The monitoring protocol should allow laboratory analysis of Electrical Conductivity (EC) and/or Total Dissolved Solids (TDS) at different depths to verify whether salinity increases with depth.

These additional (5 maximum) monitoring bores should be installed as nested bores, targeting the shallow (1– 6 m deep), intermediate (10 – 50 m deep), and deep (> 150 m) aquifers. Bores should be installed in stages, targeting specific zones where the measured impact trend exceeds the simulated ZOI. The conceptual monitoring bores should act as sentinel monitoring systems for the GDEs.

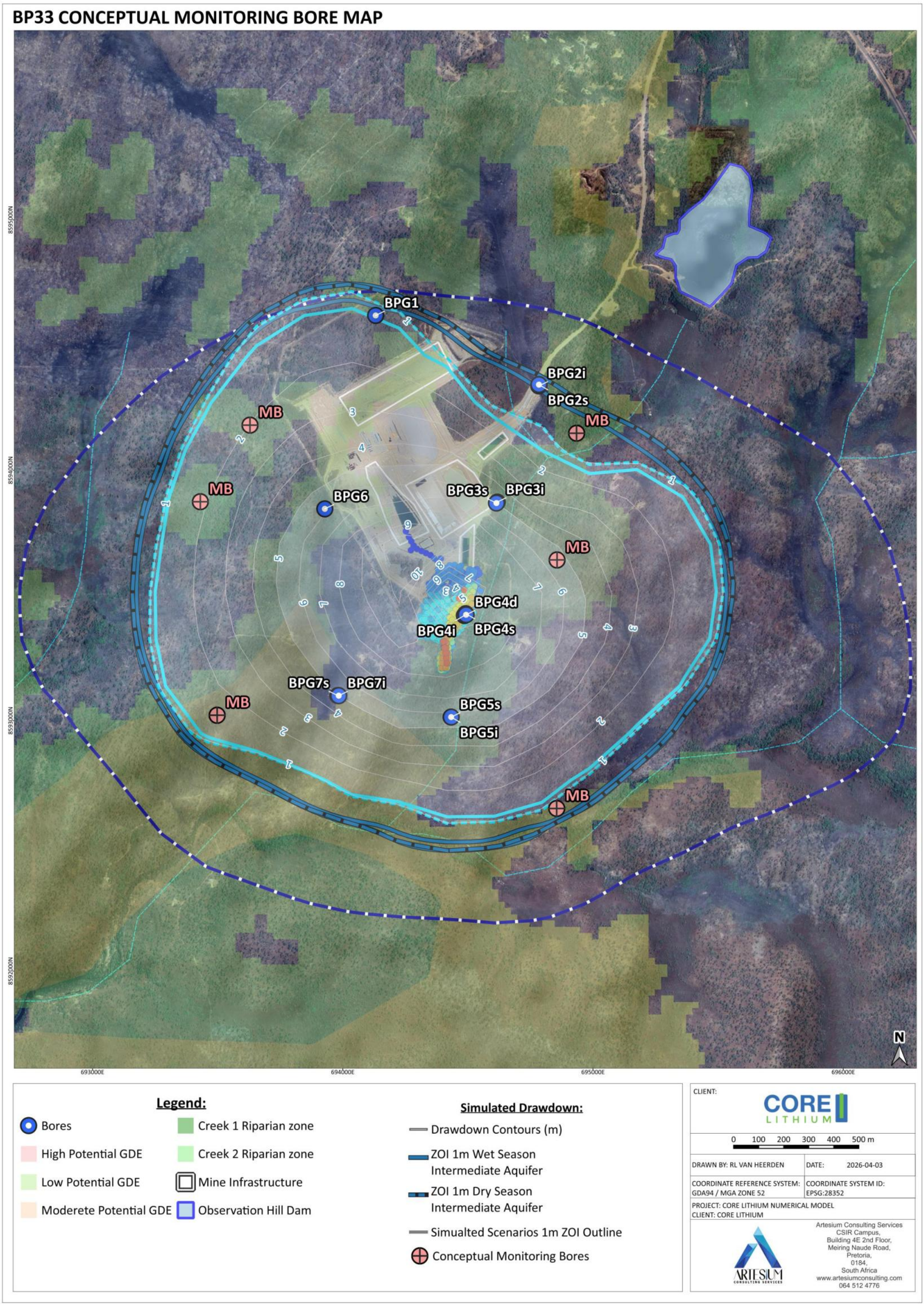

Figure 8-1: BP33 Conceptual Monitoring Bore Placement Map

9 CONCLUSIONS

From the findings of the model update, the following conclusions were made:

1. Long-term groundwater monitoring at the Grants Open Pit (2017–2025) and BP33 Box Cut (2020–2025) indicates that groundwater systems in the shallow zone at both sites are dominated by natural seasonal variability, with pre-mining water level fluctuations of approximately 5 – 6 m and ranges of up to 10 – 12 m in groundwater level. Despite sustained mining-related dewatering (approximately 600 – 750 m^3/d at Grants and 340 m^3/d at BP33), no measurable drawdown exceeding baseline seasonal variability was measured, indicating a limited zone of influence generally constrained to <400 m of the activity and largely occurring within the intermediate and deep aquifer systems, with negligible effect on shallow groundwater. At Grants, water levels have shown a net rise associated with wet climatic conditions and have stabilised towards quasi-steady-state behaviour. Short-term declines observed at BP33 are attributable to seasonal dry-period effects rather than development-induced changes. Observed vertical head differences (0.25 – 15.40 m) and nested bore responses confirm a hydraulically semi-disconnected system among shallow, intermediate, and deep aquifers, despite the absence of a distinct confining layer, thereby limiting vertical hydraulic connectivity and constraining the propagation of mining-induced drawdown.

2. The simulated fissure dewatering rates at BP33 included base-case dewatering rates peaking at ±1 696 m^3/d approximately 75 months into mining, declining to a rate of ±1 100 m^3/d as aquifer storage is depleted. The average life-of-mine dewatering rate simulated was 1 139 m^3/d. The high-case scenario indicates higher sustained inflows, peaking at 2 235 m^3/d and stabilising at a rate of 1 600 m^3/d. The BP33 box cut contributes comparatively low inflows, peaking at 260 m^3/d before the UG is developed, then reducing to an average fissure inflow of approximately 51 m^3/d.

3. The simulated ZOI for BP33 underground mining, defined by a 1 m (cutoff) boundary, extended across the shallow, intermediate, and deep aquifers at LoM, with various low-potential GDEs intersected to the south and north of the mine in the shallow aquifer. In the shallow aquifer, the ZOI extended ±2.25 km east–west and ±2.1 km north–south (±345 ha), with a maximum simulated drawdown of ±10 m confined to the decline footprint. The intermediate aquifer exhibited a slightly larger extent of approximately 395 ha, while the deep aquifer, where the bulk of underground mining is to occur, expanded significantly to ±685 ha with the deep cone extending ±3.5 km east–west and ±2.5 km north–south. No known groundwater users are currently located within either the intermediate or deep simulated impact zones at BP33.

4. Simulated groundwater discharge to drainages within the model domain decreases from a mean of 27 181 m^3/d under no-mining conditions to 24 564 m^3/d during active mining, representing an overall reduction of 10%. Not all drainages are associated with groundwater-dependent ecosystems (GDEs), and the mean annual impact on low- and moderate-potential GDEs was negligible at a <2% reduction for wet and dry seasons.

10 RECOMMENDATIONS

The following is recommended from the findings of the investigation:

1. The current monitoring network at BP33 is considered sufficient for gauging the impact from additional mining; the conceptual monitoring bores are therefore proposed in the circumstance that measured drawdown trends in the existing monitoring bores indicates exceedance of the simulated drawdown, and the ZOI is observed to intersect a GDE.

2. Hydraulic testing needs to be conducted up to the final depth of the proposed underground workings at BP33 mine (-787 mamsl). There may be deep-seated fractured zones that are not characterised by hydraulic testing (i.e., packer lugeon testing). Testing can be conducted either prior to the advancement of underground infrastructure or during operations from underground stopes.

3. The model should be updated annually, incorporating newly recorded site data and verifying and correlating model results. Including, but not limited to, the data collected from the newly installed depth-specific monitoring of hydraulic heads.

11 REFERENCES

1. Ahmad, M. & Hollis, J.A., 2013. Pine Creek Orogen: Geology and Mineral Resources. Northern Territory Geological Survey, Special Publication 5.

2. Australian Mining (2024). BP33 shines for Core Lithium. Australian Mining, [online] Available at: https://www.australianmining.com.au/bp33-shines-for-core-lithium [Accessed 6 Aug. 2025]

3. Belcher, W.R., Sweetkind, D.S. & Elliott, P.E., 2002. Probability distributions of hydraulic conductivity for hydrogeologic units. USGS WRI 2002-4212.

4. Bureau of Mineral Resources, Geology and Geophysics (BMR) & Northern Territory Geological Survey (NTGS) 1988, Darwin, Northern Territory: sheet SD52-04 [map], 2nd edn, 1:250 000 Geological Map Series (surface geology), BMR, Canberra & NTGS, Darwin.

5. Castendyk, D.N., Balistrieri, L.S., Gammons, C. and Tucci, N., 2015. Modeling and management of pit lake water chemistry 2: Case studies. Applied Geochemistry, 57, pp.289-307.

6. CloudGMS (2018) Development of a groundwater model for the Grants Lithium Project. CloudGMS Report No. V1.0, 20 September 2018.

7. CloudGMS (2019) Grants Lithium Project groundwater model addendum report. CloudGMS Report No. 1.3, 2019.

8. CloudGMS (2021) Finnis Lithium Project BP33 groundwater modelling report. CloudGMS Report No. 3.0, October 2021.

9. Core Lithium Ltd. (2024) Grants Lithium operational water management plan. Report No. 1727-17-C4, May 2024.

10. Dewandel, B. et al. (2017). A simple groundwater balance tool...application to a deeply weathered crystalline aquifer in southern India. Journal of Hydrology.

11. Domenico, P.A. & Schwartz, F.W. (1990). Physical and Chemical Hydrogeology. Wiley, New York.

12. Durand, V., Lachassagne, P., Dewandel, B. et al. (2017). Quantification of the specific yield in a two-layer hard-rock aquifer model. Journal of Hydrology, 551, 328–343.

13. Duvert, C., Lim, H.S., Irvine, D.J., Bird, M.I., Bass, A.M., Tweed, S.O., Hutley, L.B. and Munksgaard, N.C. (2022). Hydrological processes in tropical Australia: Historical perspective and the need for a catchment observatory network to address future development. Journal of Hydrology: Regional Studies, 43, p.101194.

14. Eapaea, M.P., Parry, D. & Noller, B. (2007). Dynamics of arsenic in the mining sites of Pine Creek Geosyncline, Northern Australia. Science of The Total Environment, 379(2-3), pp. 201-215.

15. Gallant, J.C., Wilson, N., Dowling, T.I., Read, A.M., Inskeep, C. and Kenyon, C. (2011). 1 second SRTM Derived Digital Elevation Models User Guide. Geoscience Australia, Canberra.

16. GHD (2017) Core Exploration Finniss Lithium Project groundwater investigation report. GHD Report No. 43/22625/02, July 2017.

17. Groundwater Enterprises (2020) BP33 groundwater investigation report. Groundwater Enterprises, November 2020.

18. Groundwater Enterprises (2021) BP33 pumping test report. Groundwater Enterprises, September 2021.

19. HydroAlgorithmics Pty Ltd (2025) AlgoMesh (mesh generation and model-building software). Available at: https://www.hydroalgorithmics.com/software/algomesh.

20. Lachassagne, P. et al. (2021). Review: Hydrogeology of weathered crystalline/hard-rock aquifers. Hydrogeology Journal, 29, 2561–2594.

21. Lee, S., Irvine, D. et al. (2024). A high-resolution map of diffuse groundwater recharge rates for Australia, Hydrology and Earth System Sciences, 28 (7), pp. 1771-1790. DOI: 10.5194/hess-28-1771-2024.

22. Lee, S., Irvine, D. J., Duvert, C., Rau, G. C., & Cartwright, I. (2024). A high-resolution map of diffuse groundwater recharge rates for Australia. Hydrology and Earth System Sciences, 28(7), 1771–1790. DOI: 10.5194/hess-28-1771-2024.

23. Maréchal, J.C. et al. (2015). Determining the vertical evolution of hydrodynamic parameters in weathered and fractured south Indian crystalline-rock aquifers. Hydrogeology Journal, 23(4).

24. NASA Jet Propulsion Laboratory (JPL). (SRTM, 2013). Shuttle Radar Topography Mission (SRTM) Version 3.0 Global 1 Arc-Second Data. NASA Earthdata. Available at: https://www.earthdata.nasa.gov/news/nasa-shuttle-radar-topography-mission-srtm-version-3.0-global-1-arc-second-data-released-over [Accessed 14 April 2025].

25. Needham, R. S., P. G. Stuart-Smith, and R. W. Page. "Tectonic evolution of the pine creek inlier, northern territory." Precambrian Research 40 (1988): 543-564.

26. Prudic, D.E. (1991). Estimates of hydraulic conductivity from aquifer-test analyses and specific-capacity data, Gulf Coast regional aquifer systems, south-central United States (Vol. 90, No. 4121). US Department of the Interior, US Geological Survey.

27. Queensland Government Department of Environment and Science (2025) SILO – Get Point Data. Available at: https://www.longpaddock.qld.gov.au/silo/point-data/ (Accessed: 6 August 2025).

28. Riveros-Iregui, D. et al. (2022). Sustainability of groundwater resources of weathered and fractured schists in the rural areas of Galicia (Spain). Environmental Earth Sciences, 81, 147.

29. Steyl, G. (2011). Estimation of Representative Transmissivities of Heterogeneous Aquifers. University of the Free State. Available at: https://scholar.ufs.ac.za/items/3b7ac488-c1b5-445e-82a4-186e04337079.

30. Tickell, S.J., Cobban, D. & Baird, C.B. (2023). Groundwater Management Zones in Darwin Rural. Northern Territory Department of Environment, Parks and Water Security, Water Resources Division Technical Report 20/2023, Darwin.

12 APPENDIX A: NUMERICAL MODELLING ASSUMPTIONS, MATERIAL PROPERTIES AND CALIBRATION

12.1 Conceptual Numerical Modelling Methodology

A three-dimensional numerical groundwater flow and transport model was developed using FEFLOW (Finite Element subsurface FLOW system), a widely accepted finite-element simulation package produced by DHI Group, Denmark. FEFLOW is extensively used internationally for modelling groundwater flow, solute transport, variably saturated conditions, density-dependent processes, and coupled groundwater–surface water interactions (DHI, 2023). The software is regarded as one of the most robust and numerically stable groundwater simulators available, particularly suited for complex geological environments and irregular geometries due to its flexible element discretisation (Trefry & Muffels, 2007).

The numerical model was constructed based on the conceptual hydrogeological understanding of the site, including stratigraphy, aquifer zonation, hydraulic parameters, groundwater inflows/outflows, and boundary conditions. The conceptual model informed all layer definitions, hydraulic conductivity distributions, recharge zones, and boundary representations, following international best practice (Anderson, Woessner & Hunt, 2015).

A triangular prism finite-element mesh was generated (refer to Figure 12-1), consisting of:

- 1 482 984 mesh elements;
- 760 892 nodes;
- 43 layers and 44 slices;
- Approx. 106 727 elements per layer;
- Total model area of 1.85521e+8 m^2 and a domain volume: 1.887e+11 m^3.

Mesh quality checks indicated 0% Delaunay-violating elements and no interior holes, confirming a stable, high-quality mesh. The mesh resolution was refined around key mining areas to provide an appropriate resolution for simulating impacts on down-gradient receptors. The mesh was generated with ALGOMESH (HydroAlgorithmics, 2025).

Dirichlet Boundary conditions were assigned to perennial rivers, estuaries, and perennial surface water features (Observation Hill Dam) with no restrictions, and to non-perennial drainages with a max flow of 0 m/d, respectively.

Non-linear recharge was incorporated using the calibrated steady-state recharge expressed as a percentage of mean annual precipitation (MAP). The recharge time series was sequenced to represent two distinct datasets: (1) a wet cycle, referenced from the cumulative rainfall departure (CRD) record (refer to Figure 2-3, for long-term CRD trends), which persisted from February 2011 to June 2025; and (2) a dry cycle lasting from

February 1980 to November 1996. These two datasets were designed to represent the effects of wet and dry climatic cycles on receptors under both mining and non-mining conditions, thereby quantifying the cumulative impact of mining activities on groundwater-dependent ecosystems (GDEs).

The model used the standard direct PCG solver for flow simulations.

The model simulates standard (saturated) groundwater flow for unconfined aquifers. The following aquifers (free, phreatic, confined, and dependent) were assigned along the model layers, as summarised in Table 12-1.

Table 12-1: Unconfined Aquifer Descriptions

Model Layer Type	Definition	Uses	Model Slices
Free	Movable slice topping an unconfined layer; surface slice follows the water table. The slice represents the actual water table, and the saturated thickness will vary dynamically, mimicking unconfined behaviour. Storage is calculated from specific yield (Sy), not from confined storage.	Typically used to represent the uppermost geological layer exposed to recharge, seepage, diffused recharge, rivers and evaporation. It can also be applied to pit lakes and natural water tables.	N/A
Phreatic	Fixed slice topping an unconfined layer and is fixed in space. The slice is treated unconfined hydraulically. Saturated thickness can change within this layer, even though the slice itself does not move.	Where vertical movement of the water table is limited and/or where the water table is known to remain close to a stratigraphic contact.	1
Dependent	Subordinate slices below the phreatic/free slice do not define the water table. Their saturation depends on the above slices (inherited unconfined conditions).	Multilayer unconfined systems. Weathered, fractured, fresh rock beneath the water table.	2 - 19
Confined	Fixed slice topping a confined layer, and the slice position remains fixed. Always treated as fully saturated. Storage is calculated from specific storage (Ss).	Aquitards or deep confining layers and/or layers that will always remain saturated.	19 - 43

12.2 Model Calibration Methodology

Both the Australian Groundwater Modelling Guidelines and ASTM D5447-04 define calibration not as curve-fitting, but as an iterative process of refining the conceptual and numerical representation of the groundwater system until the model reproduces *observed system behaviour* to a degree consistent with the study objectives (ASTM, 2010). The objective of the project was to provide dewatering rates and potential zones of influence for the planned expansion of the UG workings BP33 by updating CloudGMS's previously developed numerical model. Even though the focus was to update the existing model, this study was still undertaken following the numerical model guidelines and project flow (Figure 6-1) as set out in Barnett et al., (2012).

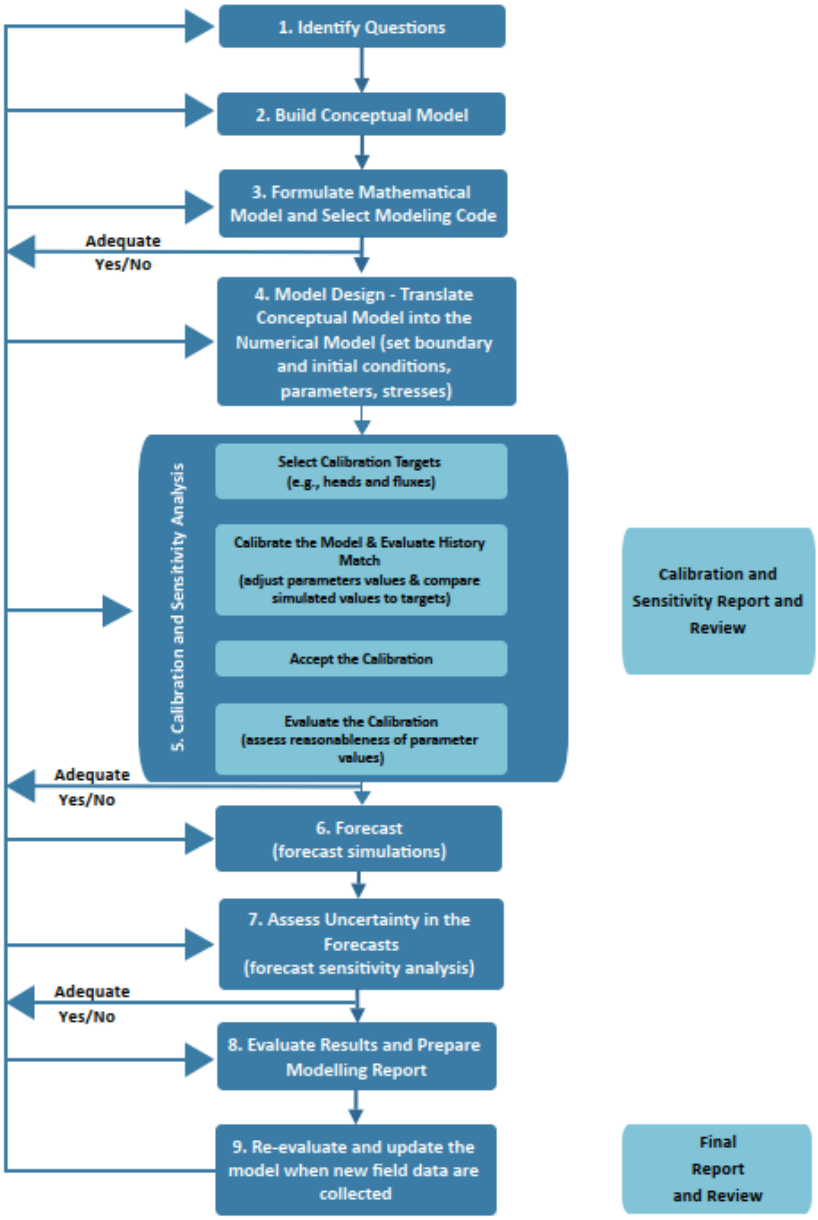

Figure 12-1: Groundwater Modelling Process Flow Diagram adapted from Barnett et al., (2012)

When assumptions were made or reference values used, a conservative approach[2] was followed aligned with the precautionary principle (NEMA, 1998). A groundwater model is a representation of the real system. It is therefore an approximation, and the level of accuracy depends on the quality of the data that is available. The purpose of the model was not to simulate the actual field conditions (i.e., every dyke and fracture), but to simulate the system behaviour with an acceptable level of confidence.

12.2.1 Steady State Calibration

Australian (Barnett et al., 2012) and American (ASTM, 2010) practices emphasise pattern reproduction rather than point-by-point head matching. The model must demonstrate that it can simulate the observed aquifer response, ideally pre-mining under steady-state (SS) conditions and during stress (operational phase). The level of calibration, effort, parameter complexity, and performance assessment must be commensurate with the decision being supported (e.g. dewatering impacts, baseflow depletion, pit lake evolution). ASTM (2010) explicitly notes that calibration does not guarantee uniqueness, and that confidence in predictions is increased through verification, sensitivity analysis, and transparent documentation, rather than through any single goodness-of-fit metric.

Calibration adjustments must remain within reasonable ranges (e.g. <10% RMSE) defined by field and laboratory data. Both trial-and-error and inverse methods are acceptable, provided:

- Parameter ranges are justified;
- Adjustments are traceable;
- Unrealistic compensating errors are avoided; and
- Steady-state calibration methodology.

According to (ASTM, 2010) guidelines steady-state calibration is appropriate when:

- A quasi-equilibrium condition is physically plausible (pre-mining);
- The objective is to represent long-term average conditions or pre-development heads;
- The steady-state solution will be used to initialise a transient model and measure the impact of stress on pre-mining conditions; and
- ASTM notes that steady-state models do not require initial conditions, but they do require careful justification of boundary conditions and recharge assumptions.

2 Conservative means that dewatering rates or environmental impacts are not underestimated. This means that in some cases more than one scenario or sensitivity analyses could be run to demonstrate ranges of modelled outputs.

Preferred steady-state calibration targets:

- Spatially distributed hydraulic heads;
- Hydraulic gradients and flow directions;
- Vertical head differences where leakage is important; and
- Integrated fluxes (e.g. regional water balance, spring/baseflow discharge).

A defensible steady-state calibration typically proceeds as follows:

- Boundary condition validation.
- Ensure boundaries represent natural controls where possible and are sufficiently distant to avoid artificial constraint.
- Recharge and discharge consistency.
- Recharge estimates must be consistent with climate, geology, and independent studies. Water balance closure is a required check.
- It is acceptable to remove up to e.g. 5% of outlier data points where measurement impediments e.g. suspected clogged or collapsed borehole or measurement errors are suspected in the data cleanup process.

The model was calibrated in steady state with pre-mining hydraulic heads measured during previous fieldwork investigations. The calibrated pre-mining SS water balance and operational phase water balance is shown in Table 12-2.

Table 12-2: Summarised Calibrated Steady State Pre-mining Model Water Balance

Component		Pre-mining	
		Model Domain	
		Inflow (m^3/d)	Outflow (m^3/d)
1	Recharge	18 986	
4	Baseflow		-13 275
6	Perrenial Rivers	367	-6 041
6.1	Obs hill dam	169	-107
6.2	BP33 Existing Pit Lake		-105
7	Grants Open Pit		
8	BP33 Box Cut		
	Total	**19 522**	**-19 527**
	Balance	**-4**	
	Balance Error (%)	**0%**	

The measured pre-mining groundwater levels for Grants were referenced in the SS calibration and stretched from June 2017 to January 2022. At BP33 water levels were first measured in October 2022 and the Box Cut construction commenced in August 2023. The average observed water levels across these time periods for the mines were referenced for steady state calibration and the simulated vs measured hydraulic heads are summarised in Figure 12-2 and Figure 12-3.

The calibration achieved a Root Mean Square Error (RMSE) of 7.67% and a Standardised Root Mean Square Error (SRMS) of 11.63%. After 4 bores were removed from the calibration statistical calculation, the calibration statistics improved with an RMSE of 5.48 and 8.45% SRMS (refer to Figure 12-2, and Table 12-4). The RMSE measures the absolute magnitude of errors between observed and simulated values. The method for evaluating model calibration penalises large errors by squaring them. The SRMS is a normalised version of the RMSE, obtained by dividing the RMSE by the standard deviation of the observations.

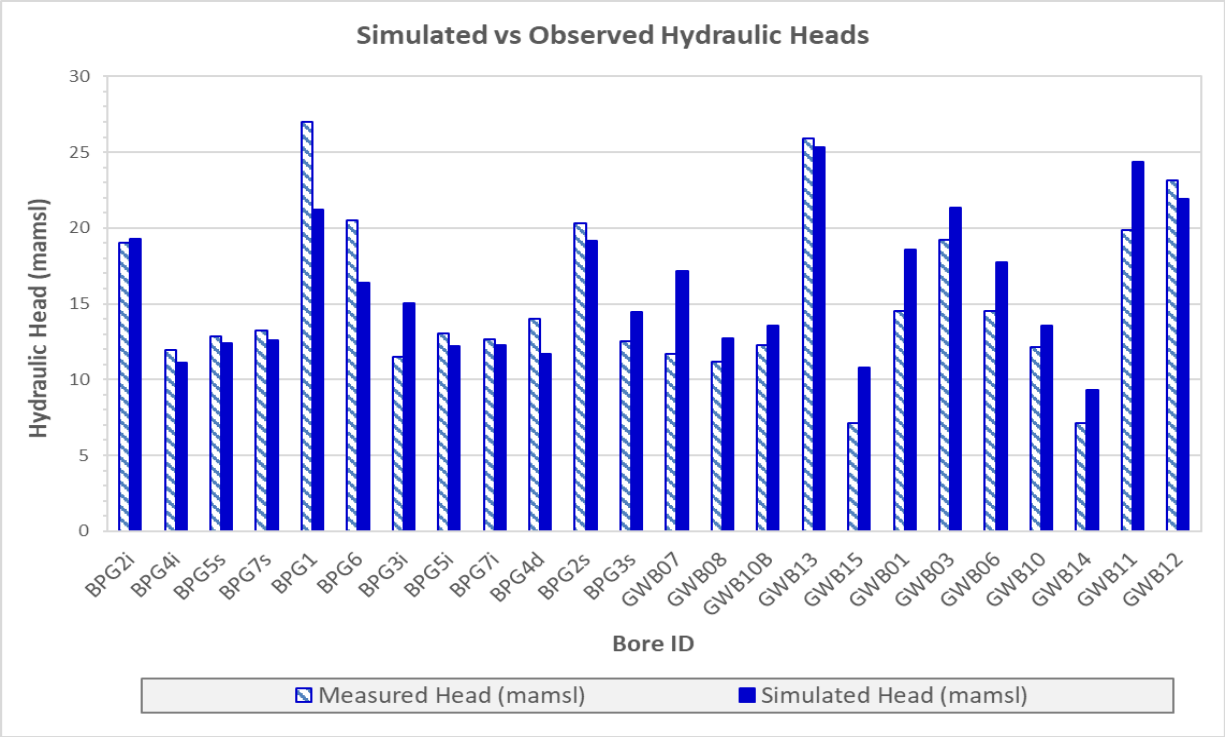

Figure 12-2: Steady State Simulated vs Measured Hydraulic Heads for Bores

The simulated vs observed hydraulic heads are shown in Figure 12-2. The R^2 value of 0.70 indicates that 70% of the variance in hydraulic head is explained by the model. This result is indicative of a moderate to good calibration of regional gradients, with local variance not excellently presented. Most of the heads plotted below the 1:1 line, indicating slight underprediction of heads in higher-lying areas.

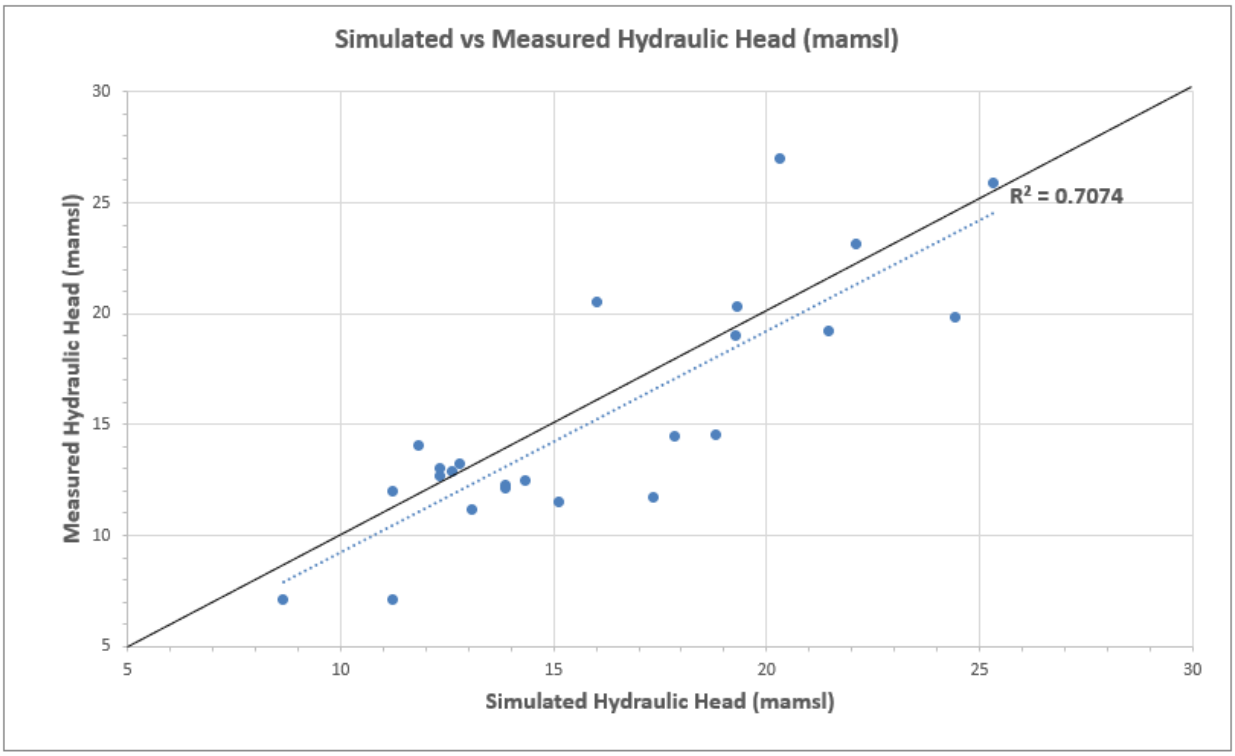

Figure 12-3: Steady State Simulated vs Observed Hydraulic Heads Correlation

The model was therefore considered adequately calibrated under steady-state conditions and ready for transfer to transient simulation or calibration. A list of assumptions and data certainty is summarised in **Table** 12-3 for the steady state model calibration.

Table 12-3: Steady State Model Limitations and Assumptions

Input parameter	Source, Parameter, or Assumption Description	Data Uncertainty
Topography (DEM)	SRTM topography data was used and cross-referenced Gallant et al. (2011), SRTM provides a vertical accuracy of ±9.8 m at 90% confidence	Low
Rivers, streams, drainages	Generated from the model DEM, to ensure drainages are placed at appropriate low-lying places in the model topography.	Low
Lithology	The regional and local geology, derived from the 1:250 000-scale geological map (SD 52-4 Darwin, 1988) and cross-reference from previous reports and literature.	Moderate
Weathered Zone Thickness	Derived from previous model conducted.	Moderate
Geological structures	Only one geological structure was derived for the BP33 mine, and no geological structure were included in the previous model.	High
Neighbouring Boreholes and pumping rates	From the previous report, no groundwater users were reported within the vicinity of the Grants or BP33 mines The only groundwater receptor would be the Groundwater dependent ecosystems and riparian zones along the drainages.	Moderate

Input parameter	Source, Parameter, or Assumption Description	Data Uncertainty
Current (As built) surface facilities	The current Grants Open Pit and Box Cut was given by the client as detailed surveyed data.	Low
Future LoM plans Schedules	The LoM schedules for the underground at Grants and BP were provided in excel format as requested.	Low
LoM Backfill Schedules	The backfill schedules were provided in excel format and had to be reworked into volumes with depth over time.	Moderate
Grants Pit Dewatering.	Three months of complete data sets (when referring to the data on a monthly scale) were derived from the client. The client confirmed that the dewatering rates used in the model was accurate.	Low
Grants pit lake bathymetry measurements	The pit lake water level is measured and given the pit volume stage curves generated was cross-referenced with the data provided by the client and a good fit/correlation was achieved, accurate pit lake bathymetry could be calculated.	Low
Rainfall	The SILO dataset was used for all model calibrations and simulations. On-site recorded data was referenced to be unreliable and needs to be verified.	Moderate
Boundary conditions	Perrenial drainages in the model boundary were represented by BC's with no max or min flow constraint on the boundary condition. The old underground workings (pit lakes) were also represented this way. Non-perrenial drainages and were assigned in the model as BC's with max flow of 0 m^3/d.	Low
Recharge	The recharge across the model domain was calibrated according to the measured monitoring data. The previously applied nett-recharge could not be calibrated with the model parameters previously used in the model.	High
Initial Hydraulic Heads	The initial pre-mining hydraulic heads were recorded with seasonal fluctuations in at Grants, but not at BP33.	Moderate
Shallow Hydraulic Conductivity Values	Multiple hydraulic tests have been conducted at Grants and BP33, with the modelled hydraulic conductivities calibrated towards the harmonic mean.	Moderate
Deep Hydraulic Conductivity Values	There was no packer or pump test data available for the deeper >150 mamsl, and the hydraulic conductivities were extrapolated with depth	High

Table 12-4: Steady State Pre-model Calibration Hydraulic Heads Statistical Summary

Obs no	Site name	X	Y	Z (mamsl)	Slice	Measured Head (mamsl)	Simulated Head (mamsl)	Residual Error Above or below actual (m) - RE	Absolute Error (m) - AE	Root Square Error (m) - RSE
1	BPG4s– Removed	694 491.50	8 593 426.80	15.00	4	19.02	19.27	-0.24	0.24	0.06
2	BPG2i	694 783.70	8 594 336.40	20.75	7	11.97	11.10	0.87	0.87	0.76
3	BPG4i	694 486.00	8 593 419.50	15.00	9	12.86	12.43	0.43	0.43	0.19
4	BPG5s	694 433.30	8 593 013.80	15.57	3	13.21	12.62	0.59	0.59	0.34
5	BPG7s	693 980.40	8 593 099.80	15.00	4	26.98	21.24	5.74	5.74	32.95
6	BPG1– Removed	694 131.50	8 594 618.00	31.63	6	20.52	16.39	4.13	4.13	17.02
7	BPG6	693 928.50	8 593 845.60	25.00	10	11.50	15.05	-3.55	3.55	12.63
8	BPG3i	694 617.50	8 593 872.60	14.41	9	13.05	12.18	0.87	0.87	0.76
9	BPG5i	694 433.30	8 593 013.80	15.57	10	12.68	12.27	0.41	0.41	0.17
10	BPG7i	693 984.00	8 593 099.40	15.00	10	14.03	11.71	2.32	2.32	5.38
11	BPG4d	694 492.90	8 593 422.60	15.00	10	20.30	19.15	1.15	1.15	1.32
12	BPG2s	694 784.20	8 594 341.60	20.75	2	12.51	14.43	-1.92	1.92	3.68
13	BPG3s	694 614.30	8 593 868.70	14.41	4	11.72	17.19	-5.47	5.47	29.97
14	GWB07 – Removed	693 665.60	8 598 650.30	17.00	10	11.17	12.75	-1.58	1.58	2.50
15	GWB08	693397.00	8599573.00	15.28	10	12.29	13.53	-1.24	1.24	1.53
16	GWB10B	693371.20	8599562.20	14.40	3	25.92	25.30	0.62	0.62	0.38
17	GWB13	692336.10	8597999.60	29.75	1	7.12	10.79	-3.68	3.68	13.53
18	GWB15	692564.00	8599891.60	8.34	11	14.54	18.55	-4.01	4.01	16.10
19	GWB01	693066.10	8599025.30	20.69	12	19.25	21.34	-2.10	2.10	4.39
20	GWB03	692610.10	8598916.50	22.79	9	14.50	17.74	-3.23	3.23	10.44
21	GWB06	693635.44	8598651.18	17.50	4	12.15	13.53	-1.38	1.38	1.91
22	GWB10	693365.00	8599565.00	14.98	1	7.13	9.31	-2.18	2.18	4.76
23	GWB14	692559.40	8599891.50	8.45	1	19.85	24.36	-4.51	4.51	20.32
24	GWB11– Removed	692925.90	8598064.50	22.86	9	23.13	21.92	1.21	1.21	1.45
25	GWB12	691885.60	8598665.90	26.62	10	19.02	19.27	-0.24	0.24	0.06
					Average	**15.31**	**16.01**	**-0.70**	**2.23**	**7.61**
					Minimum	**7.12**	**9.31**	**-5.47**	**0.24**	**0.06**
					Maximum	**26.98**	**25.30**	**5.74**	**5.74**	**32.95**
					Correlation (R)	**0.83**				

ME	**-0.83**
MAE	**1.68**
RMSE	**5.48%**
SRMS	**8.45%**
Min HH in Model	**-2.00**
Max HH in Model	**35.00**
Sim HH Range	**37.00**
Min HH of Obs	**7.12**
Max HH of Obs	**26.98**
Obs HH Range	**19.86**

***ME: Mean Error**

****MAE: Mean Absolute Error**

*****RMSE: Root Mean Square Error**

******SRMSE: Standardised Root Mean Square Error**

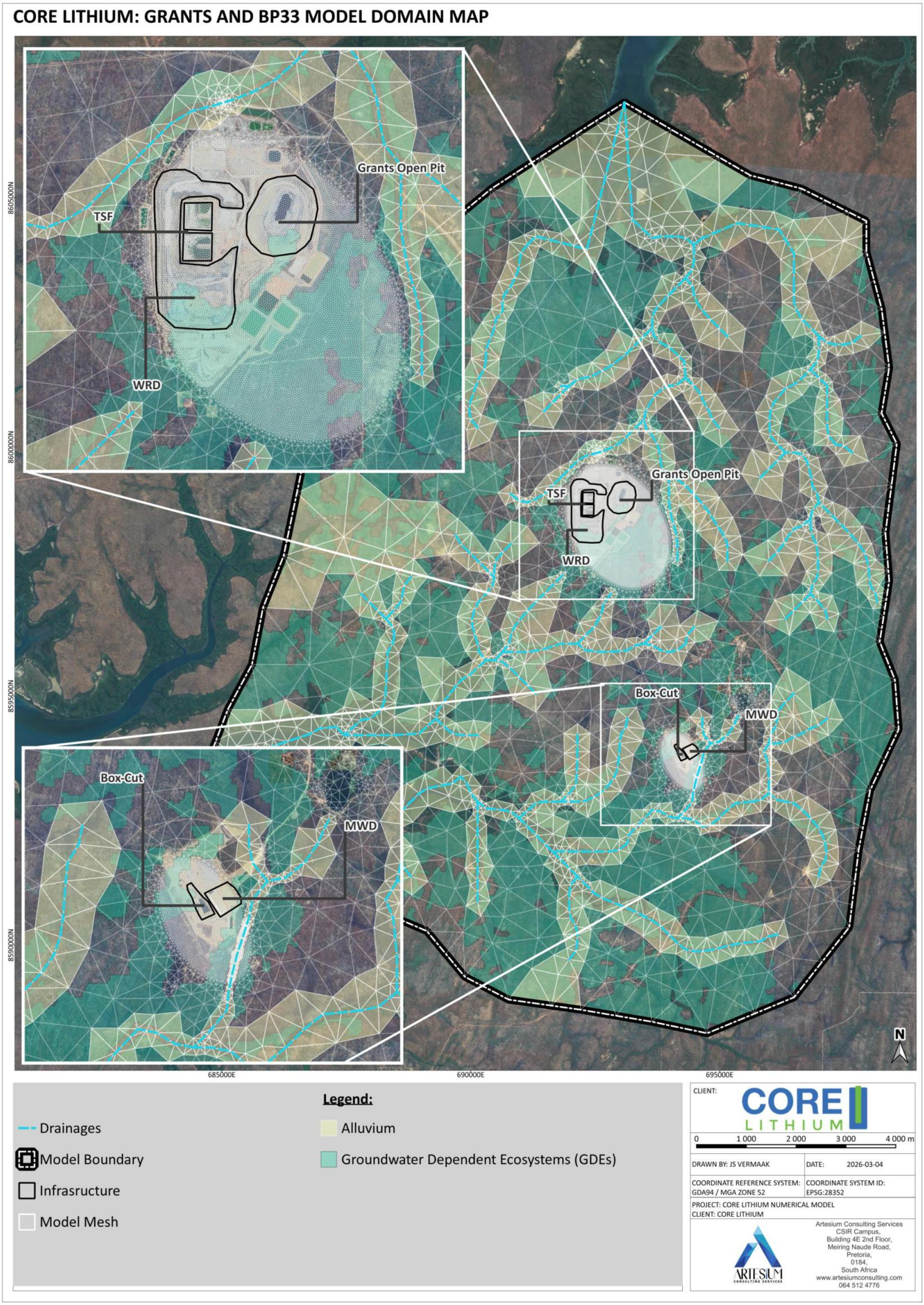

Figure 12-4: Model Domain Map

12.2.2 Transient State Model Calibration

The purpose of the transient calibration is to enable the simulation of seasonal pre-mining water-level fluctuations and transient groundwater/fissure-water inflow rates for the BP33 Box Cut. The introduction of specific storage (Ss) and specific yield (Sy) are parameters added in the transient simulations. The same calibration statistics apply as in the steady-state models, but are calculated from the transient data.

The transient model calibration was conducted from January 2017 to January 2026 (9 years). The Box Cut development times were also referenced by the client, and gave the box cut a short development time (5 months). The Grants open cut was mined linearly. The transient pit dewatering rates, along with the transient measured hydraulic heads, were used as a reference for the transient calibration.

The graph (Figure 12-5) compares simulated transient dewatering rates against average measured groundwater inflows for BP33 Box Cut over a 105-month period.

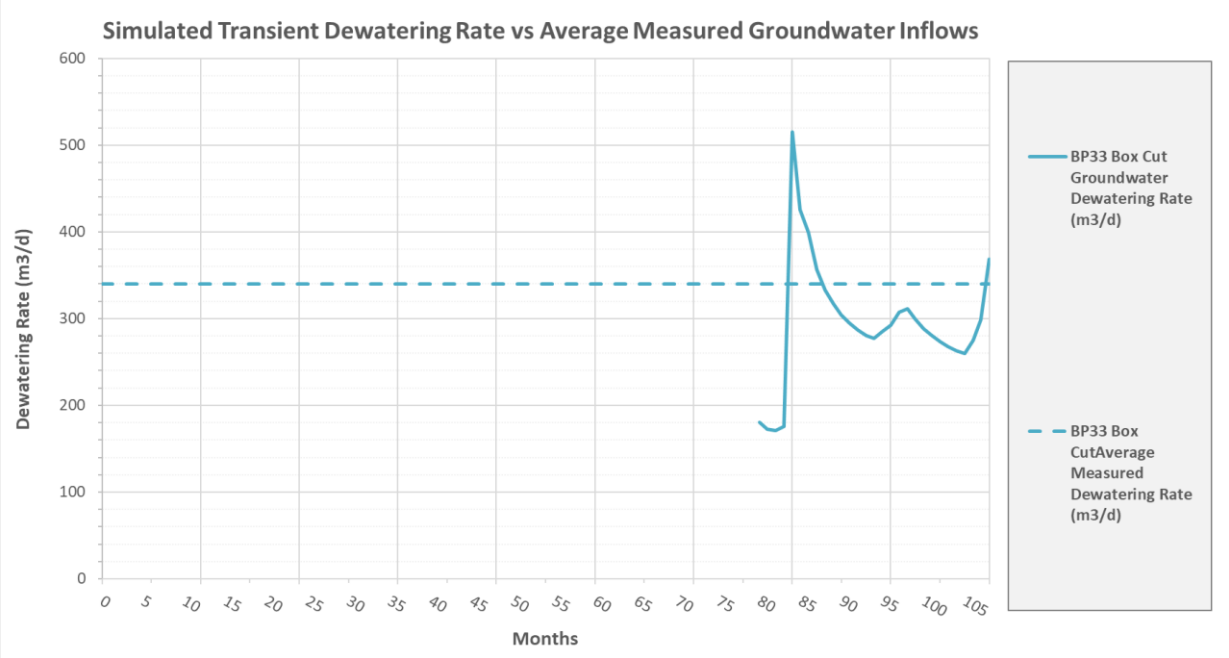

Figure 12-5: Simulated Transient Dewatering Rate vs Average measured Groundwater Inflows

At BP33, the simulated dewatering rate peaked at approximately ±515 m³/d before stabilising in the range of 280 – 350 m³/d toward the end of the calibration period, compared to an estimated average measured dewatering rate of approximately 340 m³/d. While this represents a modest underestimation, the calibration at BP33 is considered satisfactory when assessed against the full suite of calibration targets. In particular, groundwater levels within the upper 40 m below ground level (mbgl) were well reproduced at both BP33, and on this basis the simulated inflow rates at BP33 are regarded as sufficiently calibrated for the purposes of the predictive modelling.

The simulated vs observed hydraulic heads for BP33 bores area summarised in Table 12-5 and Table 12-6 and displayed graphically from Figure 12-7 to Figure 12-9. The transient simulated vs measured figures plot the

measured bore groundwater levels (dots) vs the transient simulated bore water levels (solid line) and error bars (±5 m) to represent the seasonal fluctuations observed in the monitoring data. The graphs show the calibrated parameters of the base case model. The average RMSE for the transient hydraulic head was 2.59% and SRMS was 2.47%. The P95 RMSE was 3.41 and SRMS was 3.26 with the P05 RMSE 2.95% and the SRMS was 2.82%. This indicates that the average water levels along with the seasonal peaks were matched with a sufficient level of calibration.

The simulated ZOI for the current (January 2026) is presented graphically in Figure 12-6 for BP33. The simulated ZOI overpredicts the ZOI relative to the measured groundwater levels in the bores. Given the level of transient calibration for parameters pre-mining and compared to observed dewatering rates at Grants open cut and BP33 box cut, the model is considered sufficiently calibrated. The model's overprediction of ZOI relative to measured values aligns with the precautionary principle and should be used as a tool to assess the maximum possible future impacts.

The primary tool to assess the impact of mining on the underlying aquifers should always be anchored on the measured groundwater levels in the bores (refer to the monitoring protocol as detailed in Section 8).

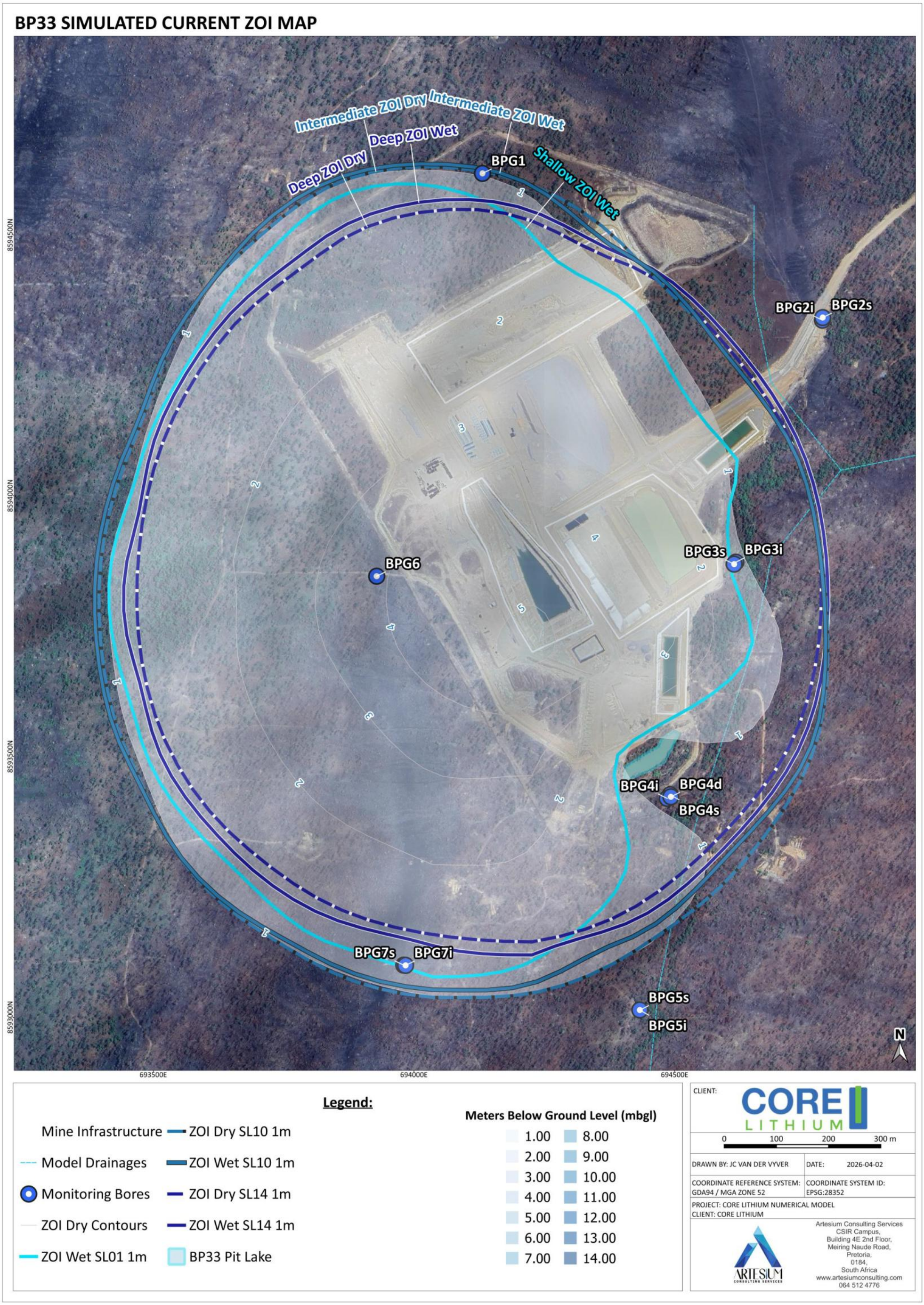

Figure 12-6: Simulated ZOI for the Current Conditions (January 2026) for BP33

Table 12-5: BP33 Transient Hydraulic Head Calibration Statistical Analysis

Avgerage of Bores		BPG1 TS_Cal	BPG1 Meas	BPG2s TS_Cal	BPG2s Meas	BPG2i TS_Cal	BPG2i Meas	BPG3s TS_Cal	BPG3s Meas	BPG3i TS_Cal	BPG3i Meas	BPG4s TS_Cal	BPG4s Meas	BPG4i TS_Cal	BPG4i Meas
P95		23.42	31.82	19.99	21.40	19.90	20.75	14.58	11.77	15.00	14.08	10.04	14.67	11.91	15.10
-2.47%	RMSE	-8.95%		-1.51%		-0.91%		-3.00%		-0.98%		-4.93%		-3.40%	
2.46%	SRMS	8.56%		1.44%		0.87%		2.86%		0.94%		4.71%		3.25%	
Average		20.60	26.62	18.95	19.98	19.03	18.82	13.49	11.12	13.65	11.62	8.73	13.10	10.27	11.43
-2.95%	RMSE	-6.41%		-1.10%		-0.22%		-2.52%		-2.16%		-4.65%		-1.24%	
2.82%	SRMS	6.13%		1.05%		0.21%		2.41%		2.07%		4.45%		1.18%	
P05		18.40	22.85	18.40	18.17	18.43	16.73	12.65	10.37	12.61	6.75	7.59	11.03	8.87	2.55
-6.90%	RMSE	-4.74%		-0.24%		-1.82%		-2.44%		-6.24%		-3.66%		-6.73%	
6.60%	SRMS	4.53%		0.23%		1.74%		2.33%		5.96%		3.50%		6.44%	
	Max Hydraulic Head	33.00	32.20												
	Minimum Hydraulic Head	-60.90	-66.00												
		Simulated	Observed												

Table 12-6: BP33 Transient Hydraulic Head Calibration Statistical Analysis – Continued

Avgerage of Bores		BPG4d TS_Cal	BPG4d Meas	BPG5s TS_Cal	BPG5s Meas	BPG5i TS_Cal	BPG5i Meas	BPG6 TS_Cal	BPG6 Meas	BPG7s TS_Cal	BPG7s Meas	BPG7i TS_Cal	BPG7i Meas
P95		12.44	15.48	13.45	14.94	13.32	15.97	16.46	25.32	14.95	15.11	14.00	15.00
-2.47%	RMSE	-3.24%		-1.58%		-2.83%		-9.44%		-0.17%		-1.06%	
2.46%	SRMS	3.10%		1.51%		2.70%		9.02%		0.16%		1.02%	
Average		10.73	13.78	12.08	12.31	11.83	12.78	12.91	20.00	11.95	12.60	11.59	12.61
-2.95%	RMSE	-3.24%		-0.24%		-1.01%		-7.55%		-0.70%		-1.08%	
2.82%	SRMS	3.10%		0.23%		0.97%		7.22%		0.67%		1.03%	
P05		9.30	11.28	10.66	9.58	10.50	10.14	10.49	15.59	9.87	9.43	9.80	9.88
-6.90%	RMSE	-2.10%		-1.16%		-0.39%		-5.43%		-0.48%		-0.08%	
6.60%	SRMS	2.01%		1.11%		0.37%		5.19%		0.45%		0.08%	
	Max Hydraulic Head	33.00	32.20										
	Minimum Hydraulic Head	-60.90	-66.00										

Table Notes:

Sim: Simulated Hydraulic Head

Meas: Measured Hydraulic Head

RMSE: Root Mean Square Error

SRMS: Scaled Root Mean Square

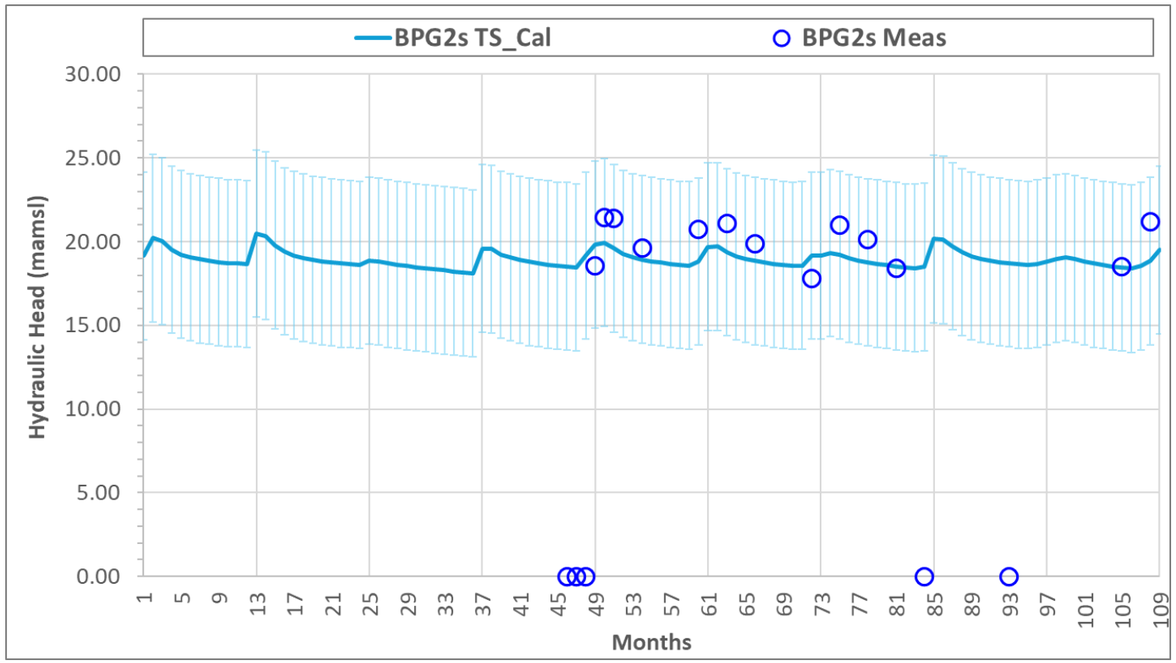

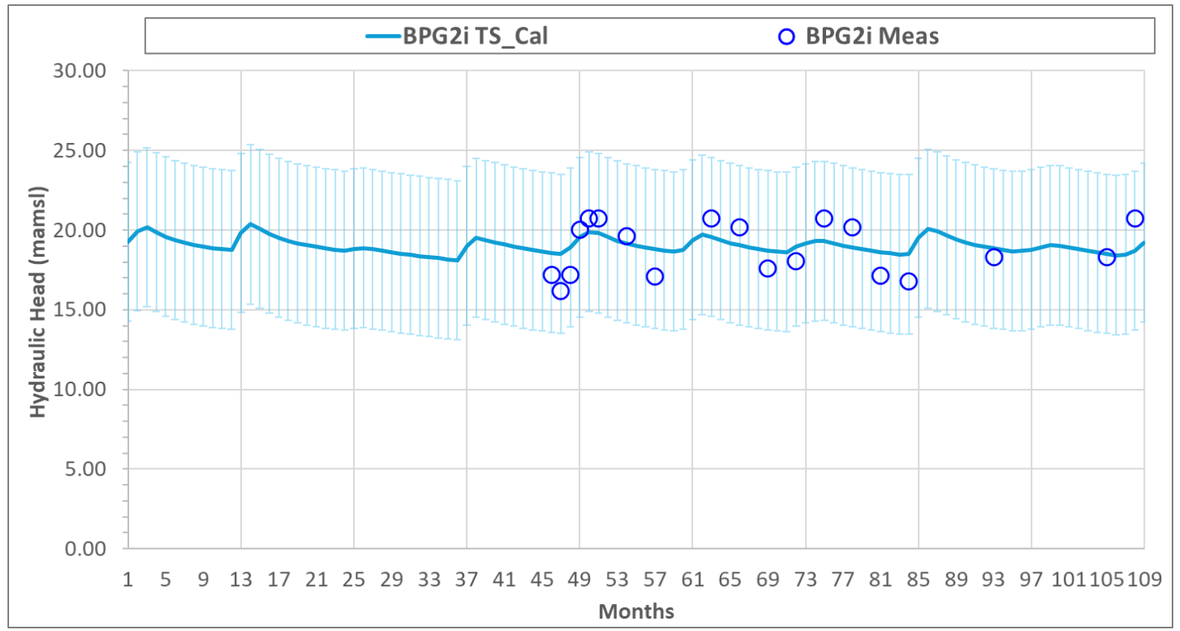

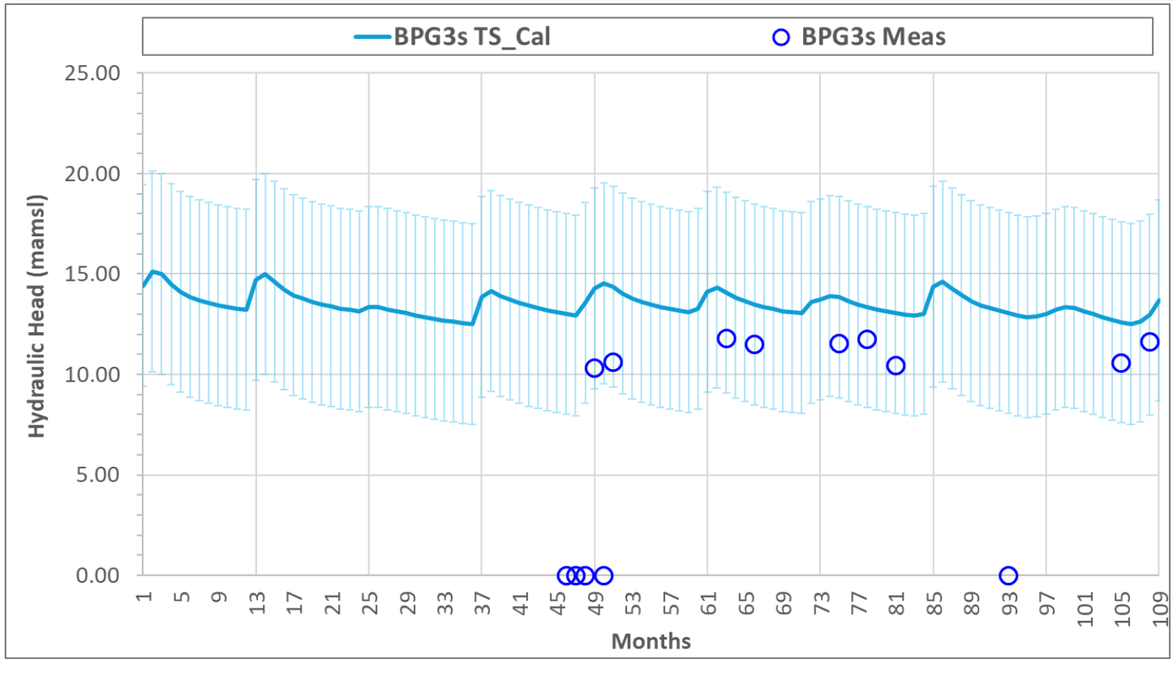

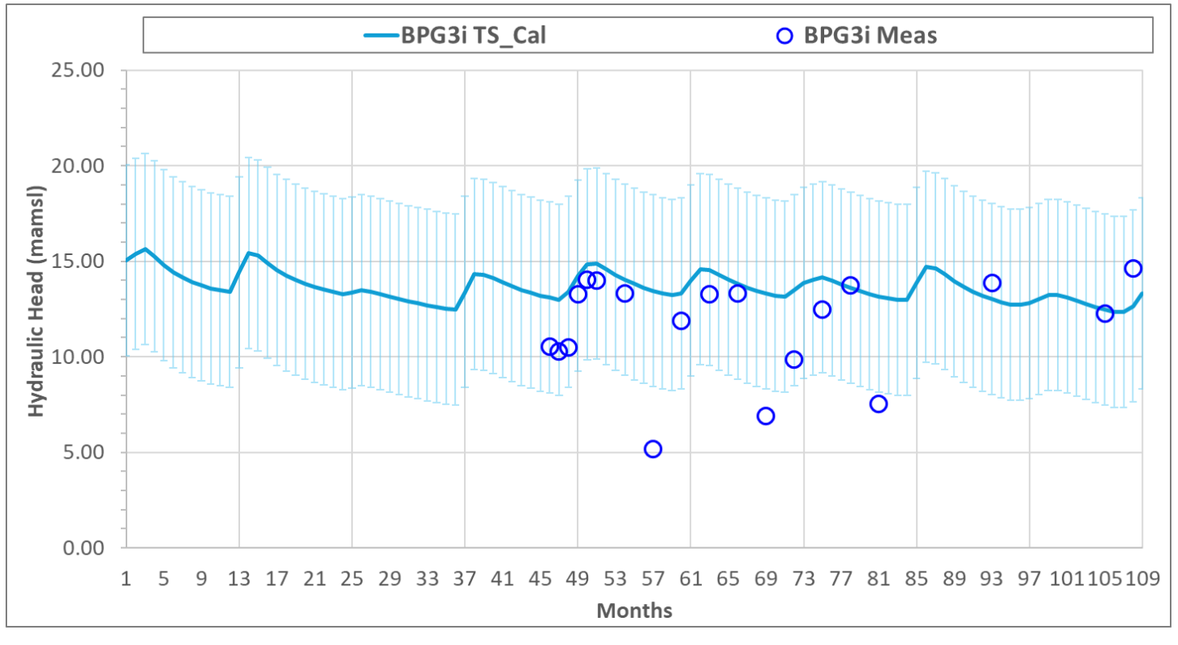

Figure 12-7: Simulated vs Measured Transient Hydraulic Heads for BPG2s, BPG2i, BPG3s, and BPG3i

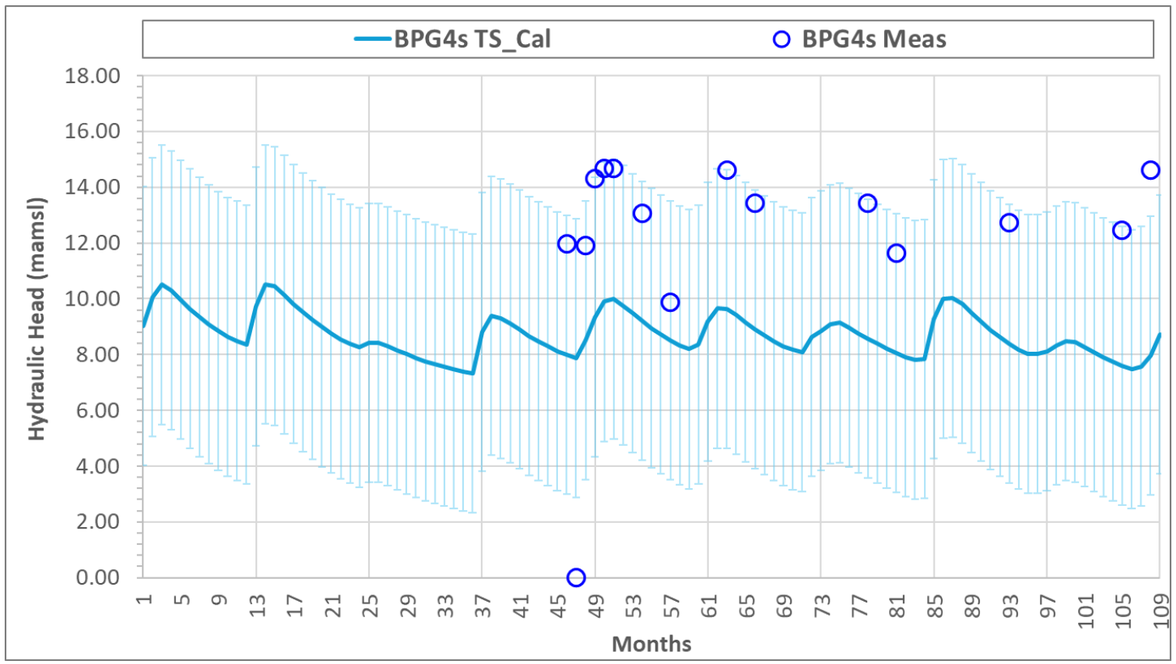

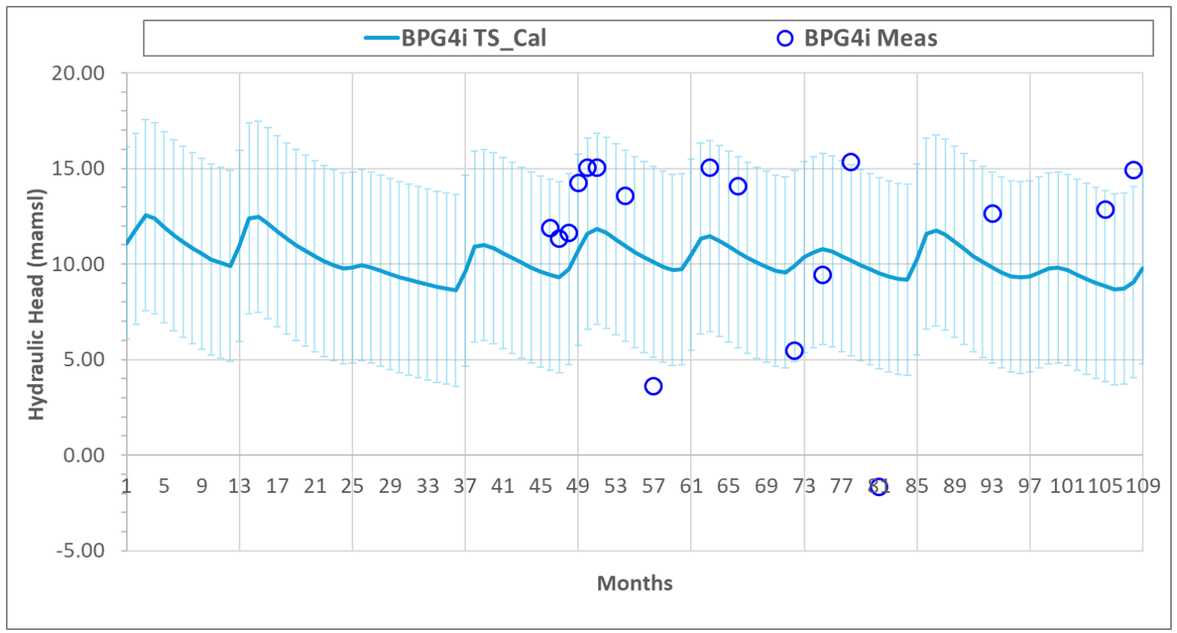

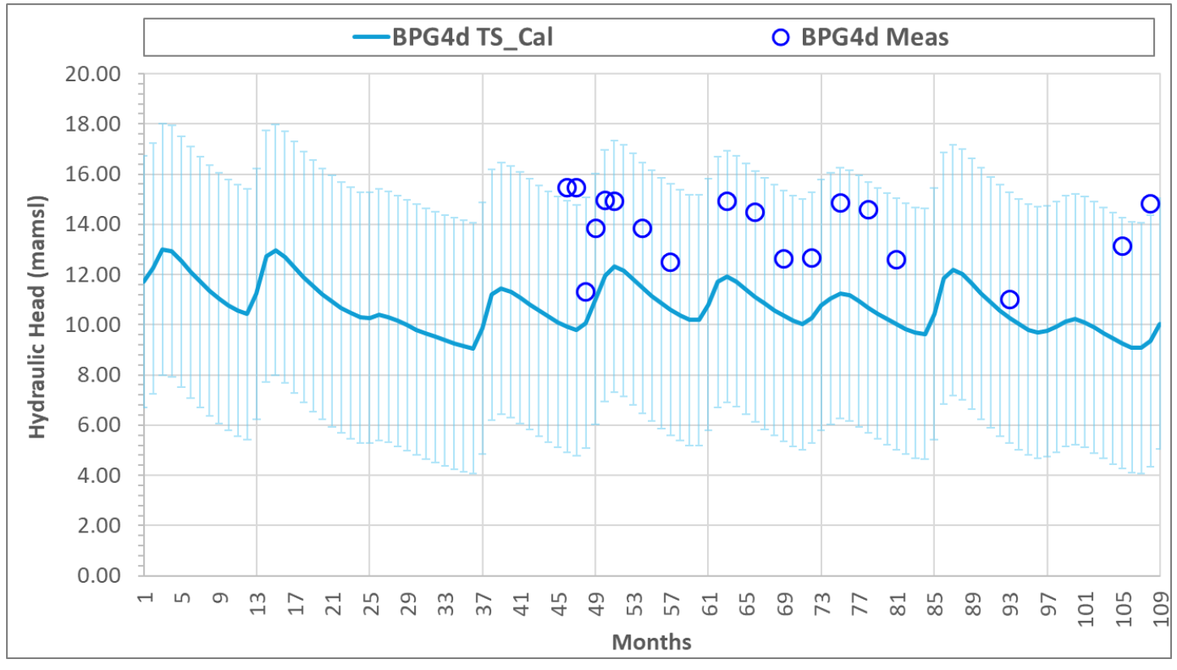

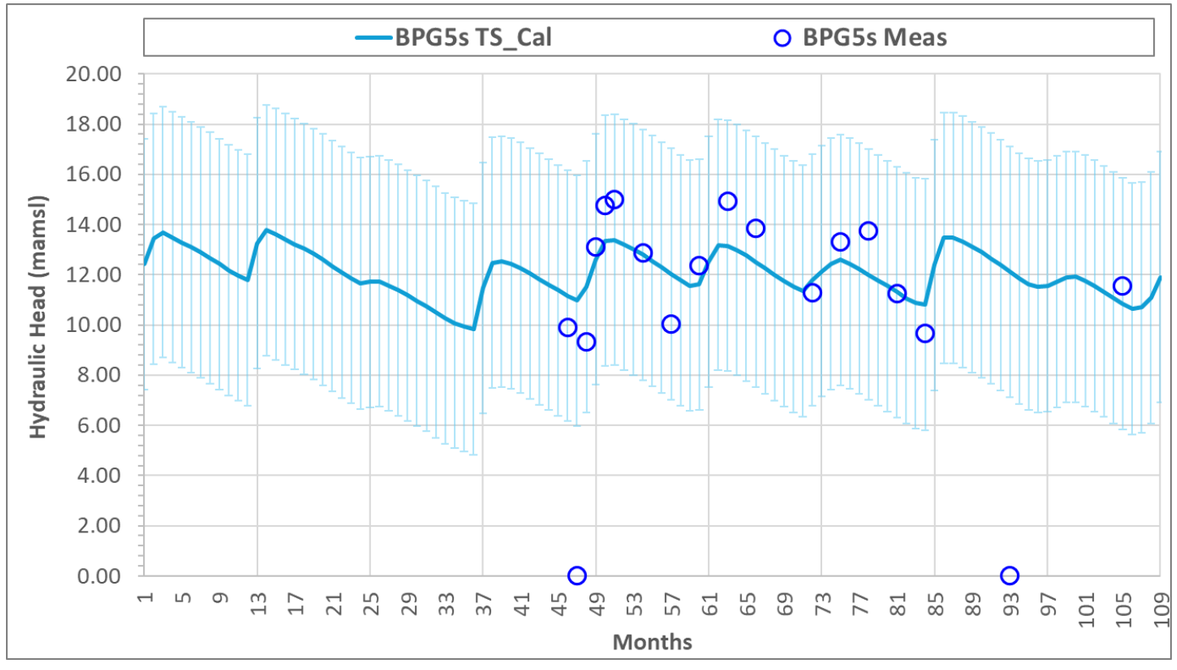

Figure 12-8: Simulated vs Measured Transient Hydraulic Heads for BPG4s, BPG4i, BPG4ds, and BPG5s

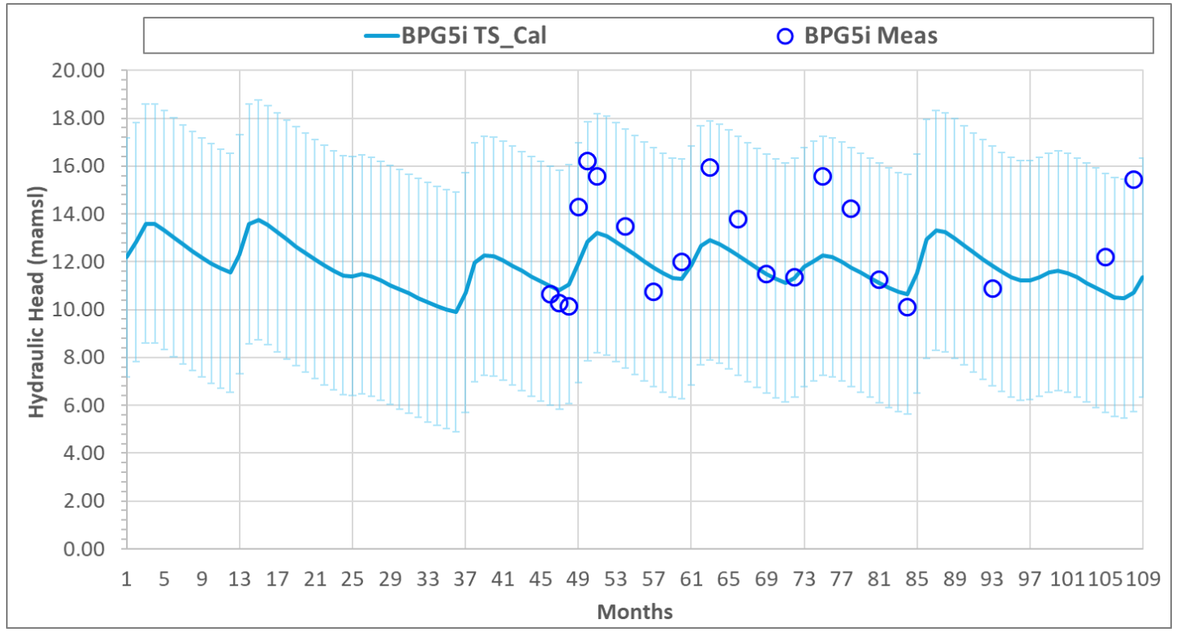

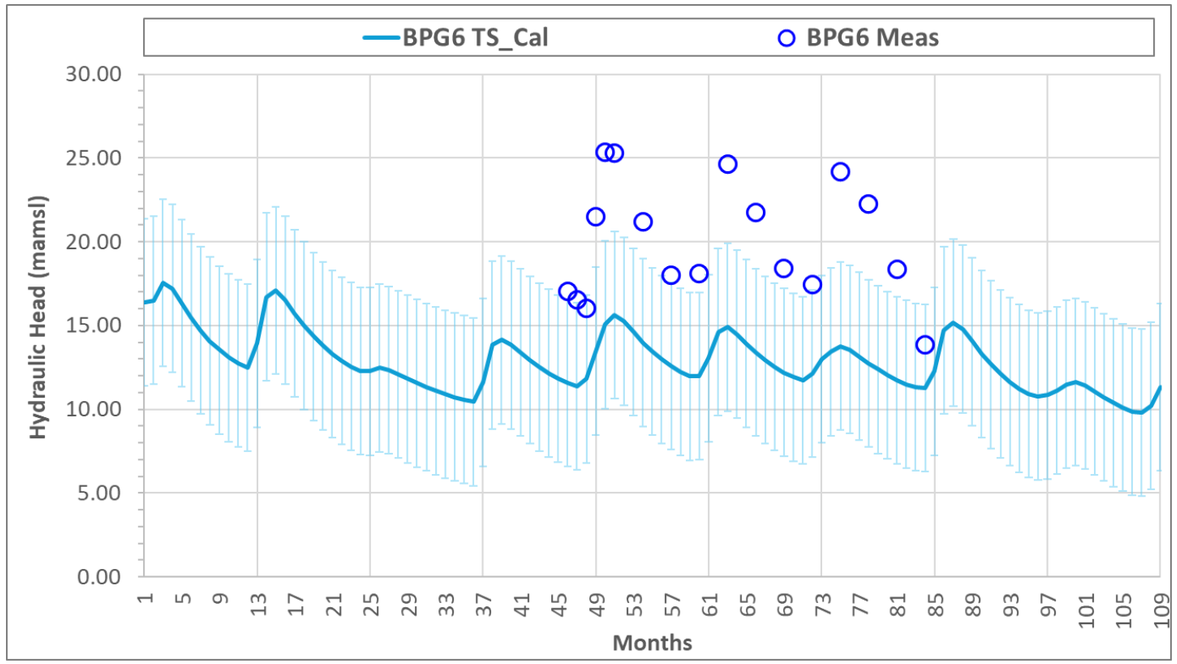

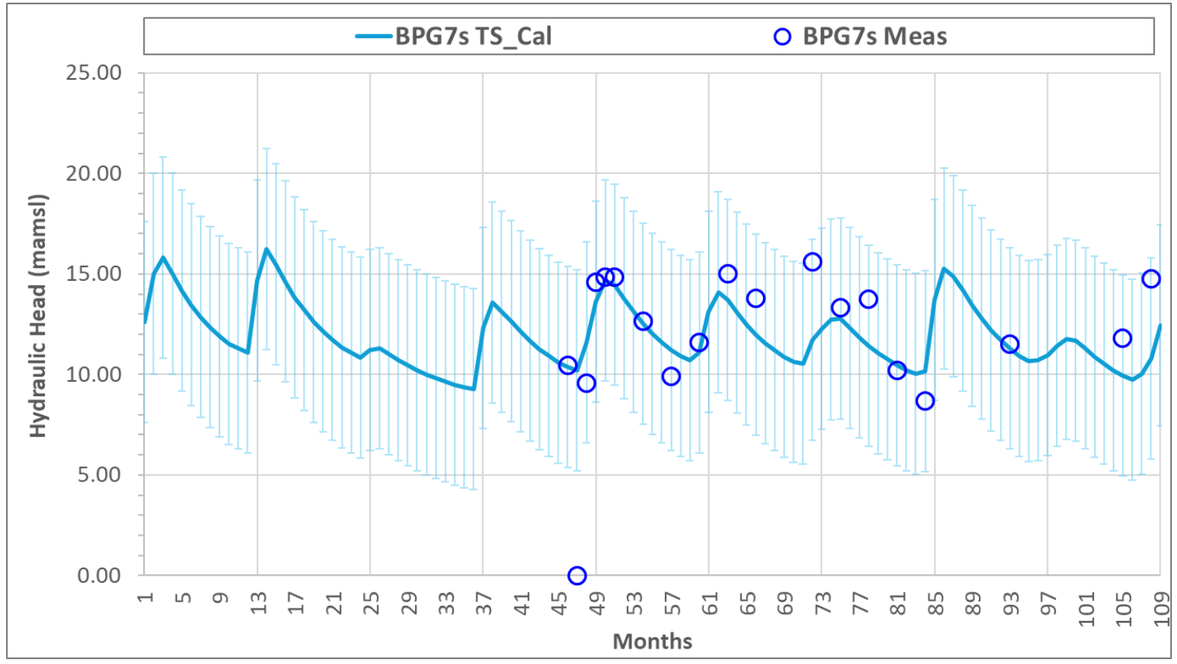

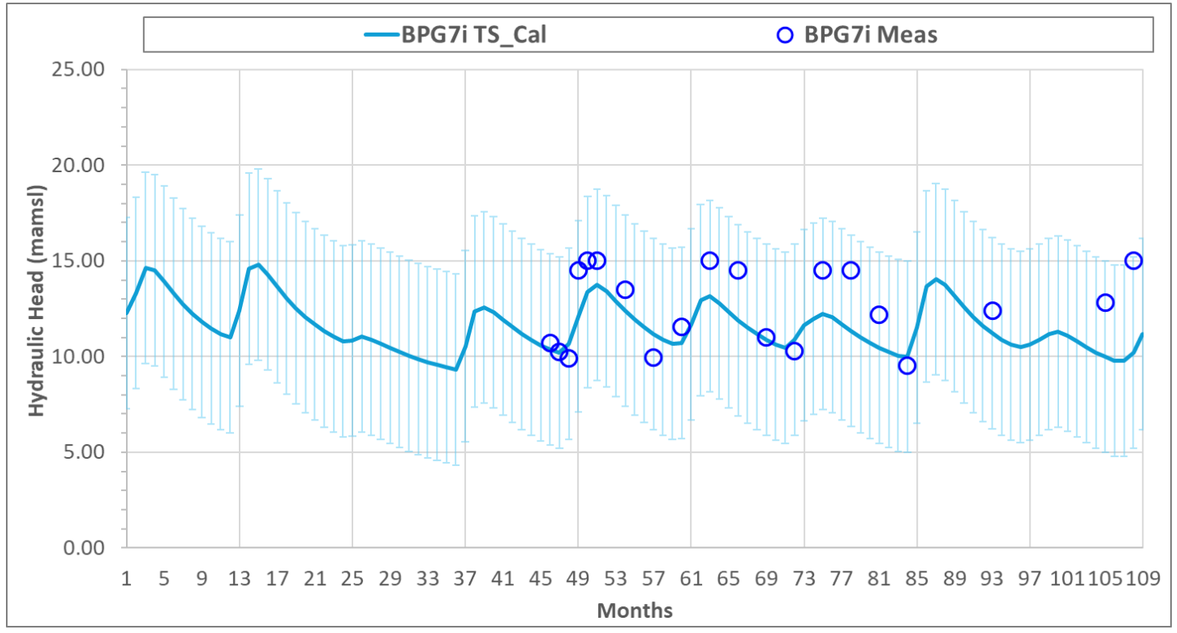

Figure 12-9: Simulated vs Measured Transient Hydraulic Heads for BPG5i, BPG6, BPG7s, and BPG7i

12.2.3 Sensitivity Analysis Results

The sensitivity analysis was conducted with the scenarios as specified in Section 3.8.1. The sensitivity analysis provided a bracketed range for dewatering rates and delineated ZOIs. The dewatering ranges for BP33 UG are shown in Figure 12-10, and the BP33 box cut inflows are provided in Figure 12-11.

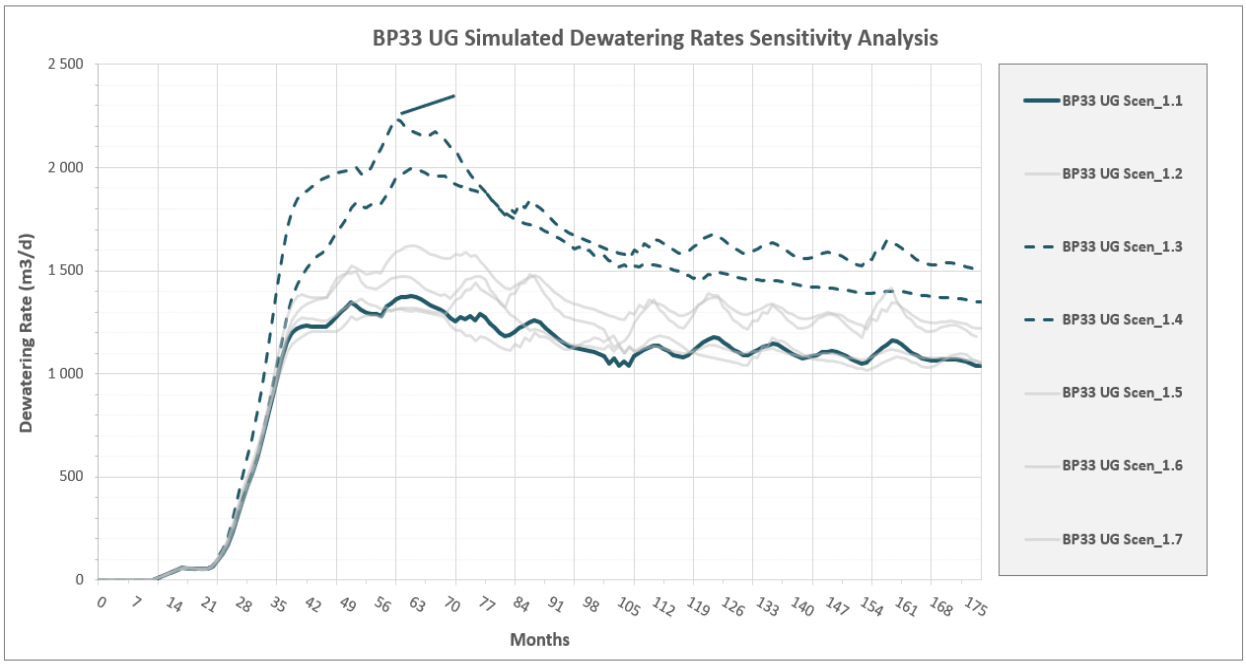

Figure 12-10: Simulated BP33 UG Dewatering Rates for all the Scenarios (Base Case and High Case Highlighted)

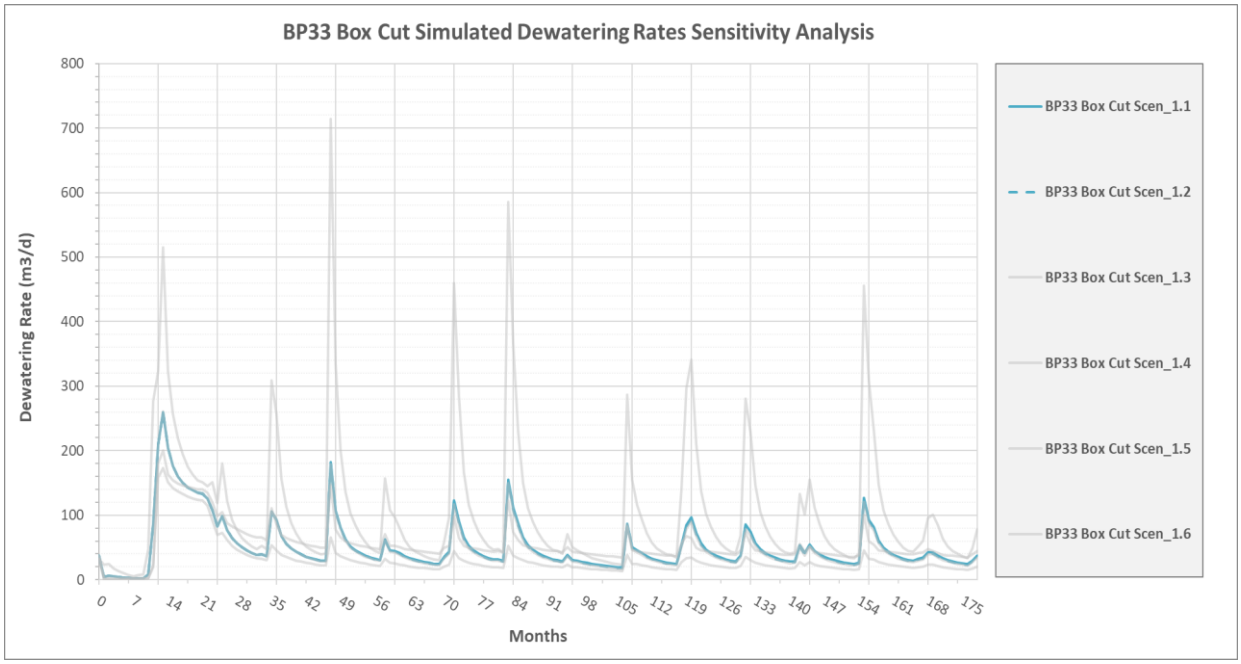

Figure 12-11: Simulated BP33 Box Cut Dewatering Rates for all the Scenarios with the Base Case Highlighted

- The simulated ZOIs are summarised in Scenario 1.1 (Base case) produced moderate ZOI extents across all depths and both mines, serving as the reference against which all other scenarios are compared.

- Scenario 1.2 (Medium K — 5 × hydraulic conductivity in deep layers) produces values very similar to Scenario 1.1, with only a modest increase in deep aquifer ZOI. Higher K allows drawdown to transmit laterally.

- Scenario 1.3 (High K — 10 × hydraulic conductivity) produces the largest ZOIs in the table, especially in the deep aquifer. This scenario represents a high-case scenario for the assessment and highlights the importance of conducting deep packer tests to verify deep hydraulic conductivity.

- Scenario 1.4 (High Sy — 10 × specific yield as Sy) produces smaller ZOIs — notably below even the base case (e.g. BP33 Shallow drops to 985 m). High Sy acts as a hydraulic buffer: a larger storage means the aquifer absorbs more water per unit of head decline before drawdown propagates outward, so the ZOI contracts significantly.

- Scenario 1.5 (50% recharge) produces ZOIs slightly below the base case. Less recharge means less water available to limit drawdown.

- Scenario 1.6 (Double recharge) produces the most compressed ZOIs in several shallow and intermediate aquifers (e.g. BP33 Shallow: 670 m). Greater recharge inputs counteract simulated drawdown.

- Scenario 1.7 (Dry cycle) shows moderate ZOI extents broadly in line with the base case. A drier climate reduces recharge availability over the LoM period, marginally increasing drawdown relative to a wetter cycle, but the effect is less dramatic than K or Sy changes because the dominant drivers of ZOI extent are aquifer transmissivity and storage.

Table 12-7 and the following was concluded:

- Scenario 1.1 (Base case) produced moderate ZOI extents across all depths and both mines, serving as the reference against which all other scenarios are compared.

- Scenario 1.2 (Medium K — 5 × hydraulic conductivity in deep layers) produces values very similar to Scenario 1.1, with only a modest increase in deep aquifer ZOI. Higher K allows drawdown to transmit laterally.

- Scenario 1.3 (High K — 10 × hydraulic conductivity) produces the largest ZOIs in the table, especially in the deep aquifer. This scenario represents a high-case scenario for the assessment and highlights the importance of conducting deep packer tests to verify deep hydraulic conductivity.

- Scenario 1.4 (High Sy — 10 × specific yield as Sy) produces smaller ZOIs — notably below even the base case (e.g. BP33 Shallow drops to 985 m). High Sy acts as a hydraulic buffer: a larger storage

means the aquifer absorbs more water per unit of head decline before drawdown propagates outward, so the ZOI contracts significantly.

- Scenario 1.5 (50% recharge) produces ZOIs slightly below the base case. Less recharge means less water available to limit drawdown.
- Scenario 1.6 (Double recharge) produces the most compressed ZOIs in several shallow and intermediate aquifers (e.g. BP33 Shallow: 670 m). Greater recharge inputs counteract simulated drawdown.
- Scenario 1.7 (Dry cycle) shows moderate ZOI extents broadly in line with the base case. A drier climate reduces recharge availability over the LoM period, marginally increasing drawdown relative to a wetter cycle, but the effect is less dramatic than K or Sy changes because the dominant drivers of ZOI extent are aquifer transmissivity and storage.

Table 12-7: Max Distance ZOI Reached from Mining for Each Scenario

Max Distance from Mining Infrastructure (m)			
Mine	**BP33**		
Aquifer	**Shallow**	**Intermediate**	**Deep**
Scenario 1.1	1 310	1 350	1 870
Scenario 1.2	1 310	1 410	1 900
Scenario 1.3	1 435	1 500	2 820
Scenario 1.4	985	960	1 340
Scenario 1.5	1 350	1 260	1 600
Scenario 1.6	670	800	1 530
Scenario 1.7	780	1 510	1 750

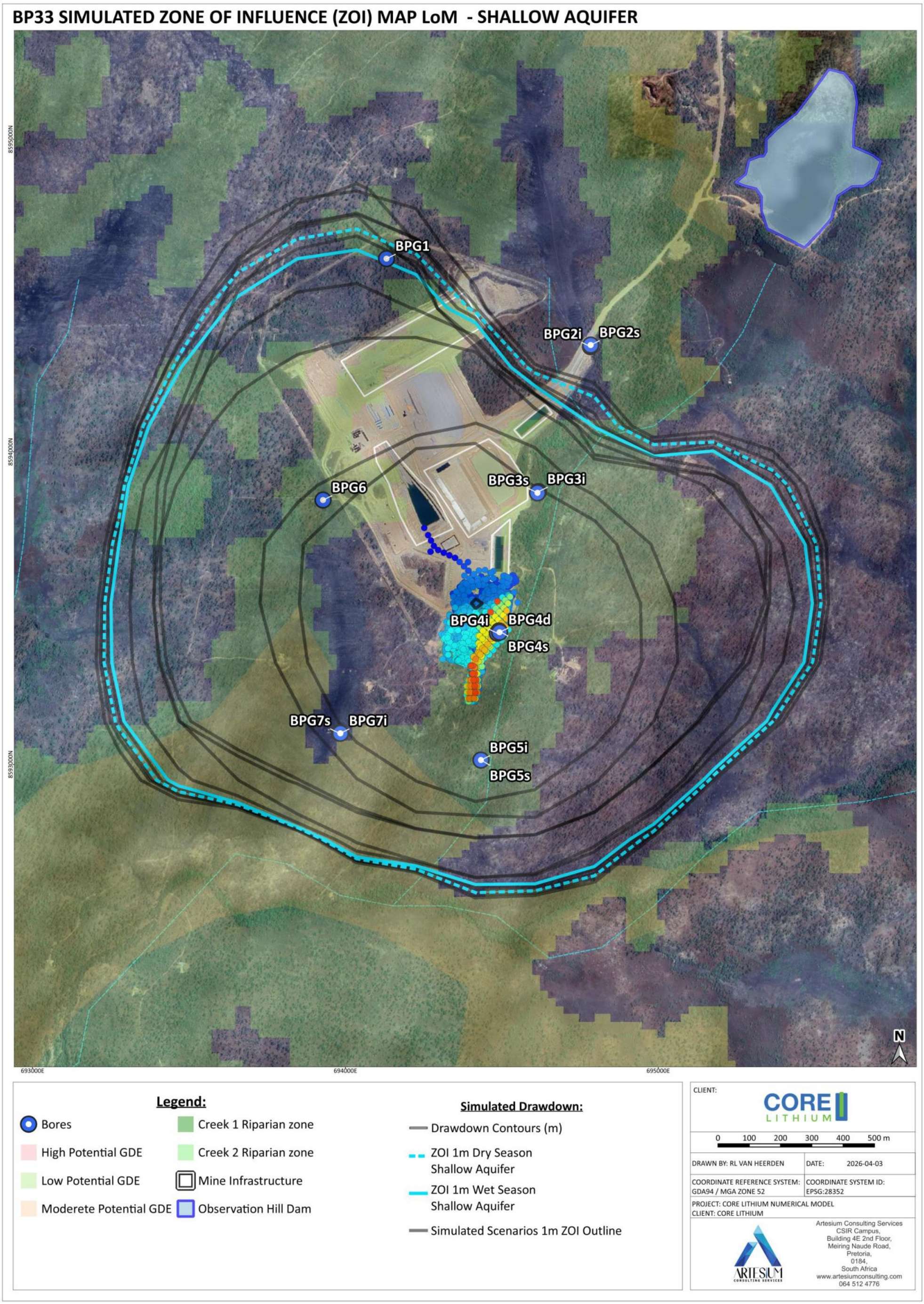

Figure 12-12: BP33 Simulated ZOIs for all Sensitivity Simulations with Base Case Highlighted measured in the Shallow Aquifer (Model Layer 1)

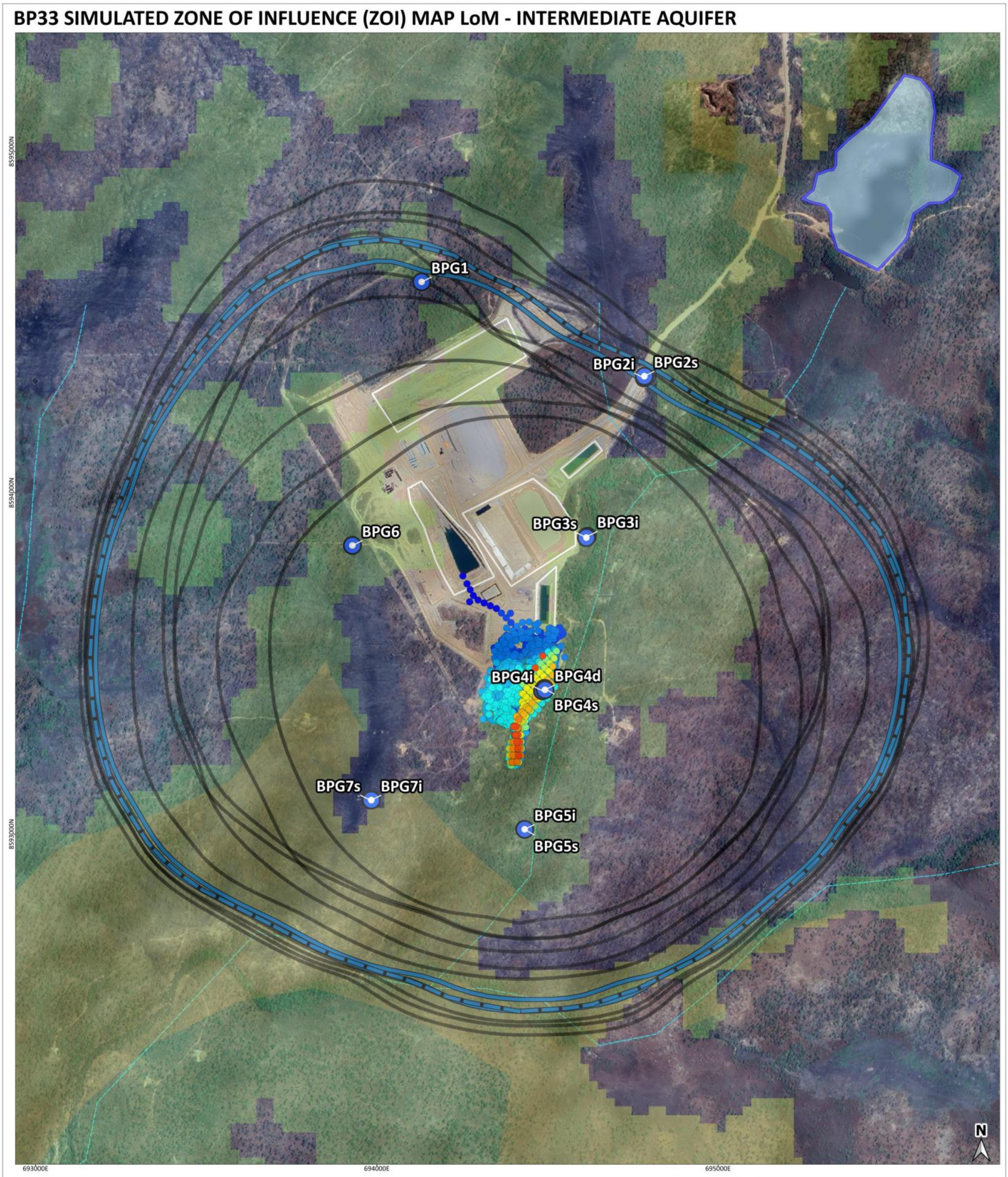

Figure 12-13: BP33 Simulated ZOIs for all Sensitivity Simulations with Base Case Highlighted measured in the Intermediate Aquifer (Model Layer 10)

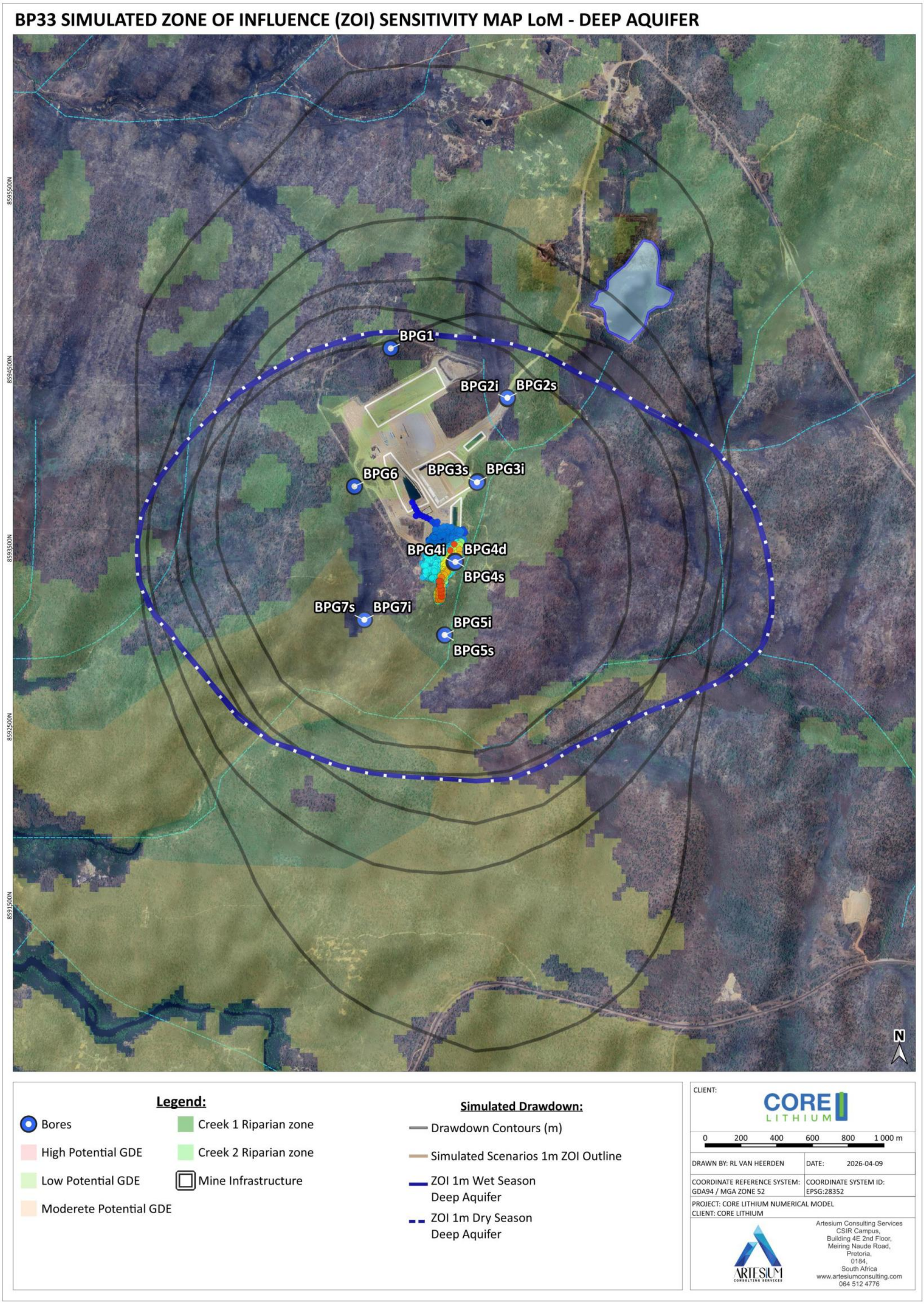

Figure 12-14: BP33 Simulated ZOIs for all Sensitivity Simulations with Base Case Highlighted measured in the Deep Aquifer (Model Layer 14)

Table 12-8: Model Parameters

Layer	Hydraulic Zone	Elevation (mamsl)	Thickness (m)	Cumulative Depth (mbgl)	Transmissivity (m^2/d)	Avg Hydraulic Conductivity K (m/d)	Hydraulic Conductivity Kx (m/d)	Hydraulic Conductivity Ky (m/d)	Hydraulic Conductivity Kz (m/d)	Ss (1/m)	S (1)	Specific Yield	Ass_R (mm/a)	Ass_R (mm/d)	Recharge (%)	Recharge (m/d)
1	Sand, silt, clay	20	4	4	12.13	2.94E+00	4.20E+00	4.20E+00	4.20E-01	2.42E-04	1.00E-03	1.00E-02	100	0.274	6.51%	2.74E-04
1	Shale, siltstone, phyllite	20	4	4	10.11	2.45E+00	3.50E+00	3.50E+00	3.50E-01	2.42E-04	1.00E-03	1.00E-02	70	0.192	4.55%	1.92E-04
1	Alluvium	20	4	4	18.48	4.48E+00	6.40E+00	6.40E+00	6.40E-01	2.42E-03	1.00E-02	8.00E-02	150	0.411	9.76%	4.11E-04
2	Weathered/Fractured	15.875	4	8	0.22	5.26E-02	7.51E-02	7.51E-02	7.51E-03	1.45E-04	6.00E-04	7.20E-03				
3	Weathered/Fractured	11.75	4	12	0.22	5.26E-02	7.51E-02	7.51E-02	7.51E-03	1.45E-04	6.00E-04	7.20E-03				
4	Weathered/Fractured	7.625	4	17	0.22	5.26E-02	7.51E-02	7.51E-02	7.51E-03	1.45E-04	6.00E-04	7.20E-03				
5	Weathered/Fractured	3.5	4	21	0.22	5.26E-02	7.51E-02	7.51E-02	7.51E-03	1.45E-04	6.00E-04	7.20E-03				
6	Weathered/Fractured	-0.625	4	25	0.22	5.26E-02	7.51E-02	7.51E-02	7.51E-03	1.45E-04	6.00E-04	7.20E-03				
7	Weathered/Fractured	-4.75	8	33	0.43	5.26E-02	7.51E-02	7.51E-02	7.51E-03	7.27E-05	6.00E-04	7.20E-03				
8	Weathered/Fractured	-13	17	50	0.87	5.26E-02	7.51E-02	7.51E-02	7.51E-03	3.64E-05	6.00E-04	7.20E-03				
9	Fractured/Fresh	-29.5	17	66	0.57	3.45E-02	5.01E-02	5.01E-02	3.34E-03	3.64E-05	6.00E-04	6.00E-03				
10	Fractured/Fresh	-46	17	83	0.57	3.45E-02	5.01E-02	5.01E-02	3.34E-03	3.64E-05	6.00E-04	6.00E-03				
11	Fractured/Fresh	-62.5	17	99	0.02	1.11E-03	1.61E-03	1.61E-03	1.07E-04	3.64E-05	6.00E-04	6.00E-03				
12	Fractured/Fresh	-79	24	123	0.03	1.11E-03	1.61E-03	1.61E-03	1.07E-04	2.48E-05	6.00E-04	6.00E-03				
13	Fractured/Fresh	-103.226	24	147	0.04	1.63E-03	2.36E-03	2.36E-03	1.57E-04	2.48E-05	6.00E-04	6.00E-03				
14	Fresh Rock	-127.452	24	172	0.01	3.07E-04	4.46E-04	4.46E-04	2.97E-05	1.24E-05	3.00E-04	4.50E-03				
15	Fresh Rock	-151.677	24	196	0.01	2.89E-04	4.20E-04	4.20E-04	2.80E-05	1.24E-05	3.00E-04	4.50E-03				
16	Fresh Rock	-175.903	24	220	0.01	2.70E-04	3.92E-04	3.92E-04	2.61E-05	1.24E-05	3.00E-04	4.50E-03				
17	Fresh Rock	-200.129	24	244	0.01	2.34E-04	3.40E-04	3.40E-04	2.27E-05	1.24E-05	3.00E-04	4.50E-03				
18	Fresh Rock	-224.355	24	269	0.01	2.20E-04	3.20E-04	3.20E-04	2.13E-05	1.24E-05	3.00E-04	4.50E-03				
19	Fresh Rock	-248.581	24	293	0.01	2.07E-04	3.00E-04	3.00E-04	2.00E-05	1.24E-05	3.00E-04	4.50E-03				
20	Fresh Rock	-272.806	24	317	0.00	1.93E-04	2.80E-04	2.80E-04	1.87E-05	1.24E-05	3.00E-04	4.50E-03				
21	Fresh Rock	-297.032	24	341	0.00	1.65E-04	2.40E-04	2.40E-04	1.60E-05	8.26E-06	2.00E-04	3.00E-03				
22	Fresh Rock	-321.258	24	365	0.00	1.57E-04	2.28E-04	2.28E-04	1.52E-05	8.26E-06	2.00E-04	3.00E-03				
23	Fresh Rock	-345.484	24	390	0.00	1.49E-04	2.16E-04	2.16E-04	1.44E-05	8.26E-06	2.00E-04	3.00E-03				
24	Fresh Rock	-369.71	24	414	0.00	1.41E-04	2.04E-04	2.04E-04	1.36E-05	8.26E-06	2.00E-04	3.00E-03				
25	Fresh Rock	-393.935	24	438	0.00	1.24E-04	1.80E-04	1.80E-04	1.20E-05	8.26E-06	2.00E-04	3.00E-03				
26	Fresh Rock	-418.161	24	462	0.00	1.17E-04	1.70E-04	1.70E-04	1.13E-05	8.26E-06	2.00E-04	3.00E-03				
27	Fresh Rock	-442.387	24	487	0.00	1.10E-04	1.60E-04	1.60E-04	1.07E-05	8.26E-06	2.00E-04	3.00E-03				
28	Fresh Rock	-466.613	24	511	0.00	1.03E-04	1.50E-04	1.50E-04	1.00E-05	8.26E-06	2.00E-04	3.00E-03				
29	Fresh Rock	-490.839	24	535	0.00	9.64E-05	1.40E-04	1.40E-04	9.33E-06	8.26E-06	2.00E-04	3.00E-03				
30	Fresh Rock	-515.065	24	559	0.00	8.27E-05	1.20E-04	1.20E-04	8.00E-06	8.26E-06	2.00E-04	3.00E-03				
31	Fresh Rock	-539.29	24	584	0.00	7.88E-05	1.14E-04	1.14E-04	7.63E-06	8.26E-06	2.00E-04	3.00E-03				
32	Fresh Rock	-563.516	24	608	0.00	7.48E-05	1.09E-04	1.09E-04	7.24E-06	8.26E-06	2.00E-04	3.00E-03				
33	Fresh Rock	-587.742	24	632	0.00	7.10E-05	1.03E-04	1.03E-04	6.87E-06	8.26E-06	2.00E-04	3.00E-03				
34	Fresh Rock	-611.968	24	656	0.00	5.92E-05	8.60E-05	8.60E-05	5.73E-06	8.26E-06	2.00E-04	3.00E-03				
35	Fresh Rock	-636.194	24	680	0.00	5.57E-05	8.08E-05	8.08E-05	5.39E-06	4.13E-06	1.00E-04	1.00E-03				
36	Fresh Rock	-660.419	24	705	0.00	5.21E-05	7.56E-05	7.56E-05	5.04E-06	4.13E-06	1.00E-04	1.00E-03				
37	Fresh Rock	-684.645	24	729	0.00	4.85E-05	7.04E-05	7.04E-05	4.69E-06	4.13E-06	1.00E-04	1.00E-03				
38	Fresh Rock	-708.871	25	754	0.00	4.13E-05	6.00E-05	6.00E-05	4.00E-06	4.13E-06	1.00E-04	1.00E-03				
39	Fresh Rock	-733.97	23	777	0.00	3.86E-05	5.60E-05	5.60E-05	3.73E-06	4.13E-06	1.00E-04	1.00E-03				
40	Fresh Rock	-757.323	24	802	0.00	3.58E-05	5.20E-05	5.20E-05	3.47E-06	4.13E-06	1.00E-04	1.00E-03				
41	Fresh Rock	-781.548	24	826	0.00	2.76E-05	4.00E-05	4.00E-05	2.67E-06	4.13E-06	1.00E-04	1.00E-03				
42	Fresh Rock	-805.774	24	850	0.00	2.76E-05	4.00E-05	4.00E-05	2.67E-06	4.13E-06	1.00E-04	1.00E-03				
43	Fresh Rock	-830	170	1 020	0.00	2.76E-05	4.00E-05	4.00E-05	2.67E-06	5.88E-07	1.00E-04	1.00E-03				

13 Appendix B: Simulated Hydraulic Heads for LoM

Table 13-1: Statistical Summary of Simulated LoM Hydraulic Heads for BP33

Statistical Summary	BPG1 Scen_1.1	BPG2s Scen_1.1	BPG2i Scen_1.1	BPG3s Scen_1.1	BPG3i Scen_1.1	BPG4s Scen_1.1	BPG4i Scen_1.1
Max	25	24	20	15	15	11	13
P95	24	24	20	14	14	10	11
P90	23	23	20	14	14	9	11
Arithmetic Mean	21	21	19	11	11	0	-13
P50	21	21	19	10	10	-2	-17
P05	19	19	18	8	8	-4	-19
Min	17	18	17	6	6	-4	-20

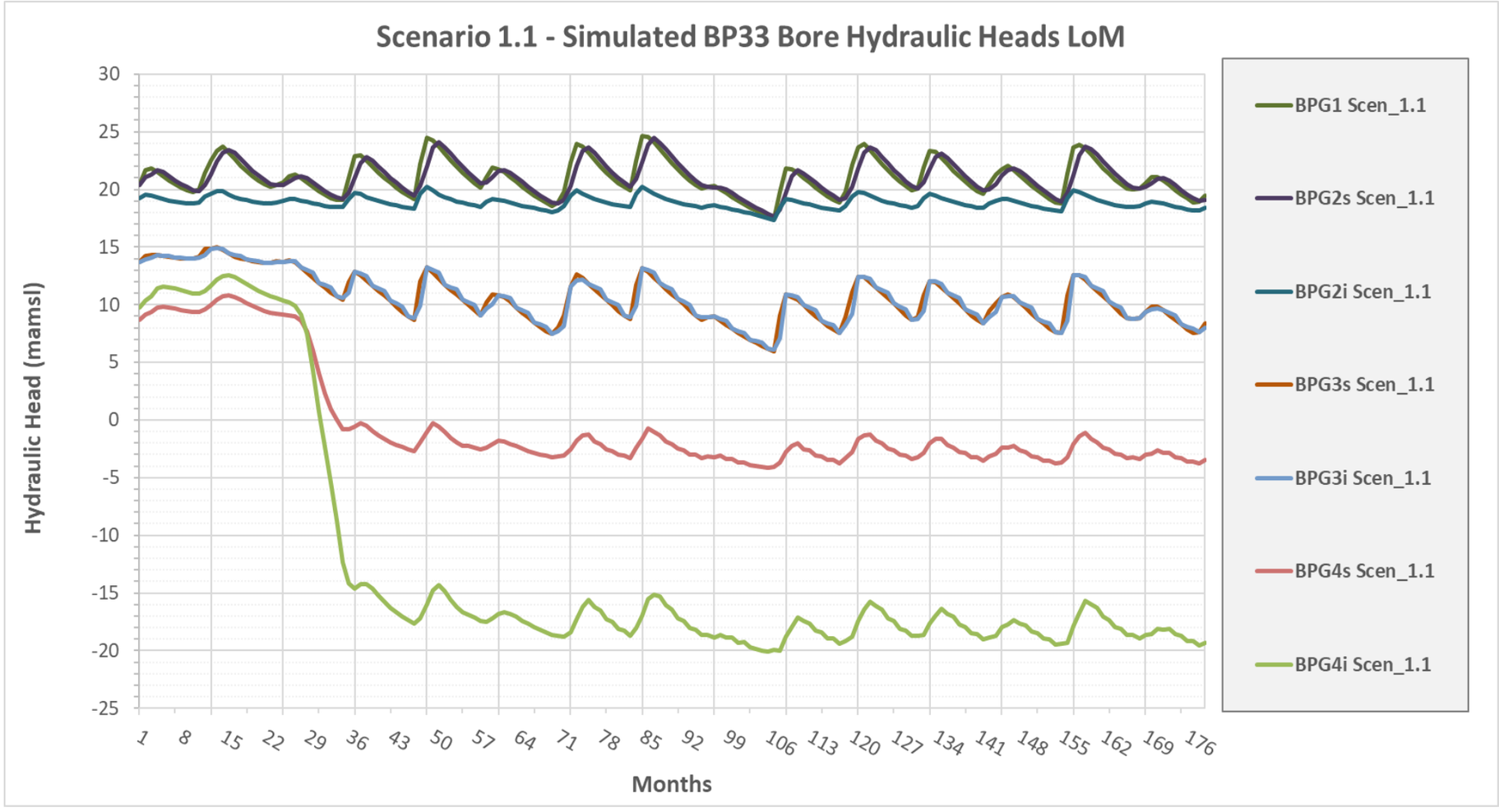

Figure 13-1: Simulated Hydraulic Heads for Bores at BP33 for LoM – Scenario 1.1

Table 13-2: Statistical Summary of Simulated LoM Hydraulic Heads for BP33 – Continued

Statistical Summary	BPG4d Scen_1.1	BPG5s Scen_1.1	BPG5i Scen_1.1	BPG6 Scen_1.1	BPG7s Scen_1.1	BPG7i Scen_1.1
Max	13	14	14	18	15	14
P95	12	13	12	16	13	12
P90	11	12	12	15	13	12
Arithmetic Mean	-24	8	6	11	9	8
P50	-32	7	5	11	9	8
P05	-33	5	3	8	6	5
Min	-34	3	2	6	5	4

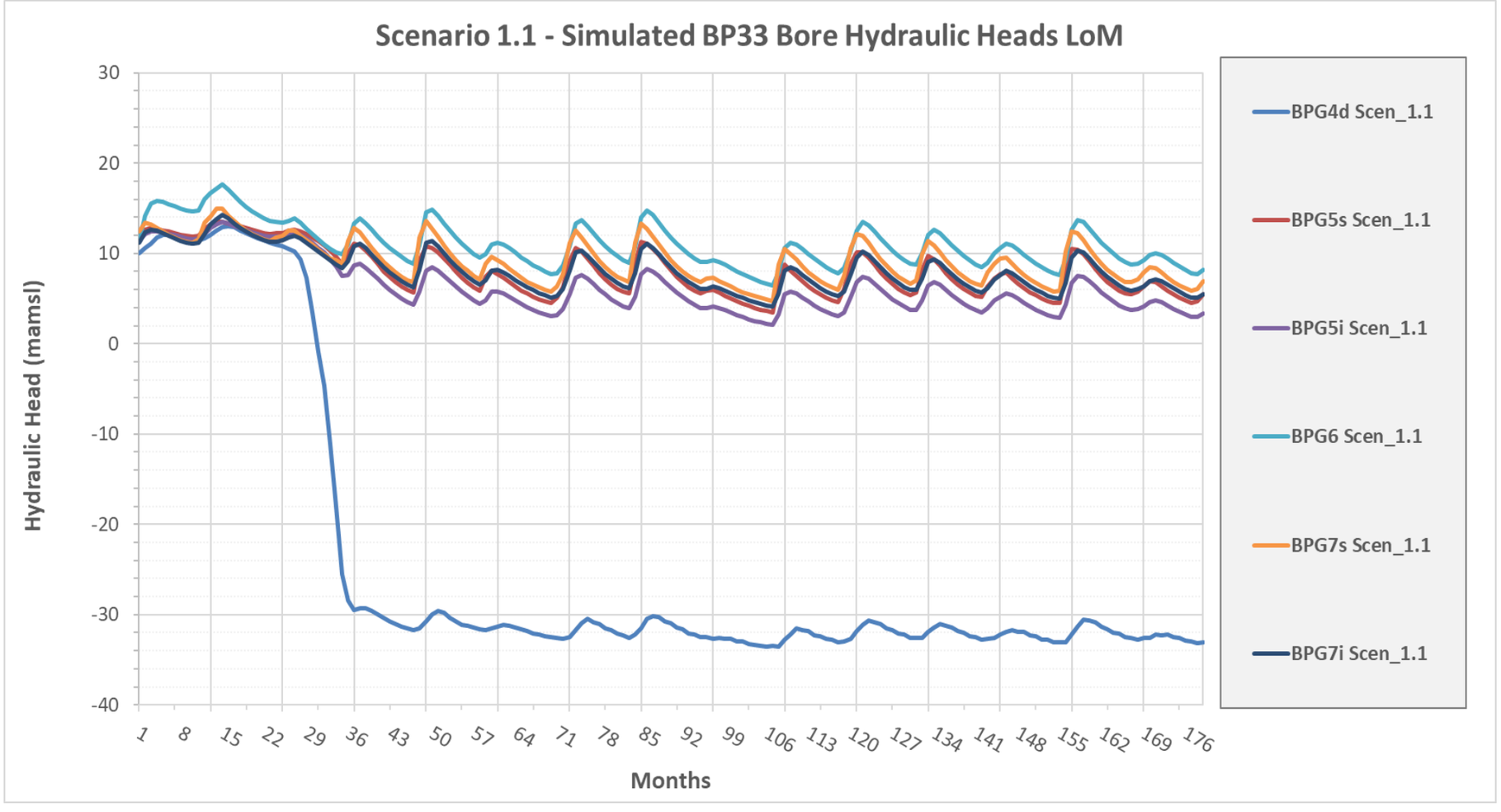

Figure 13-2: Simulated Hydraulic Heads for Bores at BP33 for LoM – Scenario 1.1 - Continued